

Aus der Klinik I für Innere Medizin
der Universität zu Köln
Direktor: Prof. Dr. med. Michael Hallek

Die Rolle des macrophage migration inhibitory factor bei der Entstehung von
Hauttumoren in der Maus

Inaugural-Dissertation zur Erlangung der Würde eines
doctor rerum medicinalium
der Hohen Medizinischen Fakultät
der Universität zu Köln

vorgelegt von
Tania Marina Brocks
aus Dortmund

Promoviert am 15. Dezember 2010

Gedruckt mit Genehmigung der Medizinischen Fakultät der Universität zu Köln
im Jahre 2010

Die in dieser Arbeit angegebenen Experimente sind nach entsprechender Anleitung durch Herrn Privatdozent Dr. Günter Fingerle-Rowson von mir selbst ausgeführt worden.

ACKNOWLEDGEMENTS

As we travel through our life, rarely do we stop and thank the people that have joined us on our way and continue to be company along our paths. Without those people, our being on this planet would not have been the same. It has been those people who were instrumental for my development. Not only as a scientist, but most importantly, as a person.

First, I would like to dedicate my greatest appreciation to my grandmother Zlata Gressner for being the biggest supporter of my career, the best mentor I have ever had, and for her tremendous faith in me. Without her, Granny, I would have never made it to where I am now. I will never be able to repay her for everything she has done for me, but I can only hope that I made her somehow proud.

Heartfelt thank you deserve my godmother Danuško and grandaunt Babka for always being there, as family, and offering sound advice and comforting words when I needed them most.

A grateful acknowledgement goes to my PhD advisor, Dr. Günter Fingerle-Rowson, for the freedom to pursue scientific ideas in his lab and providing me with the opportunity for becoming a well-rounded, creative, and independent scientist.

All that I have been able to achieve during my graduate research studies would not have been possible without the intellectual and emotional support of my lab mates, namely Nadine, Dana, Julian, Nils and Oleg. I hugely appreciate our unconditional friendships! In particular, my gratitude extends to lively Astrid, whose vigorousness I have always admired.

I am so much obliged to my mother-in-law to have become part of my life. Never had I thought it could feel so good to have one. And that is because it is her, Hilde.

Finally, I would like to thank the love of my life, Christian, whose support, warmth and love (and not to forget all the raspberry tartlets, and his funny moves that made me laugh!) throughout this process, although he was thousands of miles away, has made all the difference!

Meiner Großmutter Zlata Gressner

TABLE OF CONTENTS

	Page
ABBREVIATIONS.....	15
1 INTRODUCTION	
1.1 MACROPHAGE MIGRATION INHIBITORY FACTOR (MIF).....	21
1.2 ORGANISATION OF THE <i>MIF</i> GENE LOCUS.....	21
1.3 STRUCTURE OF THE MIF PROTEIN.....	22
1.4 EXTRACELLULAR AND INTRACELLULAR MIF.....	24
1.5 EXPRESSION PATTERN OF MIF.....	27
1.6 MIF IN THE SKIN.....	29
1.7 MIF AND TUMORIGENESIS.....	30
1.8 MIF IN EPITHELIAL TUMORS.....	30
1.9 MIF AND UVB RADIATION.....	32
1.10 AIMS OF THE STUDY.....	32
1.11 EXPERIMENTAL SET-UP.....	32
2 MATERIALS & METHODS	
2.1 INSTRUMENTS.....	43
2.2 CHEMICALS.....	44
2.3 SPECIAL REAGENTS/KITS.....	46
2.4 SOFTWARE.....	46
2.5 ETHICS STATEMENT.....	47
2.6 ANIMALS.....	47
2.7 ANIMAL WELFARE.....	48
2.8 REASONS FOR THE CHOICE OF MOUSE STRAINS FOR THE EXPERIMENTS.....	48
2.9 BREEDING STRATEGIES.....	49
2.10 GENOTYPING.....	50

2.11 GENOMIC DNA PREPARATION.....	50
2.12 POLYMERASE CHAIN REACTION (PCR).....	51
2.13 GENOTYPING <i>MIF</i> MICE.....	52
2.14 GENOTYPING <i>K14HPV8-CER</i> MICE.....	53
2.15 GENOTYPING OF <i>K14-CRE</i> MICE.....	56
2.16 AGAROSE GEL ELECTROPHORESIS.....	58
2.17 TWO STAGE-CARCINOGENESIS WITH 7,12- DIMETHYLBENZ(A)ANTHRACENE (DMBA) AND PHORBOL-12- MYRISTATE-ACETATE (TPA).....	59
2.18 ONE STAGE CARCINOGENESIS WITH BENZO(A)PYRENE (B[A]P).....	59
2.19 UV-B IRRADIATION.....	60
2.20 RESCUE OF IMMUNE CELL HOMING BY INTRA-EPIDERMAL INJECTIONS OF MIF.....	60
2.21 HISTOLOGY.....	61
2.22 IMMUNOHISTOCHEMISTRY.....	61
2.23 IMMUNOFLUORESCENCE.....	62
2.24 IMMUNOFLUORESCENT ANALYSIS OF CRYOSECTIONED MURINE SKIN TUMOR TISSUE.....	63
2.25 PREPARATION OF EPIDERMAL SHEETS.....	63
2.26 EUKARYOTIC CELL CULTURE CONDITIONS.....	64
2.27 PREPARATION OF MURINE EMBRYONIC FEEDERS FOR PRIMARY MURINE KERATINOCYTES.....	64
2.28 ISOLATION OF PRIMARY MURINE KERATINOCYTES.....	65
2.29 TRYPSINIZATION.....	67

2.30 COUNTING.....	67
2.31 FREEZING AND THAWING OF CELLS.....	68
2.32 PREPARATION OF CELL LYSATES.....	68
2.33 QUANTIFICATION OF PROTEINS.....	69
2.34 SDS POLYACRYLAMIDE GEL ELECTROPHORESIS (SDS- PAGE).....	70
2.35 PROTEIN TRANSFER.....	72
2.36 IMMUNOBLOTTING AND DEVELOPMENT.....	73
2.37 ANTIBODIES FOR IMMUNOBLOTTING.....	74
2.38 GENERATION OF CHEMICALLY COMPETENT CELLS.....	74
2.39 TRANSFORMATION OF CHEMICALLY COMPETENT CELLS.....	76
2.40 AMPLIFICATION OF $\Delta NTP53R175H$	77
2.41 DIGESTION OF PSC_AEGFPFG2.....	78
2.42 LIGATION OF DIGESTED PSC VECTOR AND $\Delta NTP53R175H$ INSERTION SEQUENCE.....	79
2.43 CONTROL DIGESTION OF CLONED PLASMIDS FOR ITR FUNCTIONALITY.....	79
2.44 Statistical Analysis.....	80

3 RESULTS

3.1 GENOTYPING TO DETERMINE THE <i>MIF</i> STATUS WITH THREE PRIMERS WAS RELIABLE.....	81
3.2 APPLICATION OF A CHEMICAL CARCINOGENESIS IN A CLASSICAL TWO-STAGE PROTOCOL WITH DMBA AND TPA SHOWS	

THAT MIF-DEFICIENCY IN MICE TURNS THEM PRONE TO INCREASED SKIN TUMOR FORMATION.....	82
3.3 CHEMICAL SKIN CARCINOGENESIS WITH DMBA AND TPA INDUCES PREDOMINANTLY BENIGN TUMORS AND HAIR FOLLICLE NEOPLASIAS IN MIF-DEFICIENT 129S1 MICE.....	85
3.4 CHEMICAL SKIN CARCINOGENESIS WITH BENZO(A)PYRENE REVEALS A DISTINCT DIFFERENCE BETWEEN TUMOR NUMBERS IN MIF-DEFICIENT AND CONTROL MICE AND THEIR SEXES.....	86
3.5 THE TUMOR SPECTRUM INDUCED BY CHEMICAL SKIN CARCINOGENESIS WITH BENZO(A)PYRENE DISPLAYS A SHIFT FROM BENIGN TO MALIGN ENTITIES, OF WHICH MOST OCCUR IN MIF-DEFICIENT MICE.....	90
3.6 THE INDUCTION OF SKIN TUMORS BY IRRADIATION WITH UV-B COULD NOT BE COMPLETED DUE TO UNFORESEEN CIRCUMSTANCES, WHICH TERMINATED IN EUTHANASIA OF THE EXPERIMENTAL ANIMALS.....	92
3.7 SKIN TUMOR DEVELOPMENT IN MICE WITH A <i>K14HPV8-CER</i> -TRANSGENIC BACKGROUND CONFIRMS THAT MIF PROTECTS THE MURINE SKIN FROM NEOPLASTIC EVENTS.....	97
3.8 THE GENERATION OF MICE WITH EPIDERMIS-SPECIFIC DEFICIENCY OF WAS ONLY PARTIALLY SUCCESSFUL, AS IT WAS NOT POSSIBLE TO GENERATE A SUFFICIENT NUMBER OF AGE- & SEX-MATCHED MICE TO START A CHEMICAL SKIN TUMOR INDUCTION.....	100
3.9 EXPRESSION PATTERN OF MIF IN MURINE SKIN SHOWS HIGH PROTEIN LEVELS IN KERATINOCYTES COMPARED TO THOSE IN DERMAL CELLS.....	103
3.10 IMMUNOHISTOCHEMICAL DETECTION OF MIF EXPRESSION IN MURINE SKIN REVEALS NUCLEAR SIGNALS IN KERATINO- AND SEBOCYTES OF DIFFERENT INTENSITIES.....	104

3.11 NUCLEAR MIF WAS DETECTED AND CONFIRMED BY WESTERN BLOT.....	106
3.12 NUCLEAR MIF EXPRESSION IN HACAT CELLS, MURINE SKIN AND SKIN TUMORS WAS CONFIRMED BY CONFOCAL MICROSCOPY.....	110
3.13 PRESENTATION OF THE METHOD HOW MIF EXPRESSION AT CYTOPLASMIC AND NUCLEAR LEVELS IN SINGLE CELLS OF HOMEOSTATIC AND NEOPLASTIC EPIDERMIS WAS HISTOPATHOLOGICALLY EVALUATED.....	111
3.14 HISTOPATHOLOGICAL SCORE OF MIF EXPRESSION AT CYTOSOLIC AND NUCLEAR LEVELS IN SINGLE CELLS OF HOMEOSTATIC AND NEOPLASTIC EPIDERMIS REVEALS THE DIMINISHMENT OF THE STRONG NUCLEAR MIF SIGNAL IN MURINE SKIN TUMOR TISSUE.....	113
3.15 EXPRESSION OF JAB1, THE INTRACELLULAR BINDING PARTNER FOR MIF, IN MURINE SKIN IS MAINLY CYTOPLASMIC IN KERATINOCYTES, BUT ALSO OCCURS IN SEBACEOUS NUCLEI.....	114
3.16 COMPARISON BETWEEN JAB1 AND MIF EXPRESSION IN EPIDERMAL TUMORS OF MICE TREATED WITH CHEMICAL CARCINOGENS REVEALS NO SIGNIFICANT CHANGES REGARDING THE EXPRESSION PATTERN OF JAB1 COMPARED TO HOMEOSTATIC SKIN.....	115
3.17 CD44 EXPRESSION IN MURINE SKIN AND ITS TUMORS AFTER CHEMICAL CARCINOGENESIS IS UNCHANGED AND RESTRICTED TO THE BASAL EPIDERMAL LAYERS.....	116
3.18 THE MIF RECEPTOR CD74 IS EXPRESSED BY IMMUNE CELLS IN THE MURINE SKIN.....	117
3.19 IMMUNOHISTOCHEMICAL DETECTION OF CD74 EXPRESSION IN MURINE SKIN TUMORS AFTER CHEMICAL CARCINOGENESIS	

SHOWS LESS CD74-POSITIVE CELLS IN MIF-DEFICIENT TISSUE.....	118
3.20 <i>K14HPV8-CER</i> -TRANSGENIC MIF-DEFICIENT MICE PRESENT A HIGHER NUMBER OF CD74-POSITIVE CELLS EMBEDDED INTO THE EPIDERMIS COMPARED TO NON-TRANSGENIC MIF KO MICE, AS UNRAVELED BY IMMUNOHISTOCHEMICAL DETECTION.....	119
3.21 IMMUNOHISTOCHEMICAL DETECTION OF B CELLS BY B220 (CD45R) EXPRESSION IN MURINE SKIN AFTER CHEMICAL CARCINOGENESIS PRESENTS INCREASED INVASION OF B CELLS INTO MIF-DEFICIENT SKIN TUMOR TISSUE.....	120
3.22 IMMUNOFLUORESCENT DETECTION OF F4/80-EXPRESSING CELLS IN MURINE SKIN BEFORE AND AFTER CHEMICAL CARCINOGENESIS IMPRESSES BY AUGMENTED ACCUMULATION OF F4/80-POSITIVE CELLS IN THE TUMOR STROMA.....	121
3.23 IMMUNOHISTOCHEMICAL DETECTION OF F4/80 EXPRESSION IN THE ASYMPTOUS SKIN OF <i>K14HPV8-CER</i> -TRANSGENIC MIF-DEFICIENT MICE AND ITS NEOPLASIA SHOWS SIMILAR AMOUNTS OF F4/80-POSITIVE CELLS RELATIVE TO COMPARABLE TISSUES OF NON-TRANSGENIC MIF KO MICE.....	123
3.24 IMMUNOFLUORESCENT DETECTION OF CD3 EXPRESSING T CELLS IN MURINE SKIN BEFORE AND AFTER CHEMICAL CARCINOGENESIS REVEALS NO APPARENT INCREASE OF T CELL NUMBERS IN TUMOR TISSUE.....	125
3.25 THE ANALYSIS OF THE PROPORTIONS OF IMMUNE CELLS IN HOMEOSTATIC EPIDERMIS AND DERMIS TO TUMOR AND STROMAL TISSUE IN COMPARISON REVEAL MASSIVE DIFFERENCES BETWEEN MIF-DEFICIENT AND WILD-TYPE CONTROL MICE.....	126
3.26 EPIDERMAL MOUSE KERATINOCYTES DO NOT EXPRESS CD74, BUT A SUBPOPULATION OF EPIDERMAL CELLS DOES, AND	

CD74-EXPRESSING CELLS INVADE THE EPIDERMIS UPON SKIN TUMOR FORMATION.....	130
3.27 EPIDERMAL DENDRITIC CELLS ARE POSITIVE FOR CD74 AND F4/80.....	132
3.28 COMPARISON OF CD74 ⁺ CELL NUMBERS AFTER CHEMICAL SKIN CARCINOGENESIS WITH DMBA/TPA OR B(A)P REVEALS SIMILAR RELATIONS WITHIN MIF-DEFICIENT AND CONTROL TISSUES, AND HINTS AT A GENERAL TUMOR-PROTECTING FEATURE OF MIF IN MURINE SKIN TUMORIGENESIS AFTER CHEMICAL INDUCTION.....	134
3.29 IMMUNOFLUORESCENT DETECTION OF THE HISTOCOMPATIBILITY ANTIGEN HLA I-A IN SKIN SAMPLES BEFORE AND AFTER CHEMICAL CARCINOGENESIS WITH DMBA/TPA REVEALS THAT MIF-DEFICIENT SKIN AND TUMORS HARBOR SIGNIFICANTLY LESS I-A ⁺ CELLS THAN CONTROL TISSUES.....	135
3.30 CONTENT OF Lcs IN THE EPIDERMAL SHEETS OF WILD-TYPE AND MIF-DEFICIENT MOUSE EARS IS THE SAME.....	136
3.31 LC NUMBERS IN UNTREATED AND NEOPLASTIC SKIN AFTER CHEMICAL TUMORIGENESIS WITH DMBA/TPA SHOW A DRASTIC DIMINISHMENT IN MIF-DEFICIENT TISSUE SAMPLES.....	140
3.32 LANGERIN AND CD74 DISPLAY CO-EXPRESSION IN EPIDERMAL SHEETS.....	141
3.33 Lcs DO NOT EXPRESS DETECTABLE AMOUNTS OF MIF IN EPIDERMAL SHEETS.....	142
3.34 INTRA-EPIDERMAL INJECTIONS OF MIF RECONSTITUTE THE LC POPULATION IN MIF-DEFICIENT MICE TO NORMAL WILD-TYPE LEVELS.....	145

3.35 ISOLATED PRIMARY MURINE KERATINOCYTES OF MIF-DEFICIENT AND WILD-TYPE MICE DISPLAY NO MORPHOLOGICAL DIFFERENCES.....	147
3.36 SUCCESSFUL DEVELOPMENT OF AN AAV2-MEDIATED TRANSFORMATION OF PRIMARY MURINE KERATINOCYTES WITH GFP AND PRESENTATION OF THE DESIGN FOR A MALIGNANT TRANSFORMATION.....	154
4 DISCUSSION.....	154
4.1 MIF IN THE HUMAN EPIDERMIS.....	157
4.2 THE POTENTIAL ROLE OF THE MIF RECEPTOR CD74 IN MURINE SKIN CARCINOGENESIS.....	159
4.3 LANGERHANS CELLS AND SKIN IMMUNITY.....	159
4.4 INFLUENCE OF CHEMICAL CARCINOGENS ON LANGERHANS CELLS.....	161
4.5 LANGERHANS CELLS AND HPV.....	163
5 SYNOPSIS.....	165
6 REFERENCES.....	167
7 PUBLICATION LIST.....	175
8 VITA.....	176

ABBREVIATIONS

A	Adenine
AA	Alopecia areata
AAV	Adeno-associated virus
AD	Atopic dermatitis
AEC	3-amino-9-carbazole
AFX	Atypical fibroxanthoma
AP-1	Activator protein 1
APC	Antigen-presenting cell
APS	Ammonium persulfate
Asp	Asparagine
ATP	Adenosine triphosphate
B(a)P	Benzo(a)pyrene
bp	Base pair(s)
BCC	Basal cell carcinoma
BPB	Bromophenol blue
BSA	Bovine serum albumin
C	Cytosine
C-terminus	Carboxyl-terminus
CARE	<i>Cis-acting Rep-dependent element</i>
CD	Cluster of Differentiation
CDKI	Cyclin-dependent Kinase inhibitor
CER	Complete early region
CLL	Chronic lymphocytic Leukemia
CSN5	COP9 signalosome subunit 5
CXCR	CXC chemokine receptor

D	Aspartic acid
DAPI	4',6-diamidino-2-phenylindole
DC	Dendritic cell
ddH ₂ O	Double-distilled water
DDT	D-Dopachrome Tautomerase
DMBA	7,12-dimethylbenz[<i>a</i>]anthracene
DMEM	Dulbecco's Modified Eagle Medium
DMSO	Dimethyl sulfoxide
DNA	Deoxyribonucleic acid
E	Glutamine (Glu)
EDTA	Ethylene diamine tetraacetic acid
EGF	Epidermal growth factor
EGFP	Enhanced green fluorescent protein
EMT	Epithelia-mesenchymal transition
ERK	Extracellular signal-regulated kinase
EtOH	Ethanol
EV	Epidermodysplasia verruciformis
F1-n	Offspring generation
FBS	Fetal bovine serum
FELASA	Federation of European Laboratory Animal Science
FGFR-1	Fibroblast growth factor receptor 1
G	Guanine
GV-SOLAS	Gesellschaft für Versuchstierkunde
H&E	Hematoxylin and eosin
HF	Hair follicle
HIF-1 α	Hypoxia-inducing factor 1 α
hiMIF	Heat-inactivated MIF
HRP	Horse raddish peroxidase

HPV	Human papilloma virus
HSPG	Heparan sulfate proteoglycan
IFE	Interfollicular epidermis
IFN	Interferon
Ig	Immunoglobulin gene
IHC	Immunohistochemistry
IL	Interleukin
IP	Immune privilege
ITR	Inverted terminal repeat
JAB1	c-Jun activating binding protein 1
K14	Keratin 14
kb	Kilobases
KCl	Potassium chloride
kD or kDa	Kilo Dalton
KH ₂ PO ₄	Monopotassium phosphate
KO	Knockout
KOH	Potassium hydroxide
L	Leucine (Leu)
LB	Liquid broth
LC	Langerhans cell
mAbs	Monoclonal antibodies
MAPK	Mitogen-activated protein kinase
MEF	Murine embryonic fibroblast
MFH	Malign fibrous histiocytoma
MgCl ₂	Magnesium chloride
MHC	Major histocompatibility complex
MIF	Macrophage migration inhibitory factor
MIF ^{-/-}	MIF knockout mouse

MIF ^{+/+}	MIF wild-type mouse
MnCl ₂	Manganese chloride
MOPS	3-(N-morpholino)propanesulfonic acid
mRNA	Messenger RNA
MSH	Melanocyte-stimulating hormone
N-terminus	Amino-terminus
NaCl	Sodium chloride
Na ₂ EDTA	Disodium ethylenediamine tetraacetate
NaPP	Tetra-sodium diphosphate
NF-κB	Nuclear factor kappa B
(NH ₄) ₂ SO ₄	Ammonium sulfate
Na ₂ HPO ₄ ·7H ₂ O	Disodium hydrogen phosphate, heptahydrate
NaOH	Sodium hydroxide
NK cells	Natural killer cells
NMR	Nuclear magnetic resonance
NMSC	Non-melanoma skin cancers
NP-40	Nonyl phenoxypolyethoxylethanol
NTP	Nucleoside triphosphate
O.D.	Optical density
ORF	Open reading frame
ORS	Outer root sheath
P	Parental generation
PARP	Poly(ADP-ribose) polymerase
PBMC	Peripheral blood mononuclear cells
PBS	Phosphate buffered saline
PCR	Polymerase chain reaction
PLA-2	Phospholipase A2
PTP	protein tyrosine phosphatase

R	Arginine (Arg)
Rac1	Ras-related C3 botulinum toxin substrate 1
rmuMIF	Recombinant murine MIF
RNA	Ribonucleic acid
RNAi	RNA interference
rpm	Rounds per minute
RT	Room temperature
SCC	Squamous cell carcinoma
SCF	Skip-cullin-F-box protein complex
SDS	Sodium dodecyl sulfate-lauryl
SDS-PAGE	SDS-Polyacrylamide gel electrophoresis
shRNA	Short hairpin RNA
siRNA	Small interfering RNA
SP-1	Specificity protein 1
Src kinase	Sarcoma kinase
ssDNA	Single-stranded DNA
T	Thymine
T4	Bacteriophage T4
Taq	<i>Thermus aquaticus</i>
TBS	Tris-buffered saline
TCL1	T-cell leukemia 1
TE	Tris/EDTA buffer
TEMED	Tetramethylethylenediamine
tg	Transgenic
TGF- β	Transforming growth factor- β
Th1 and Th2	T helper cell 1 and 2
TNCB	2,4,6-trinitrochlorobenzene
TNF	Tumor necrosis factor

TPA	12-O-tetradecanoylphorbol-13-acetate
Tris	Tris-(hydroxymethyl)-aminomethane
UVB	Ultraviolet B
VP1-3	Viral capsid proteins
WT	Wild-type

1 INTRODUCTION

1.1 MACROPHAGE MIGRATION INHIBITORY FACTOR (MIF)

Macrophage migration inhibitory factor (MIF) was first described in 1966 by Barry Bloom and John David when they both, independently from each other, isolated a protein from cultures of antigen-sensitized lymphocytes that could act at a distance to inhibit the random movement or migration of phagocytes [1, 2]. It was one of the first soluble, non-immunoglobulin cytokines, which could be analyzed *in vitro*. This molecule was named macrophage migration inhibitory factor (MIF) and its activity was reported over the next 20 years to alter phagocytosis, macrophage adherence, spreading and to increase phagocyte tumoricidal potential [3-5].

In 1989, human MIF was cloned and a molecular analysis of the biological, biochemical, and biophysical properties was approached [6].

1.2 ORGANISATION OF THE *MIF* GENE LOCUS

The gene for murine MIF is located on chromosome 10 [7, 8] and the human gene maps to chromosome 22q11.2 [9]. Both genes are very small (approximately 1.7 kb in size) and show a similar intron-exon organization. The *mif* gene consists of three exons of 107, 162 and 66 bp and two introns of 188 and 94 bp. The sequence identity within *mif* RNA transcripts between mouse and human is very high (70.4%, 86.4% and 67.5% for exons 1, 2, and 3). Consensus sequences, which indicate the presence of transcription factor binding sites, have been found in the murine as well as in the human MIF promoter [8]. The promoter region contains enhancer and regulatory binding domains, which are implicated to respond to the proto-oncogene *c-fos* [10, 11]. Other domains are a SP-1 sequence, a cAMP responsive element (CREB) and an AP-1 sequence. Further upstream are a cytokine-1 (CK-1) site and a nuclear factor- κ B site (NF- κ B) (Fig. 1).

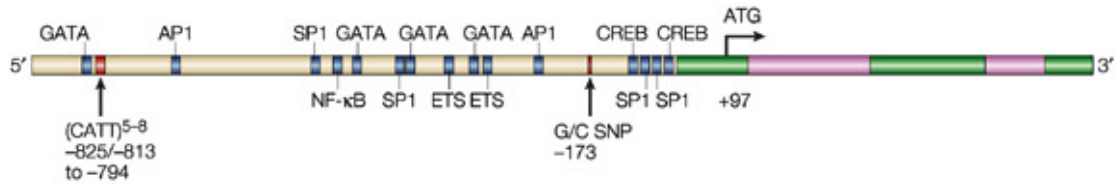


Fig. 1: Structure of the *mif* gene. It is composed of three short exons (green) and two introns (pink).

1.3 STRUCTURE OF THE MIF PROTEIN

Human and mouse *mif* cDNA were cloned from the Jurkat T cell and the the AtT-20 pituitary cell line [12] and the brain [10], and the recombinant proteins were expressed. In both species, the primary protein has a length of 115 amino acids and a molecular mass of 12.5 kDa. The initiating methionine is post-translationally removed and the mature protein starts with a proline at position 1.

Determination of the three-dimensional structure of mouse and human MIF was done by X-ray crystallography [13, 14] and by NMR spectroscopy [15] and led to the discovery of a new protein folding. All X-ray studies showed that MIF is a trimer of identical subunits with the overall dimensions of 35 x 50 x 50 Å (Fig. 2). The secondary structure of the MIF monomer consists of two antiparallel α-helices and six β-strands, four of which form a mixed β-pleated sheet that is highly similar to MHC molecules. Three monomers assemble to a α/β structure consisting of six α-helices surrounding three β-sheets that form a barrel with a solvent accessible channel. This orientation is unusual for a eukaryotic protein. Stabilization of the trimer is guaranteed by several hydrogen bonds between the β-sheets and one of the α-helices and the C-terminus. Hydrophobic bonds stabilize one of the leucine-rich hydrophobic regions.

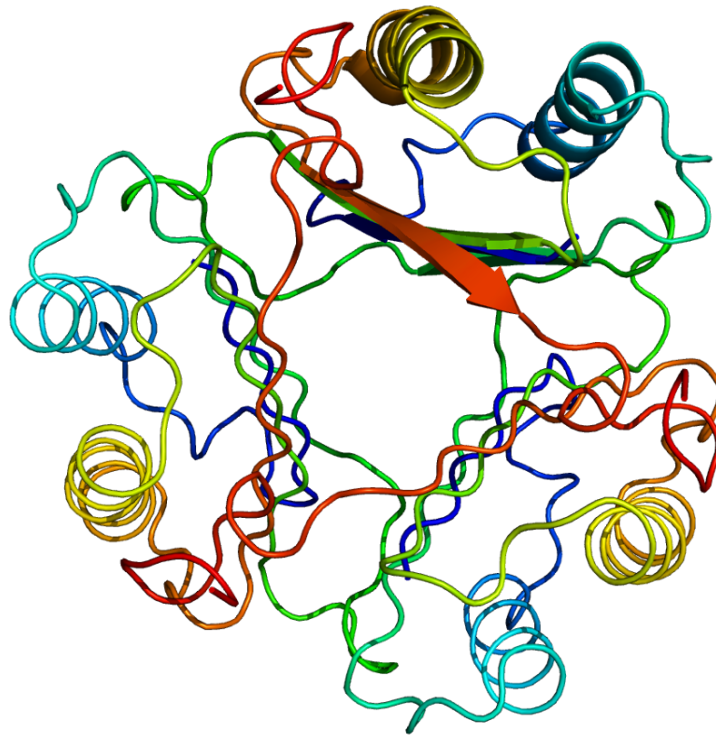


Fig. 2: The active form of MIF as a homotrimer (source: PDB Protein Data Bank).

Considering the three-dimensional structure of MIF and other enzymes, a similarity between bacterial tautomerase and human D-dopachrome tautomerase (DDT) can be found. In the genome of mice and men, the gene for DDT lies only at 80 kb distance from MIF and it is likely that the MIF/DDT locus evolved as a duplication event during evolution. DDT shares amino acid sequence homology with MIF to about 30%, whereas the crystal structure, its overall topology and trimeric formation is almost identical to MIF [16]. The protein GIF (glycosylation inhibition factor), which was investigated by Japanese scientists in the 1990s, was found to be identical to MIF with respect to its sequence and structure [17, 18]. Knowledge on the physiologic substrate of MIF and the importance of this enzymatic activity is scarce [19].

1.4 EXTRACELLULAR AND INTRACELLULAR MIF

Until today, two different ways of signal transduction have been described for MIF: an extracellular and an intracellular signaling pathway.

The first receptor found to bind extracellular MIF was CD74 [20]. CD74 is a non-polymorphic type II integral membrane protein, which was initially believed to function as an MHC class II chaperone only [21]. With the discovery of MIF as a ligand for CD74, its additional role as an accessory signaling molecule started to become clearer. In macrophages, MIF binds with high affinity to the extracellular domain of CD74, thereby activating the mitogen-activated protein kinase (MAPK) pathway and cellular proliferation [20]. CD74 is known to involve other receptors for efficient signal transduction and a second transmembrane co-receptor, the adhesion molecule CD44, appears to be required for the phosphorylation of the ERK1/2 kinases by MIF [22] (Fig. 3). The activation of both receptors is also necessary for MIF-mediated protection of the cell from apoptosis. CD44 is a cell-surface glycoprotein, a receptor for hyaluronic acid and involved in cell-cell interactions, cell adhesion, and migration. This protein participates in a wide variety of cellular functions including lymphocyte activation, recirculation and homing, hematopoiesis, and tumor metastasis. Transcripts for this gene undergo complex alternative splicing that results in many functionally distinct isoforms; however, the full-length nature of some of these variants has not been determined. Alternative splicing is the basis for the structural and functional diversity of this protein, and may be related to tumor metastasis.

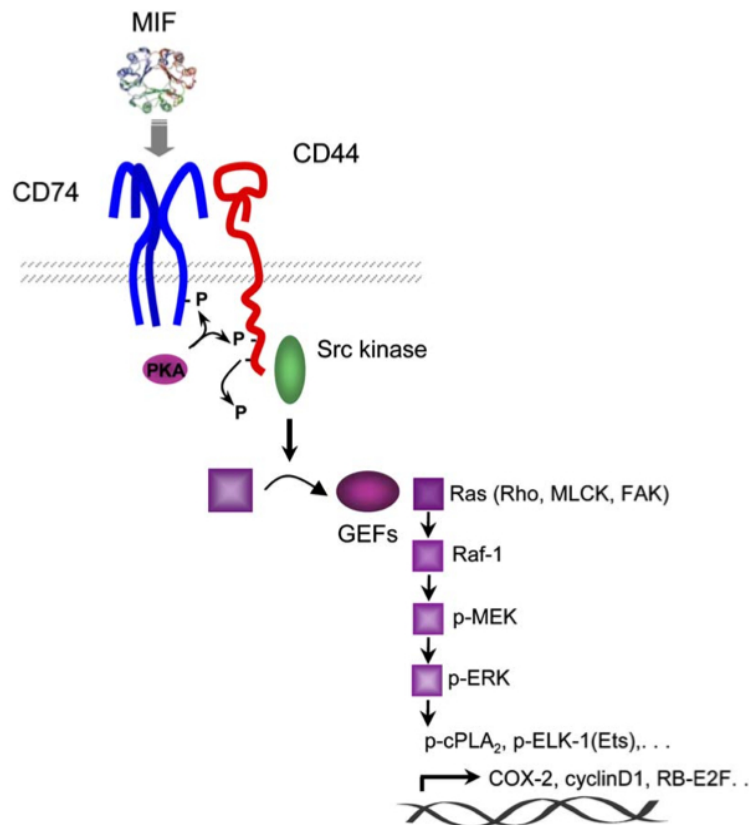


Fig. 3: Model of MIF signal transduction involving MIF binding to CD74 and activation of the CD44 co-receptor (source: Shi et al., 2006).

In B lymphocytes, MIF initiates a signaling cascade activating NF- κ B via the Src kinase Syk and Akt. This activation is mediated by translocation of the CD74-intracellular domain, which gets released by intramembraneous regulated proteolysis upon MIF stimulation [23].

MIF was also identified to be a noncognate ligand for the chemokine receptors CXCR2 and CXCR4 [24]. By interaction with those two receptors, MIF is able to promote the recruitment of monocytes as well as T cells into inflamed tissue. It is also known that CXCR2 co-localizes with CD74, which suggests that MIF may signal via a combined CD74/CD44/CXCR2 complex.

Since MIF's affinity for CXCR2 is particularly high, it was hypothesized that MIF may possess structural motives shared by canonical CXCR2 ligands, namely the conserved N-terminal Glu-Leu-Arg (ELR) motif [25]. Sequence alignment and structural modeling indeed revealed a pseudo-(E)LR motif (Asp-44-X-Arg-11) constituted by non-adjacent residues in neighboring loops but with identical

parallel spacing as in the authentic ELR motif. Structure-function analysis demonstrated that mutation of residues R11, D44, or both preserve proper folding and the intrinsic catalytic property of MIF but severely compromises its binding to CXCR2 and abrogates MIF/CXCR2-mediated functions in chemotaxis and arrest of monocytes on endothelium under flow conditions. R11A-MIF and the R11A/D44A-MIF double mutant exhibited a pronounced defect in triggering leukocyte recruitment to early atherosclerotic endothelium in carotid arteries perfused *ex vivo* and upon application in a peritonitis model. The function of D44A-MIF in peritoneal leukocyte recruitment was preserved as a result of compensatory use of CXCR4. In conjunction, the data published by Weber *et al.* in 2008 identified a pseudo-(E)LR motif as the structural determinant for MIF's activity as a non-canonical CXCR2 ligand, epitomizing the structural resemblance of chemokine-like ligands with chemokines and enabling selective targeting of pro-inflammatory MIF/CXCR2 interactions.

MIF is also abundantly expressed in the cytosol and intracellular MIF involves another pathway by direct binding and inhibitory interaction with JAB1/CSN5 (JAB = c-jun activating binding protein 1) (Fig. 4).

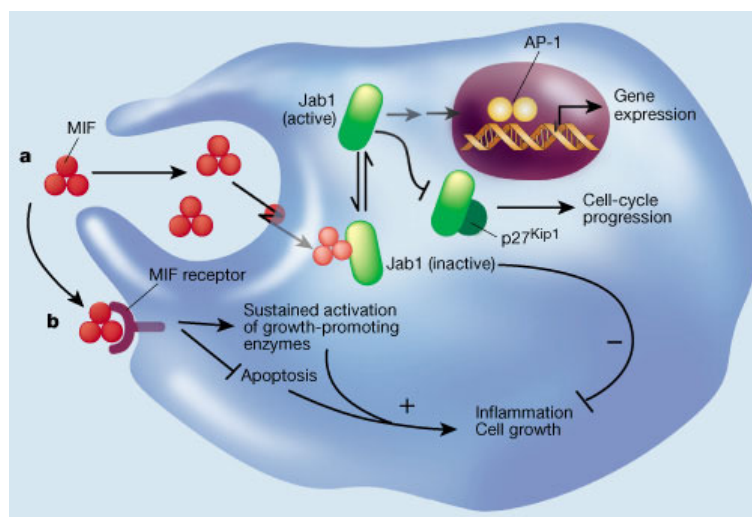


Fig. 4: Pathways by which MIF may regulate inflammation and the proliferation of target cells (source: Bucala, 2000).

a, Kleemann et al. (2000) suggest that MIF can be taken up into target cells by endocytosis. This probably occurs when MIF is present at high extracellular concentrations. Once in the cytoplasm, MIF interacts with JAB1, inhibiting it. In the absence of MIF, JAB1 activates a transcription factor, AP-1, that activates

pro-inflammatory genes; JAB1 also leads to the degradation of a cell-cycle inhibitor, p27^{Kip1}. In the presence of MIF, however, JAB1 cannot exert these effects, leading to negative effects on inflammation and cell growth.

***b,** At low concentrations, MIF may bind to a specific receptor, leading directly to intracellular signals that have a positive effect on inflammation and cell growth.*

JAB1/CSN5 functions also as subunit 5 of the COP9 signalosome (CSN), which is located in the nucleus and the cytoplasm [26-28]. The CSN consists of eight subunits, which are highly similar to the subunits of the 26S proteasome [29, 30], which is the major proteolytic system of the cell [31]. JAB1 specifically binds to p27^{Kip1}, a cyclin-dependent kinase inhibitor (CDKI), and promotes its degradation via the proteasome [32]. Inhibition of Jab1 by MIF antagonizes JAB1-dependent regulation of p27^{Kip1} and stabilizes this CDKI [26]. Data showing that MIF regulates the cell cycle also suggest that these effects are mediated via the SCF complex. MIF co-regulates the activity of the skip-cullin-F-box protein complex (SCF complex) and affects proteasomal control of intracellular protein degradation via inhibition of JAB1 [33, 34]. Another known function of JAB1/CSN5 is the co-activation of AP-1 transcription [35, 36]. Additionally known targets of JAB1/CSN5 are the tumor suppressor p53 or hypoxia-inducing factor-1 α (HIF-1 α) [27, 37].

1.5 EXPRESSION PATTERN OF MIF

MIF mRNA and protein have been detected in a wide variety of tissues and cell types. Since there is no cell line or tissue known to be negative for MIF, one can assume that MIF is a ubiquitously expressed protein. Its baseline expression in nearly all tissues can also be induced to high levels by a variety of stimuli depending on the cellular context.

Expression of MIF is already observed during early development. Kobayashi *et al.* studied the expression of MIF mRNA during embryogenesis of mice and showed that expression of MIF during organogenesis parallels tissue specification. MIF mRNA was found in somites, precartilaginous primordia in ribs

and vertebrae, branchial arches, limb buds, neural tissues, all muscle cell types and during organogenesis of liver, kidney, testis, skin, intestine, adrenal gland and pancreas [38, 39]. This broad expression pattern of MIF mRNA in embryogenesis continues during adult life.

Immunohistochemical analysis of various tissues revealed that MIF is present in a wide spectrum of tissues [40]. MIF protein is detected in cells of the immune system such as monocytes/macrophages [41], T and B lymphocytes [42] [43], NK cells [44], basophiles/mast cells [45] and eosinophils [46]. Endocrine organs such as the anterior pituitary gland [35], the adrenal cortex, the Leydig cells of the testis, the epithelial cells of the epididymis and pancreatic β -cells [47] have also been reported to be a source of MIF production [40]. Other MIF synthesizing cells are smooth and skeletal muscle cells [48], gastric parietal cells [49], keratinocytes and fibroblasts [50], hepatocytes, peripheral and central neurons [51]. Even erythrocytes have been reported to contain MIF [52] and soluble MIF protein is constitutively present in serum and plasma [53].

1.6 MIF IN THE SKIN

Shimizu *et al.* performed several analyses of MIF in human skin. Their immunohistochemical studies showed that MIF is expressed especially in the basal layer of the human epidermis [54]. They also evaluated MIF serum levels in psoriasis vulgaris and found an elevation due to the up-regulation of MIF production by peripheral blood mononuclear cells [53]. In 1999, Shimizu *et al.* could show that UVB irradiation induced an increased release of MIF by human keratinocytes [55]. In 2005, they presented data showing expression of MIF in rats during embryonic development. MIF mRNA was detectable in the developing epidermis and hair germinal cells from embryonic day (E16) on. From E19 on, moderate levels of MIF expression were seen in the epidermis and epithelial sheath cells of growing hair follicles. Expression intensity was increased in postnatal epidermis and hair follicles on day 3 [56].

1.7 MIF AND TUMORIGENESIS

In hepatocellular carcinomas, colon cancers and prostate cancers, high levels of MIF expression are correlated with unfavorable clinical prognosis [57-59]. There are several possible mechanisms for MIF's role in tumor formation and metastasis. Firstly, MIF seems to affect the two arms of the adaptive immune system, namely the Th1 and the Th2 routes. The first route activates macrophages and neutrophils by secretion of IL-2, IL-12m, IFN γ , and TNF α . The Th2 route, which acts as a counterpart to Th1 activates cytokines including IL-4, IL-5, IL-13, and IL-10. MIF also affects innate immunity by sustaining the macrophage viability via the MAPK pathway and thereby leading to a sustained inflammatory reaction [60]. MIF is also capable of inducing angiogenesis and it has been reported that MIF enhances tumor-associated neovascularization [61, 62], and there is evidence that MIF is able to modulate VEGF bioactivity [63]. In accordance with MIF's role in angiogenesis, monoclonal antibodies (mAbs) against MIF or MIF antisense mRNA, have been shown to inhibit angiogenesis in tumors [64].

Another mechanism for MIF acting as a tumor promoter could be the inhibition of p53-dependent apoptosis and growth inhibition. The functional interaction of MIF with p53 was shown in 1999 by Hudson *et al.* who demonstrated that MIF was able to inhibit the transcriptional activity of p53, e.g., the induction of p21 by p53 [65]. Analysis of a MIF knockout mouse model [66] confirmed this hypothesis by showing that the p53-dependent activity in murine embryonic fibroblasts (MEFs) was increased in MIF knockout MEFs compared to wild-type controls. It has been hypothesized that tumor-associated macrophages are able to promote the malignant potential of the tumor [8]. The ability of MIF to preserve macrophage viability via inhibition of p53 may therefore lead to tumor progression and the development of metastases. MIF also has a direct effect on T lymphocytes. Bacher *et al.* showed that mitogen- and antigen-induced activation of Th2 lymphocytes greatly depend upon autocrine MIF secretion [42]. As mentioned before, Th2 lymphocytes suppress the immune system, thereby further enabling tumor growth and development [50], provided evidence for a role of MIF in the suppression of Th1 lymphocytes. They observed that MIF inhibited the action of cytotoxic T lymphocytes. Since they are essential in

antitumor activity via cytolysis of tumor cells, increased MIF levels in tumor cells may lead to immune escape of the tumor. Hence, the immunological effects of MIF may play an important role in the development of tumors.

In 2004, Ichiyama *et al.* demonstrated that mono- and multinuclear cells infiltrate inflamed tissue [67]. They could also show that these cells stained positive for MIF. In vitro experiments revealed active secretion of MIF by macrophages in response to phagocytosis of particles. These results can be adapted to tumor-infiltrating macrophages. Given the effects of MIF on immune surveillance and its growth stimulatory effects, MIF might not only prolong the survival of macrophages, but also that of transformed cells.

1.8 MIF IN EPITHELIAL TUMORS

In a study by Meyer-Siegler *et al.*, MIF increased cell viability and tumor invasiveness [68]. Using prostate cancer cell lines they demonstrated, that androgen-independent but not androgen-dependent cell lines required MIF-activated signal transduction pathways for both growth and invasion and that the MIF cell surface receptor CD74 was only detectable in androgen-independent tumor cells. Inhibition of CD74 or MIF resulted in decreased MIF secretion, cellular proliferation, and tumor invasion.

Rendon *et al.* obtained further evidence for a role of MIF in epithelial tumorigenesis using a siRNA mediated MIF knockdown technology in a human lung adenoma cell line: Decreased expression of MIF resulted in a reduction in both cell invasiveness and cell migration, in parallel with a reduction of Rac1 [69]. Consistent with these findings, opposite effects were observed when MIF was over-expressed. Taken together, these data underline the importance of MIF in metastasis and invasiveness and thus, tumor progression.

Repp *et al.* showed that MIF inhibits NK cell-mediated lysis of melanoma cells [70]. In 2007, Culp *et al.* presented data demonstrating that interference with MIF expression in a mouse melanoma cell line inhibited the tumor establishment via up-regulating antiangiogenic thrombospondin-1 [71]. Interference with MIF expression led to a delayed tumor formation marked by the absence of intratumoral vasculature in MIF RNAi-treated xenograft tumors.

The induction of non-melanoma skin cancers (NMSC) by UVB irradiation in BALB/c mice, published by Martin *et al.* in 2009, revealed that MIF-deficient mice have a significantly diminished acute inflammatory response to UVB exposure, as measured by dermal neutrophil infiltration and edematous response [72]. These knockout mice also show significantly lower VEGF concentrations in whole skin. Furthermore, there was a significant increase in p53 activity and epidermal cell proliferation following an acute UVB insult. In response to chronic UVB exposure, MIF-deficient mice showed a reduction in tumor incidence, significantly less angiogenesis, and delayed tumor progression.

These findings provide evidence that MIF may influence immune reactions related to skin tumor growth, but other data about a direct involvement of MIF in epidermal tumors is not available.

The preliminary work that led to this thesis was based on experiments with MIF knockout mice. In 2003, Fingerle-Rowson *et al.* showed that subcutaneous injections of a carcinogenic aromatic carbohydrate called benzo[a]pyrene (B[a]P) induced smaller fibrosarcomas in MIF-deficient C57Bl/6 mice than in wild-type controls. This finding was initially explained with the inhibitory activity of MIF in p53 activity [66]. Nevertheless, in contrast to these findings, topical application of the carcinogen B(a)P led to significantly increased formation of skin tumors in MIF knockout compared to wild-type controls [33]. A repetition of this experiment with the same outcome was published two years later [73]. Controversial or even opposite functions of cytokines in dependence of the tissue context are not rare in scientific literature. The most prominent example may be the transforming growth factor- β (TGF- β): The disruption of the TGF- β signaling pathway in the epidermis results in a distortion of the hair follicle cycle and augmented formation of squamous cell carcinomas (SCCs) [74]. In contrast, in mesenchymal cells or in breast cancer, TGF- β acts as a tumor-promoter inducing EMT [75].

1.9 MIF AND UVB RADIATION

In addition to the aspects of MIF in combination with UVB, there is an experiment that was published in 2009, in which MIF-transgenic (MIF tg) and wild-type mice were exposed to chronic UVB irradiation showed that MIF tg mice developed skin tumors earlier and in higher numbers compared to their WT controls. The first tumor appeared in week 14. After acute UVB exposure, fewer sunburned cells in the epidermis of the MIF tg mice were found than the WT mice. The epidermis derived from the MIF tg mice exhibited substantially decreased levels of p53, Bax and p21 after UVB exposure in comparison with the WT mice. Collectively, these findings suggest that chronic UVB exposure enhances MIF production, which may inhibit the p53-dependent apoptotic processes and thereby induce photocarcinogenesis in the skin [76].

1.10 AIMS OF THE STUDY

Starting with the observation that MIF acts as tumor promoter in most tissues, but as tumor suppressor in the epidermis, the first aim of this study was to further ascertain the postulated tumor suppressor function of MIF in four mouse models of non-melanoma skin tumorigenesis. The second aim investigated which biological properties of MIF may inhibit tumor formation in the epidermis.

1.11 EXPERIMENTAL SET-UP

To address the question whether and by which mechanism MIF affects the development of epidermal non-melanoma skin cancer, we designed different approaches to test its role in the induction of epidermal skin tumors.

First, the chemical one stage carcinogenesis protocol with B(a)P was repeated, as performed by Fingerle-Rowson *et al.* in 2007, with weekly topical administration of B(a)P onto shaved dorsal skins of MIF-deficient and wild type control mice. Knowledge of the metabolism and action of B(a)P is restricted to that it becomes epoxidized at mitochondrial level and that this epoxide metabolite

is able to bind to the base guanine of the DNA resulting in an overall distortion of the original DNA structure. Obviously, B(a)P may affect a large number of genes and its effects are not restricted to *ras* only.

Second, the classical two-stage protocol, which includes a single application of the chemical carcinogen 7,12-dimethylbenz[*a*]anthracene (DMBA) followed by repeated treatment with the mitogenic phorbol ester 12-O-tetradecanoylphorbol-13-acetate (TPA) as tumor promoter, was applied. The advantage of this experimental design is given by the well-defined mechanism for the oncogenic action of DMBA/TPA. DMBA introduces a mutation into codon 61 of the *ras* gene and TPA is required for the clonal expansion of the mutated clone.

Third, MIF-deficient mice and wild type controls were exposed to UVB radiation according to a protocol provided to us by Dr. Stefan Beissert from the University Hospital at Munster, Germany [77]. UVB radiation is epidermis-specific, as it cannot penetrate the dermis. Thus, the epidermis functions as a UVB radiation filter (Fig. 5).

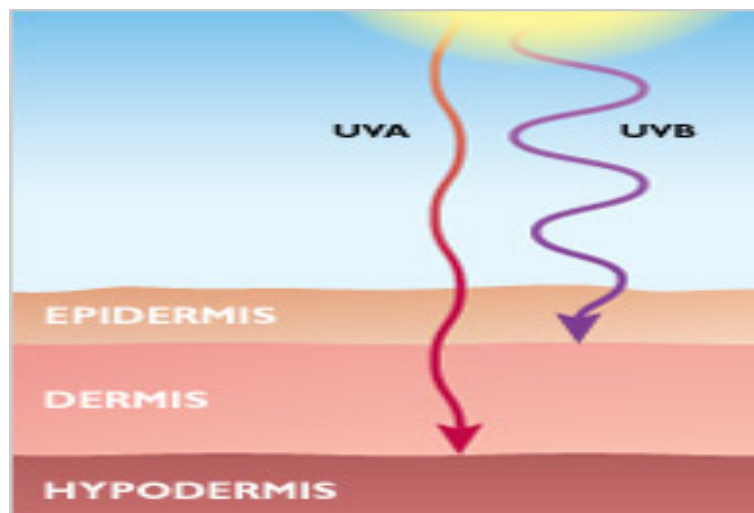


Fig. 5: Comparison of penetration depths of UV-A and UV-B radiation on incidence onto the skin surface (source: LA ROCHE-POSAY).

Fourth, we crossbred MIF-deficient mice with mice, transgenic for the early genes *E2*, *E6* and *E7* of the human papilloma virus isotype 8 under control of the human keratin-14 promoter (K14HPV8-CER mice), and performed a lifetime

observation of those K14HPV8-CER transgenic and MIF-deficient or MIF wild-type mice for the development of skin tumors. The project was done in collaboration with Dr. Paolo Marcuzzi and Prof. Dr. Herbert Pfister from the Institute of Virology at University Hospital Cologne.

A role of human papillomavirus (HPV) infection in skin cancer development is well established in patients with the rare, inherited disorder of epidermodysplasia verruciformis (EV) [78, 79]. EV is characterized by the life-long occurrence of multiple flat warts and macular lesions, which are induced by a group of at least 20 HPV types, so-called EV-HPV [80]. There is a high risk of developing SCC later in life. In contrast to the plurality of EV-associated HPVs in benign tumors, only a few virus types, predominantly HPV5 or HPV8, are found in the cancers and are regarded as a high risk. Sensitive detection techniques frequently identified EV-HPVs also in healthy skin and NMSC of the general population. They are particularly prevalent in immunosuppressed organ transplant recipients [81-83]. The meaning of these findings for skin carcinogenesis is still uncertain because no single high-risk HPV types predominate in NMSC of non-EV patients and low viral loads suggest that only a minority of tumor cells contain HPV DNA [84]. However, the presence of antibodies against HPV8 capsids has recently been shown to be associated with cutaneous SCC [85, 86] and with the development of large numbers of precancerous actinic keratoses [87], which may suggest that this EV-type also plays a role in NMSC in the general population.

Extensive studies have linked the efficiency of mucosal HPV types (e.g., HPV16) in promoting cancer development to activities of their major oncoproteins E6 and E7, which interfere with the regulation of both the cell cycle and apoptosis. Comparatively, little is known about cutaneous HPV and much of the data suggests that the oncogenes of HPV from skin and mucosa have only a few shared properties. Thus, in contrast to HPV16, the E6 proteins of the EV-associated HPV5 and HPV8 do not interfere with p53 [88-90]; however, they can still induce morphologic transformation and anchorage-independent growth in rodent cells [89, 91]. A contribution to NMSC development may be expected from the inhibition of apoptosis by E6 proteins of, for example, HPV5 [92]. If cells with DNA damage caused by transient

exposure to the UV component of sunlight cannot be eliminated by apoptosis, somatic mutations may accumulate and eventually lead to cancer. The E7 proteins of HPV5 and HPV8 have a much weaker interaction with the tumor suppressor pRB than that of HPV16, and only transform rodent cells in collaboration with an activated H-ras gene [93]. Expression of the HPV8 E2 protein led to anchorage-independent growth of rodent fibroblast and the human skin keratinocyte line HaCaT [94]. Given these *in vitro* differences between the cutaneous and mucosal HPV types, one might expect a lower carcinogenic activity of cutaneous viruses.

To study the effects of the early genes of HPV8 *in vivo*, a transgenic mouse model was established at the Institute of Virology, University Hospital Cologne, Germany, with the complete early region of HPV8 (K14HPV8-CER). To direct the expression to the basal layer of squamous epithelia the genes were put under the control of the human keratin-14 promoter (Fig. 6).

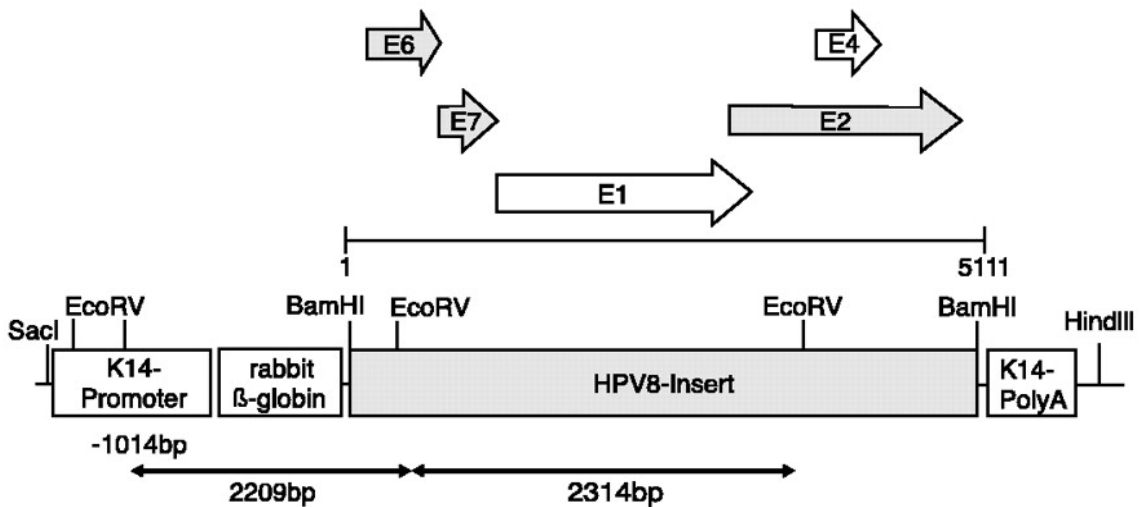


Fig. 6: Schematic overview of the open reading frames of the early genes of HPV8 (taken from Schaper et al., Cancer Research 2005).

Transgenic mice were backcrossed for up to six generations into both FVB/N and Bl6 mouse strains. HPV8 transgene-positive littermates developed lesions in the skin (single or multifocal benign tumors, characterized by papillomatosis, acanthosis, hyperkeratosis, and varying degrees of epidermal dysplasia).

Squamous cell carcinomas developed in transgenic FVB/N mice as well. Real-time reverse transcription-PCR showed highest expression levels for HPV8-E2, followed by E7 and E6. There was no consistent difference in relative viral RNA levels between healthy or dysplastic skin and malignant skin tumors. Whereas UV-induced mutations in the tumor suppressor gene *p53* are frequently detected in human skin carcinomas, mutations in *p53* were not observed either in the benign or malignant mouse tumors. Non-melanoma skin cancer developed in HPV8-transgenic mice without any treatment with physical or chemical carcinogens. This was the first experimental proof of the carcinogenic power of an epidermodysplasia verruciformis-associated HPV-type *in vivo*, which points to an impressive oncogenic potential of the EV-associated HPV8.

In the case of a difference between MIF-deficient mice and wild-type controls in induced skin tumorigenesis, a rescue experiment with intra-epidermal injections of recombinant murine MIF into MIF-deficient mice will be performed to find out whether it is possible to reverse the observed phenotype.

A successful cultivation of primary murine keratinocyte cell lines would result in the attempt to establish AAV2-mediated malign transformations with dominant negative *tp53* ($\Delta Ntp53$) or *H-ras* to be able to perform *in vitro* studies and to facilitate the study of single cell behaviour upon tumorigenesis in keratinocytes. AAVs belong to the genus Dependovirus, which in turn are members of the family Parvoviridae. They are small (20 nm), replication-defective, non-enveloped viruses that infect humans and some other primate species.

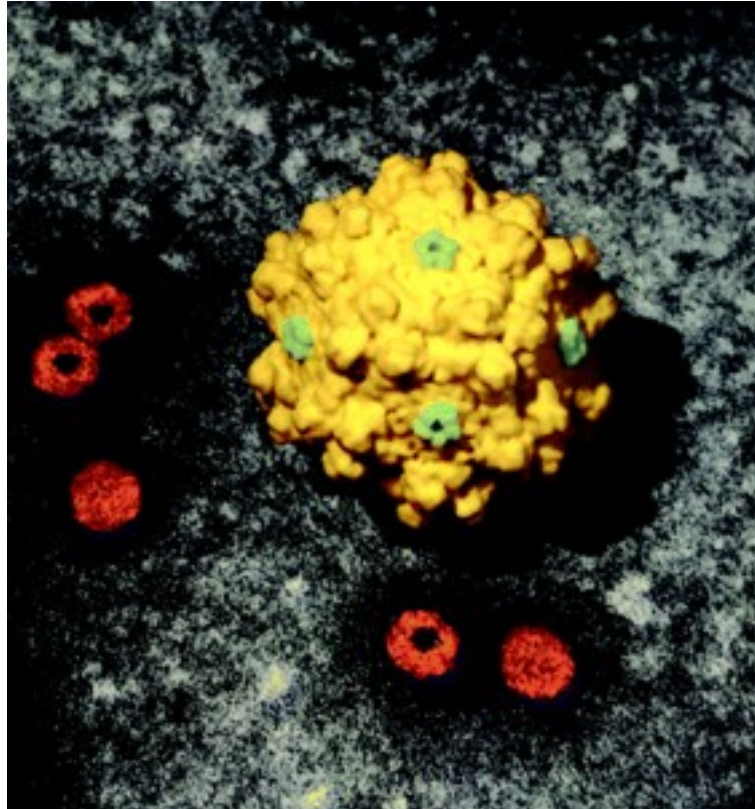


Fig. 7: The adeno-associated virus 2 (AAV2) in yellow with its HSPG receptors in green and electron microscope pictures in red.

AAVs evoke very mild immune responses and are not known to cause diseases. AAV can infect both dividing and non-dividing cells and may incorporate its genome into that of its host cell. These features make AAV a very attractive candidate for creating viral vectors for gene therapy. Wild-type AAV has attracted considerable interest from gene therapy researchers due to a number of features. Chief amongst these is the viruses' apparent lack of pathogenicity. It can also infect non-dividing cells and has the ability to stably integrate into the host cell genome at a specific site (designated AAVS1) in the human chromosome 19. The AAV genome integrates most frequently into the site mentioned, while random incorporations into the genome take place with a negligible frequency. Development of AAV's as gene therapy vectors, however, has eliminated this integrative capacity by removal of the *rep* and *cap* from the DNA of the vector. The desired gene together with a promoter to drive

transcription of the gene is inserted between the inverted terminal repeats (ITR) that aid in concatamer formation in the nucleus after the single-stranded vector DNA is converted by host cell DNA polymerase complexes into double-stranded DNA. AAV-based gene therapy vectors form episomal concatamers in the host cell nucleus. In non-dividing cells, these concatamers remain intact for the life of the host cell. In dividing cells, AAV DNA is lost through cell division, since the episomal DNA is not replicated along with the host cell DNA. Random integration of AAV DNA into the host genome is low but detectable. AAV's also present very low immunogenicity, seemingly restricted to generation of neutralizing antibodies, while they induce no clearly defined cytotoxic response. This feature, along with the ability to infect quiescent cells, presents their dominance over adenoviruses as vectors for the human gene therapy. Use of the virus does present some disadvantages. The cloning capacity of the vector is relatively limited and most therapeutic genes require the complete replacement of the virus's 4.8 kb genome. Large genes are, therefore, not suitable for use in a standard AAV vector. Options are currently being explored to overcome the limited coding capacity. The AAV ITRs of two genomes can anneal to form head to tail concatamers, almost doubling the capacity of the vector. Insertion of splice sites allows for the removal of the ITRs from the transcript. The humoral immunity instigated by infection with the wild type is thought to be a very common event. The associated neutralizing activity limits the usefulness of the most commonly used serotype AAV2 in certain applications. Accordingly the majority of clinical trials currently underway involve delivery of AAV2 into the brain, a relatively immunologically privileged organ. In the brain, AAV2 is strongly neuron-specific.

The AAV genome is built of single-stranded deoxyribonucleic acid (ssDNA), either positive- or negative-sensed, which is about 4.7 kb long. The genome comprises inverted terminal repeats (ITRs) at both ends of the DNA strand, and two open reading frames (ORFs): *rep* and *cap*. The former is composed of four overlapping genes encoding Rep proteins required for the AAV life cycle, and the latter contains overlapping nucleotide sequences of capsid proteins: VP1, VP2 and VP3, which interact together to form a capsid of an icosahedral symmetry (Fig. 8).

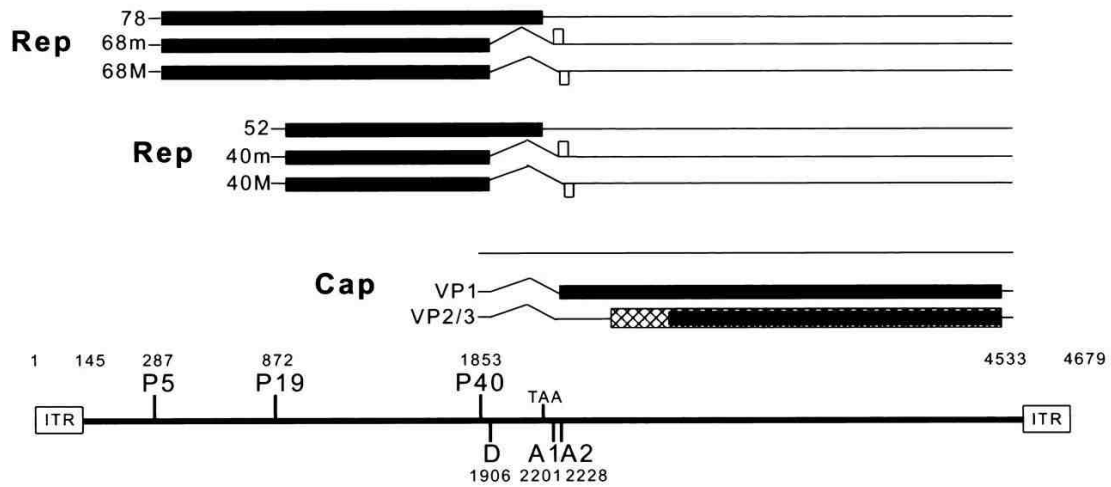


Fig. 8: Schematic gene map of the AAV2 genome. Source: www.hixonparvo.info.

The Inverted Terminal Repeat (ITR) sequences comprise 145 bases each. They were named so because of their symmetry, which was shown to be required for efficient multiplication of the AAV genome. Another property of these sequences is their ability to form a hairpin, which contributes to so-called self-priming that allows primase-independent synthesis of the second DNA strand. The ITRs were also shown to be required for both integration of the AAV DNA into the host cell genome (19th chromosome in humans) and rescue from it, as well as for efficient encapsidation of the AAV DNA combined with generation of a fully assembled, deoxyribonuclease-resistant AAV particles (Fig. 9).

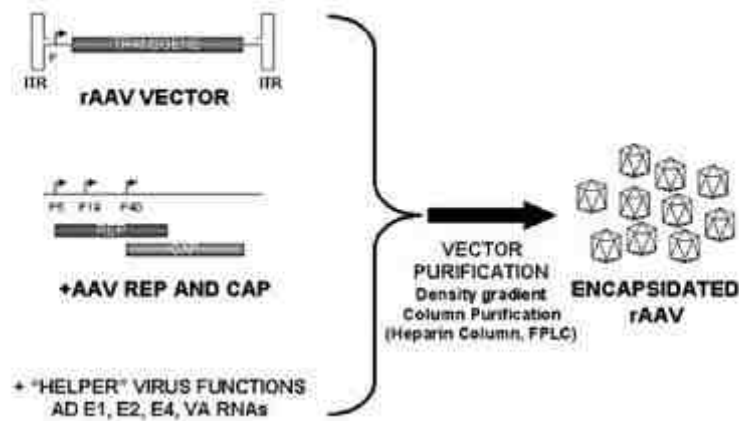


Fig. 9: AAV2 purification scheme. Source: www.vectorbiolabs.com.

With regard to gene therapy, ITRs seem to be the only sequences required *in cis* next to the therapeutic gene: structural (*cap*) and packaging (*rep*) genes can be delivered *in trans*. With this assumption many methods were established for efficient production of recombinant AAV (rAAV) vectors containing a reporter or therapeutic gene. However, it was also published that the ITRs are not the only elements required *in cis* for the effective replication and encapsulation. A few research groups have identified a sequence designated *cis-acting Rep-dependent element* (CARE) inside the coding sequence of the *rep* gene. CARE was shown to augment the replication and encapsulation when present *in cis*.

On the "left side" of the genome there are two promoters called p5 and p19, from which two overlapping messenger ribonucleic acids (mRNAs) of different length can be produced. Each of these contains an intron, which can be either spliced out or not. Given these possibilities, four various mRNAs, and consequently four various Rep proteins with overlapping sequence can be synthesized. Their names depict their sizes in kilo Daltons (kDa): Rep78, Rep68, Rep52 and Rep40. Rep78 and 68 can specifically bind the hairpin formed by the ITR in the self-priming act and cleave at a specific region, designated terminal resolution site, within the hairpin. They were also shown to be necessary for the AAVS1-specific integration of the AAV genome. All four Rep proteins were shown to bind ATP and to possess helicase activity. It was also shown that they up-regulate the transcription from the p40 promoter

(mentioned below), but down-regulate both p5 and p19 promoters.

The right side of a positive-sensed AAV genome encodes overlapping sequences of three capsid proteins, VP1, VP2 and VP3, which start from one promoter, designated p40. The molecular weights of these proteins are 87, 72 and 62 kilo Daltons, respectively. All three of them are translated from one mRNA. After this mRNA is synthesized, it can be spliced in two different manners: either a longer or shorter intron can be excised resulting in the formation of two pools of mRNAs: a 2.3 kb- and a 2.6 kb-long mRNA pool. Usually, especially in the presence of adenovirus, the longer intron is preferred, so the 2.3-kb-long mRNA represents the so-called "major splice". In this form the first AUG codon from which the synthesis of VP1 protein starts, is cut out, resulting in a reduced overall level of VP1 protein synthesis. The first AUG codon that remains in the major splice is the initiation codon for VP3 protein. However, upstream of that codon in the same open reading frame lies an ACG sequence (encoding threonine), which is surrounded by an optimal Kozak context. This contributes to a low level of synthesis of VP2 protein, which is actually VP3 protein with additional N-terminal residues, as is VP1.

Since the bigger intron is preferred to be spliced out, and since in the major splice the ACG codon is a much weaker translation initiation signal, the ratio at which the AAV structural proteins are synthesized *in vivo* is about 1:1:20, which is the same as in the mature virus particle. The unique fragment at the N terminus of VP1 protein was shown to possess the phospholipase A2 (PLA2) activity, which is probably required for the releasing of AAV particles from late endosomes. Muralidhar *et al.* reported that VP2 and VP3 are crucial for correct virion assembly [95]. More recently, however, Warrington *et al.* showed VP2 to be unnecessary for the complete virus particle formation and an efficient infectivity, and also presented that VP2 can tolerate large insertions in its N terminus, while VP1 cannot, probably because of the PLA2 domain presence [96].

As of 2006 there have been 11 AAV serotypes described. All of the known serotypes can infect cells from multiple diverse tissue types. Tissue specificity is determined by the capsid serotype and pseudotyping of AAV vectors to alter their tropism range will likely be important to their use in therapy. Serotype 2

(AAV2) has been the most extensively examined so far. AAV2 presents natural tropism towards skeletal muscle, neurons, vascular smooth muscle cells and hepatocytes.

Three cell receptors have been described for AAV2: heparan sulfate proteoglycan (HSPG), $\alpha_v\beta_5$ integrin and fibroblast growth factor receptor 1 (FGFR-1). The first functions as a primary receptor, while the latter two have a co-receptor activity and enable AAV to enter the cell by receptor-mediated endocytosis. HSPG functions as the primary receptor, though its abundance in the extracellular matrix can scavenge AAV particles and impair the infection efficiency.

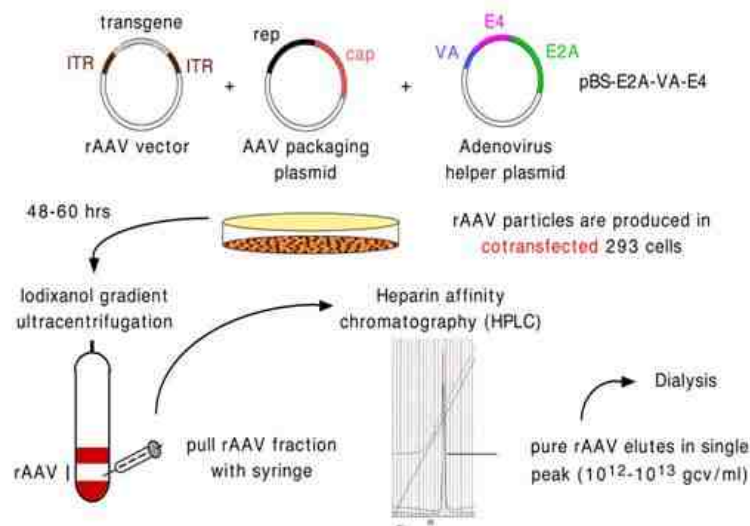


Fig. 10: Schematic overview of the production of rAAV2 particles. Source: Hansrudi Bueler.

2 MATERIAL & METHODS

2.1 INSTRUMENTS

Automatic pipettes	Gilson, Middleton, WI, USA
Balance	Ohaus, Pine Brook, NJ, USA
Cell counting chambers	Neubauer, Germany
Cell freezing containers	Nalgene, Neerijse, Belgium
Centrifuge (benchtop and cooled device)	Eppendorf, Hamburg, Germany
Centrifuge (cell culture)	Eppendorf, Hamburg, Germany
Electrophoresis system DNA	BioRad, Hercules, CA, USA
Electrophoresis system protein	Invitrogen, Karlsruhe, Germany
Film-developer	AGFA, Cologne, Germany
Films	Amersham Bioscience, Buckinghamshire, UK
Fridge and freezer	
4°C & -20°C	AEG, Stockholm, Sweden
-80°C	Sanyo, Wood Dale, IL, USA
Heater/magnetic shaker	Heidolph, Schwabach, Germany
Incubator (mammalian cell culture)	Labotect, Göttingen, Germany
Incubator (murine cell culture)	Heraeus, Hanau, Germany
Laminar flow hood	Heraeus, Hanau, Germany
Microscopes	Axiophot, Zeiss, Göttingen, Germany Leica DM4000B, Leica Camera AG, Solms, Germany
N ₂ storage tank	Thermo Scientific, Dubuque, IA, USA
PCR machine (Mastercycler Gradient EP S)	Eppendorf, Hamburg, Germany
pH meter	Mettler-Toledo, Schwerzenbach, Germany

Shaker	Heidolph, Schwabach, Germany
Spectrophotometer	BioRad, Hercules, CA, USA
Thermomixer	Eppendorf, Hamburg, Germany
Vortex	VWR, Darmstadt, Germany
Waterbath	Medingen, Freital, Germany
X-ray film exposure cassette	AGFA, Cologne, Germany

2.2 CHEMICALS

2-Mercaptoethanol	Sigma, Steinheim, Germany
5'-Bromo-deoxy-uracil (BrdU)	Sigma, Steinheim, Germany
Acetic acid	Carl Roth GmbH & Co, Karlsruhe, Germany
Acrylamid 30%	Carl Roth GmbH & Co, Karlsruhe, Germany
Agarose	Biozym, Hess. Oldendorf, Germany
Ammonium peroxdisulfate (APS)	Carl Roth GmbH & Co, Karlsruhe, Germany
Bromophenol blue	Carl Roth GmbH & Co, Karlsruhe, Germany
Bovine serum albumin	Applichem, Darmstadt, Germany
Calcium chloride	Merck, Darmstadt, Germany
DMEM	Gibco/Invitrogen, Karlsruhe, Germany
DMSO	Sigma, Steinheim, Germany
ECL	Amersham Biosciences, Buckinghamshire, UK
Ethanol	Carl Roth GmbH & Co, Karlsruhe, Germany
Ethidium bromide	Carl Roth GmbH & Co, Karlsruhe, Germany

Ethylendiamine tetra acetic acid (EDTA)	Carl Roth GmbH & Co, Karlsruhe, Germany
Fetal Bovine Serum (FBS)	Gibco/Invitrogen, Karlsruhe, Germany
Glycerol	Carl Roth GmbH & Co, Karlsruhe, Germany
Glycine	Carl Roth GmbH & Co, Karlsruhe, Germany
HEPES	Carl Roth GmbH & Co, Karlsruhe, Germany
Hydrochloric acid	Carl Roth GmbH & Co, Karlsruhe, Germany
Isopropanol	Carl Roth GmbH & Co, Karlsruhe, Germany
Magnesium chloride	Carl Roth GmbH & Co, Karlsruhe, Germany
Methanol	Carl Roth GmbH & Co, Karlsruhe, Germany
Molecular weight marker	MBI-Fermentas, St. Leon-Rot, Germany
Non fat dry milk powder	Carl Roth GmbH & Co, Karlsruhe, Germany
Nonidet P-40 (NP-40)	Sigma, Deisenhofen, Germany
Paraformaldehyde	Sigma, Deisenhofen, Germany
PBS	Gibco/Invitrogen, Karlsruhe, Germany
PCR primers	Metabion, Martinsried, Germany
Penicillin/streptomycin	Gibco/Invitrogen, Karlsruhe, Germany
Ponceau S	Carl Roth GmbH & Co, Karlsruhe, Germany
Potassium chloride	Merck, Darmstadt, Germany
Prestained protein marker	MBI-Fermentas, St. Leon-Rot, Germany
Sodium chloride	Carl Roth GmbH & Co, Karlsruhe, Germany
Sodium dodecylsulfate lauryl (SDS)	Serva Electrophoresis GmbH, Heidelberg, Germany

Sodium pyruvate	Gibco/Invitrogen, Karlsruhe, Germany
TEMED	Carl Roth GmbH & Co, Karlsruhe, Germany
Tris-(hydroxymethyl)-aminomethane	Carl Roth GmbH & Co, Karlsruhe, Germany
Triton X-100	Sigma, Deisenhofen, Germany
Trypan blue	Gibco/Invitrogen, Karlsruhe, Germany
Trypsin/EDTA	Gibco/Invitrogen, Karlsruhe, Germany

2.3 SPECIAL REAGENTS/KITS

Reagents/Kits	Supplier
ECL Detection Reagents	Amersham Bioscience, Buckinghamshire, UK
Mouse on Mouse Kit	Thermo Fisher Scientific GmbH, Schwerte, Germany
Protease Inhibitor Cocktail	Roche, Mannheim, Germany
NE-PER Nuclear and Cytoplasmic Extraction Reagents	Pierce Biotechnology, Rockford, IL, USA

2.4 SOFTWARE

Endnote

ImageJ

KC4

Microsoft Office

PhotoshopCS

Statistica

2.5 ETHICS STATEMENT

Animal maintenance and experimental procedures were approved by the ethics committee of Cologne University and were in accordance with the FELASA and GV-SOLAS Guidelines for Animal Care and Use.

2.6 ANIMALS

MIF KO mice generated by Cre-mediated deletion of the entire *mif* locus in the pure C57Bl/6 background (Fingerle-Rowson et al., PNAS 2003) were available in our laboratory, as well as *mif^{f/f}*, also generated by Fingerle-Rowson. The same MIF KO strain mice was outbred to the 129S1/SvImJ background for 6 generations and kindly provided to us by O. Petrenko, SUNY, USA. All animals were maintained in a homozygous state under virus-free conditions in a conventional animal facility.

mif^{P1G/P1G} mice on the C57Bl/6 background were created at the Institute for Genetics at the University of Cologne, Germany, by Fingerle-Rowson.

Prof. Pfister, University Hospital Cologne, Germany, kindly provided K14HPV8-CER mice on a mixed FVB/N and C57Bl/6 background. The transgene in these animals was kept as heterozygous allele.

Male *K14-cre^{+tg}* (Tg(KRT14-cre)1Amc/J, donated by Andrew McMahon, Harvard, through Prof. Carien Niessen and MD Dr. Axel Roers, Cologne) mice were cross-bred with female floxed *mif* mice (*mif^{f/f}*), both on the C57Bl/6 background. The *cre* transgene was kept in a heterozygous status in order to avoid any phenotype artifacts.

2.7 ANIMAL WELFARE

The animals were kept at a controlled atmosphere of 23°C. Semi-annual health checks showed that the mice were virus-free and only carried *Helicobacter species* as well as *Pasteurella pneumonia* without clinical signs of disease. The animals were allowed to feed and drink *ad libitum* and received a breeding diet (mouse chow) by Altromin. They were kept in type II cages at groups of four to five mice.

Breeding was done on a one to one basis and pups were weaned after 21 days.

2.8 REASONS FOR THE CHOICE OF MOUSE STRAINS FOR THE EXPERIMENTS

We used mice of the 129S1/SvImJ strain for the chemical carcinogenesis protocols, because they are more tumor-sensitive than C57Bl/6 mice. We used both strains just mentioned for the UV-B irradiation, since we did not know whether they would react differently from 129S1/SvImJ mice, and because we wanted to gain data about MIF^{P1G/P1G} mice. We had to use C57Bl/6 for the epidermis-specific knockout of *mif*, because K14-Cre-transgenic mice were only available on this background. The mice, transgenic for the *K14HPV8-CER* construct, were on a mixed FVB/N and 129S1/SvImJ background. In this lifetime observation experiment, all generations of transgenic MIF WT and MIF KO animals had equal proportions of both backgrounds.

2.9 BREEDING STRATEGIES

Breeding of most mouse strains took place in the animal facilities of the Department for Surgery, which is run by the Clinic I for Internal Medicine at the University Hospital of Cologne.

The experiment of K14HPV8-CER-induced skin tumorigenesis was performed in the vivarium of the Institute for Virology of the University Hospital of Cologne. The mice, transgenic for *K14HPV8-CER* on the FVB/N background were crossed with *mif*^{-/-} mice on the 129S1/SvImJ background. *mif*^{-/-} mice were mated with *K14HPV8-CER*-transgenic and littermates of the first generation were genotyped, and mated in a way that the second generation bred homozygous animals for the *mif* wild-type and the *mif* knockout allele, and which were heterozygous for the transgene as well. Thus, we obtained animals with equal portions of the two backgrounds, FVB/N and 129S1/SvImJ.

To get all other experimental animals with MIF WT or MIF KO genotypes, the following breedings were started and renewed upon request. MIF-deficient mice already existed and were mostly crossed with litters of other breeding pairs, although all mouse strains were inbred ones. Breedings were kept on homozygous genetic background and in detached racks to avoid any contamination or confusion about the genotypes. Wild-type controls on 129S1/SvImJ background were also kept in our facilities; C57Bl/6 wild-types were purchased when needed. Besides the MIF-deficient mice on the 129S1/SvImJ background, we also had MIF^{-/-} and MIF^{P1G/P1G} on the C57Bl/6 background, because we wanted to include a group of MIF^{P1G/P1G} mice as well as MIF WT and MIF KO on this background into the UV-B irradiation experiment, since we did not know whether they would react differently from 129S1/SvImJ mice and because we wanted to gain data about these mutated MIF mice, too. MIF^{floxed/floxed} mice on the C57Bl/6 background were needed for the epidermis-specific knockout of MIF, as *K14-Cre*-transgenic mice, with which they were crossed, were only available on this background. The first generation litters of this crossing were genotyped for *Cre* transgene positivity, were tested for their *mif* status, and *Cre*^{tg} mice, which were automatically *mif*^{+/fl}, were then

again mated with *mif^{fl/fl}* animals to obtain *K14-Cre^{+tg} mif^{fl/fl/Δepi}* or *K14-Cre^{+tg} mif^{+fl/Δepi}* in second generation. The results of genotyping these mice either displayed two bands in the first or three bands in the latter case where a band wild-type, a floxed and a knockout allele are present due to the excision of the floxed *mif* gene between the two loxP sites which can only happen in the epidermis, since Cre is under control of the human keratin-14 (K14) promoter.

2.10 GENOTYPING

Genotyping of the animals was necessary to separate the correct experimental animals from the controls, and done by polymerase chain reaction (PCR). At the time of weaning, a piece of the tail or ear was clipped, genomic DNA prepared, and the region of interest amplified by PCR with gene-specific primers.

2.11 GENOMIC DNA PREPARATION

A small piece of the clipped tail is put into a tube and lysed for at least 4 hrs in 150 µl of lysis buffer plus 1.5 µl of proteinase K (1 mg/ml) in a thermomixer at 56°C and 800 rpm.

Then, the digested tail is spinned down at 13,000 rpm for 5'. The supernatant is put into a new cup with 150 µl isopropanol, mixed, and again spinned for 5' at 13,000 rpm. Discard supernatant and wash pellet twice with 150 µl 70% ethanol. Discard ethanol and dry pellet for 1 hr at room temperature. When the pellet is dry (no more smell of ethanol), resuspend pellet in 50 µl TE buffer. Genomic DNA was stored at 4 °C o/n to resuspend DNA pellet.

Genomic DNA Lysis Buffer

100 mM Tris, pH 8.5

5 mM EDTA

0.2 % SDS

200 mM NaCl

adjust to volume of 1 l with ddH₂O

1x TE Buffer

50 mM Tris

150 mM NaCl

adjust to pH 7.5

adjust to volume of 1 l with ddH₂O

2.12 POLYMERASE CHAIN REACTION (PCR)

Amplification of DNA fragments is done by polymerase chain reaction (PCR). A piece of DNA is amplified with specific primers, binding to the region of interest. The amplification was done with a Taq polymerase by in vitro enzymatic replication. Amplified DNA itself is used as a template again, so the chain reaction generates DNA exponentially.

Set up the PCR for genotyping by pipetting the PCR Mix. Add the corresponding primers and 0.4 µl of Taq polymerase to the reaction and start the program on Eppendorf Mastercycler S gradient.

2.13 GENOTYPING *MIF* MICE

Volume [μ l]	Component
20	1x PCR Mix
1	A [10 pmol]
1	B [10 pmol]
1	C [10 pmol]
2	DNA template
0.4	Taq Polymerase (Fermentas)
25.4	Total volume

- program

Initiation	94 °C 2 min	
Denaturation	94 °C 1 min	} x 35
Annealing	62 °C 45 sec	
Elongation	72 °C 45 sec	
Final elongation	72 °C 10 min	

- primer sequences

A	5'-AGG TTA GTC ACT CTA CTG GCC-3'
B	5'-TCT CAC TGT TCT GGT GTG AGG-3'
C	5'-GGC TCC TGG TCT CAG TCA GG-3'

- fragment sizes = 383 bp (*mif*^{-/-}), 544 bp (*mif*^{+/+}), 683 bp (*mif*^{flxed})

- agarose gel

1.5%, let run with 100V

- standard marker = MassRuler DNA ladder, Low Range (Fermentas)

2.14 GENOTYPING *K14HPV8-CER* MICE

Volume [μ l]	Component
39.25	1x PCR-Mix
3	E6F [10 pmol]
3	E6R [10 pmol]
4	DNA template
0.5	Taq Polymerase (Fermentas)
0.25	BSA (Fermentas)
50	Total volume

- controls

Volume [μ l]	Component
39.25	1x PCR-Mix
3	HPV8E6FOR [10 pmol]
3	HPV8E6REV [10 pmol]
4	E6-free DNA
0.5	Taq Polymerase (Fermentas)
0.25	100x BSA
50	Total volume

Volume [μ l]	Component
33.25	1x PCR-Mix
6	HPV8E6FOR [5 pmol]
6	HPV8E6REV [5 pmol]
4	ddH ₂ O
0.5	Taq Polymerase (Fermentas)
0.25	100x BSA
25	Total volume

Volume [μ l]	Component
39.25	1x PCR-Mix
3	HPV8E6FOR [10 pmol]
3	HPV8E6REV [10 pmol]
4	E6-positive control (genomic DNA of a papilloma)
0.5	Taq Polymerase (Fermentas)
0.25	100x BSA
50	Total volume

- program

3'	94°C	
30''	94°C	} 29 x
90''	60°C	
120''	72°C	
10'	72°C	
~	4°C	

- primer sequences

HPV8E6FOR	5'– GGA TCC TTT CCT AAG CAA ATG GAC GGG – 3'
HPV8E6REV	5'– GGA TCC GCA TGC CAC AAA ATC TTG CAC AGT GAC CTC – 3'

- fragment size = 550 bp

- agarose gel

1.5%, ca. 25' with 120V

- standard marker = MassRuler DNA ladder, Low Range (Fermentas)

- dNTP Mix

Volume [μl]	Component
20	dATP [as provided by Fermentas]
20	dCTP [as provided by Fermentas]
20	dGTP [as provided by Fermentas]
20	dTTP [as provided by Fermentas]
920	ddH ₂ O
1000	Total volume

- 1x PCR Mix

Volume [μl]	Component
740	ddH ₂ O
100	10x Taq buffer with (NH ₄) ₂ SO ₄
100	MgCl ₂ [as provided by Fermentas]
60	dNTP-Mix
1000	Total volume

2.15 GENOTYPING OF *K14-CRE* MICE

Volume [μ l]	Component
21	1x PCR Mix
1	Cre3 [5 pmol]
1	Cre4 [5 pmol]
2	DNA template
0.4	Taq Polymerase (Fermentas)
25	Total volume

- controls

Volume [μ l]	Component
21	1x PCR Mix
1	Cre3 [5 pmol]
1	Cre4 [5 pmol]
2	Cre-free DNA template
0.4	Taq Polymerase (Fermentas)
25	Total volume

Volume [μ l]	Component
21	1x PCR Mix
1	Cre3 [5 pmol]
1	Cre4 [5 pmol]
2	ddH ₂ O
0.4	Taq Polymerase (Fermentas)
25	Total volume

- program

2' 94°C
45'' 94°C
45'' 62°C } 36 x
90'' 72°C
10' 72°C
~ 4°C

- primer sequences

Cre3	Forward primer	5'– CAA TTT ACT GAC CGT ACA C – 3'
Cre4	Reverse primer	5'– CAT CGC CAT CTT CCA GCA G – 3'

- fragment size = 1000 bp

- agarose gel

1.5%, let run with 100V

- standard marker = MassRuler DNA ladder, Low Range (Fermentas)

- dNTP-Mix

Volume [μl]	Component
20	dATP [as provided by Fermentas]
20	dCTP [as provided by Fermentas]
20	dGTP [as provided by Fermentas]
20	dTTP [as provided by Fermentas]
920	ddH ₂ O
1000	Total volume

- 1x PCR Mix

Volume [μ l]	Component
740	ddH ₂ O
100	10x Taq buffer with (NH ₄) ₂ SO ₄
100	MgCl ₂ [as provided by Fermentas]
60	dNTP-Mix
1000	Total volume

2.16 AGAROSE GEL ELECTROPHORESIS

PCR products as well as restriction enzyme digests were analyzed by agarose gel electrophoresis to verify the size of the fragments or products.

1x TAE buffer was boiled with the desired amount of agarose, mixed with the DNA-intercalating substance ethidium bromide (0.25 μ g/ml) and poured into the gel chamber. The comb was directly inserted and taken out when solidification occurred, before the chamber was put into the electrophoresis chamber containing 1x TAE. For smaller fragments (300-3,500 bp), 1.5% agarose was used. 300 to 500 ng of 10 μ l of PCR products were mixed with loading dye filled up with H₂O to a final volume of 20 μ l and loaded onto the gel. Depending on size of the gel, between 80-140 V and 200 mA were chosen for electrophoresis.

50x TAE Buffer

dissolve 242 g of Tris in 500 ml of ddH₂O

50 mM Na₂EDTA

57.1 ml Glacial acetic acid

adjust to volume of 1 l with ddH₂O

2.17 TWO STAGE-CARCINOGENESIS WITH 7,12-DIMETHYLBENZ(A)ANTHRACENE (DMBA) AND PHORBOL-12-MYRISTATE-ACETATE (TPA)

10 male MIF KO and WT littermates were topically treated on their dorsal skins one day 1 with 25 µg DMBA in acetone beginning after full completion of the first postnatal hair cycle (8 wks of age). After tumor initiation with DMBA, mice were treated twice a week with 50 µg TPA in acetone for a total of 20 weeks. Developing tumors with a minimal of 1 mm in any dimension were counted once weekly and measured in all three dimensions with an electronic caliper. Mice were sacrificed by cervical dislocation when tumor incidence reached 100% in both groups. Skin tumors, DMBA/TPA-treated skin adjacent to tumors as well as untreated skin were excised for further histological analysis after fixation in 4% buffered paraformaldehyde or frozen at -20°C or -80°C for biochemical analysis.

2.18 ONE STAGE CARCINOGENESIS WITH BENZO(A)PYRENE (B[A]P)

10 male and female mice per group at the age of 8 weeks were topically treated with 100 µg B(a)P in acetone two times a week on their shaved dorsal skins and tumor formation was observed over a period of 32 weeks. Developing tumors with a minimal size of 1 mm in any dimension were counted once weekly and measured in all three dimensions with an electronic caliper. Mice were sacrificed by cervical dislocation when tumor incidence reached 100% in one group. Skin tumors, B(a)P-treated skin adjacent to tumors as well as untreated skin were excised for further histological analysis after fixation in 4% buffered paraformaldehyde or frozen for biochemical analysis.

2.19 UV-B IRRADIATION

The entire dorsum of 10 female and 10 male mice within one group at the age of 8 weeks was shaven prior to initial irradiation with 2.5 kJ/m². After 4 weeks, the dose was raised to 5 kJ/m². As of week 9, 10 kJ/m² were applied for 6 months. All radiation dosages were given three times per week.

A bank of four UVB TL40W/12 (Philips) sunlamps was used, which have an emission spectrum from 280 to 350 nm, with a peak at 306 nm. These lamps deliver an average dose of 8 W/m², as measured with an IL-1700 UV detector and a SED 24 filter (both from International Light). The mice were placed in cages, 20 cm below the light bulbs for irradiation. The cage order was systematically rotated on a weekly base before treatment to compensate for uneven lamp output along the cage line. Mice were shaved with electric clippers when necessary to guarantee hairlessness of all entire dorsi.

2.20 RESCUE OF IMMUNE CELL HOMING BY INTRA-EPIDERMAL INJECTIONS OF MIF

5 MIF-deficient mice received intra-epidermal injections into their dorsal skins. 28G-needles were used for the injections. A total of 100 ng protein was solved in NaPP buffer in a total volume of 50 µl. The following proteins were injected: a heat-inactivated, denaturized recombinant murine MIF sample that had been incubated at 95°C for 10 min, native recombinant murine MIF and a structural MIF mutant called D44A-MIF. All probes had been placed on ice until injection to prevent degradation. Successful injections were visible by blister formation at the injection site. Injection sites were marked with ethanol-resistant pens. All injections were administered in a cross pattern on the back of each animal. After 3 days, the animals were sacrificed by cervical dislocation and the skin at the injection sites punched with a 6 mm biopsy punch. All skin samples were

immediately fixed with 4% buffered formaldehyde, stored at 4°C o/n and processed for immunohistochemical analysis the day after.

2.21 HISTOLOGY

Tissues were either fixed with 4% buffered formalin o/n, then processed and embedded in paraffin or embedded in O.C.T. medium and shock-frozen in isopentane and liquid nitrogen. 4 µm thick paraffin sections were dewaxed with xylene and rehydrated through a graded series of isopropanol and ethanol.

For determination of tumor types, tumor sections were stained with H&E and evaluated by a pathologist, blinded for genotypes, and classified according to the current WHO classification of skin tumors (see reference list).

2.22 IMMUNOHISTOCHEMISTRY

For immunohistochemistry, 1% hydrogen peroxide in methanol solution was used to block endogenous peroxidase activity and citric acid antigen retrieval was performed for all antibodies – except for anti-MIF – by microwaving in CitraPlus for 1 min at 600 W.

Primary antibodies against:

- B220 (1:200; Becton Dickinson, Cat. No. 550286)
- CD44 (1:400; Becton Dickinson, Cat. No. 550538)
- CD68 (1:800; Novus Biologicals, Cat. No. NB100-683)

- CD74 (1:200, Becton Dickinson, Cat. No. 555317)
- JAB1 (1:200; Becton Dickinson, Cat. No. 611618)
- MIF (1:400; Santa Cruz, Cat. No. sc-20121)

were detected by using biotin-labeled secondary antibodies produced by DAKO in conjunction with streptavidin peroxidase and a colorimetric read-out, based on 3-amino-9-carbazole (AEC).

Ready-to-use background reducing antibody diluent solution by DAKO was used as solvent for all antibodies. Counterstaining of nuclei was done using Meyer's hematoxylin.

2.23 IMMUNOFLUORESCENCE

For immunofluorescent detection of proteins in paraffin embedded material the following antibodies were used:

- Alexa Fluor 488 anti-mouse CD207 (Langerin) (eBioRMUL.2, eBioscience, Cat. No. 53-2073, 1:100)
- CD3 (AnaSpec, Cat. No. 29588, 1:50)
- CD19 (6D5, LifeSpan, Cat. No. LS-C57376, 1:50)
- F4/80 (A3-1, Abcam, Cat. No. ab6640, 1:50)
- I-A (OX6, AbCam, Cat. No. ab6403, 1:50)
- MIF (FL-115, Santa Cruz, Cat. No. sc-20121, 1:400)

In accordance to the intended color combinations, different Alexa Fluor-coupled secondary antibodies were combined and DAPI (Sigma Aldrich, D9542) was used as nuclear counterstain. All secondary antibodies for immunofluorescent detection were purchased from Molecular Probes.

2.24 IMMUNOFLUORESCENT ANALYSIS OF CRYOSECTIONED MURINE SKIN TUMOR TISSUE

For the immunofluorescent staining on cryosections, 4-micron thick samples were thawed to room temperature, fixed in ice-cold acetone at 4°C for 10 min, washed with PBS and primary antibodies were incubated in the indicated dilution at RT for 30 min. The applied secondary antibody solution (0.5-fold dilution of primary antibody), containing DAPI as counterstain, was incubated for 30 min. After final washes with PBS to remove unbound antibodies, samples were mounted in Mowiol 4-88.

2.25 PREPARATION OF EPIDERMAL SHEETS

For the assessment of the LC contents, epidermal sheets were taken from MIF-deficient and control mice. Both ear halves were placed outside up on a drop of a 3.8% ammonium thiocyanate solution for 20 min at 37°C. After the separation of the epidermis from the dermis, the epidermal sheets were covered with ice-cold acetone for fixation and incubated for 15 min at 4°C with their inside up. The fixation step was followed by a washing step with PBS. The epidermal sheets were blocked with 0.5% BSA in PBS for 20 min and washed with PBS/Tween-20 again. The Alexa Fluor 488 anti-mouse CD207 (Langerin) antibody was diluted 1:100 and DAPI as counterstain was added directly to the solution for 30 min. For double immunofluorescence stainings, the solution

contained a second primary antibody and detection of this protein was performed with Alexa Fluor 546-conjugated secondary antibodies. After repeated washing steps with PBS, the probes were mounted with Mowiol.

2.26 EUKARYOTIC CELL CULTURE CONDITIONS

All cell lines and primary cells were cultured at 37°C, a relative humidity of 90% and 5% CO₂. DMEM cell culture media was supplemented with 10% (v/v) FBS, 1% sodium pyruvate and 1% antibiotics (penicillin/streptomycin).

2.27 PREPARATION OF MURINE EMBRYONIC FEEDERS FOR PRIMARY MURINE KERATINOCYTES

Mice were mated and checked for vaginal plugs every morning. When a vaginal plug was visible (day 0.5 of gestation), the mother animal had to be sacrificed at day 14.5 by asphyxiation through CO₂. The animal was sprayed with antiseptic, and the abdominal wall opened in a sterile surrounding and manner. The embryos were taken out and put onto a 15 cm dish filled with 1x PBS. The uterus and amniotic sack were removed, too, and the embryos washed again. All red organs (= heart, liver, spleen) and heads were picked. The embryonic bodies were chopped into fine pieces by using a pair of fine scissors. The embryos were transferred into a 50 ml Erlenmeyer flask filled with 1x trypsin/EDTA and autoclaved glass beads. The tissue was trypsinized for 30 min at 37°C in an incubator while the suspension was slowly stirring. The trypsin was inhibited by adding 50 ml MEF media, containing 10% FBS (DMEM, 10% FBS, 1% sodium pyruvate, 1% antibiotics). The suspension was filtered through a 100-micron nylon mesh and the cell suspension collected in 50 ml

tubes. The cells were spun down at 400-800 x g for 10 min at RT. The supernatant was discarded, and the pellet resuspended in MEF media. The cells were counted and 3×10^6 cells per 15-cm dish cultivated in 20 ml MEF media until confluent (approx. 3 days).

2.28 ISOLATION OF PRIMARY MURINE KERATINOCYTES

On day 1, newborn mice (P1-3) were killed by decapitation. The bodies were kept cool in a beaker on ice for 1 h. Then the following procedure was performed to disinfect the bodies, using one body after the other and keeping the rest on ice:

Betaisodona/1x PBS (1:1) for 1'

1x PBS (rinse briefly)

70% EtOH for 1'

1x PBS (rinse briefly)

The bodies were transferred onto a sterile dish, and tails and limbs cut off. A lengthwise incision on the back from neck to tail was made and the mouse body unwrapped by using forceps, taking off the skin in one piece.

The skins were transferred to a dish with an antibiotic/antimycotic solution (PenStrepAmphotericin, GibCo) (1:100 in 1x PBS) w/o Ca^{2+} , Mg^{2+} and incubated for a few minutes. The skins were taken, transferred to a new 35-mm dish and spread on plastic surface with the epidermal side up. The dish was filled with 2 ml 0.025% trypsin/PBS/EDTA, so that the skins floated on top of the trypsin solution. The dish was kept at 4°C o/n. 60-mm dishes were coated with

collagen, e.g., bovine collagen I solution (4 mg/ml) to a final concentration of 20-30 µg/ml, by using 2 ml 1x PBS for each 60-mm dish, and incubated at 4°C o/n.

On day 2, the solution on collagen dishes was aspirated and washed twice w/ 1x PBS. Feeder cells (MEFs, F2) were treated with 60 µl mitomycin C (2 mg/ml) by adding it to the medium and these cells incubated at 37°C for 2 hrs. After this incubation period, mitomycin C was removed by washing the cultures with PBS twice, and culture medium was added back. The skins were taken out, and the epidermis peeled off the dermis by using forceps. The epidermal pieces were pooled in a 10-mm dish, and the epidermis minced into very small pieces using two scalpels. These epidermal fragments were suspended in 1.5 ml FAD medium with serum (50 µM Ca²⁺, 10% FBS Gold; pre-treated with 2 g Chelex 100 per 50 ml o/n at 4°C; sterile filtered). The 2-ml tube was shaken for 30' at RT w/ 1,000 rpm. The mitomycin C-treated feeder cells were washed with 1x PBS, trypsin/EDTA added, the plate rinsed and trypsin added. The dish was incubated for a few minutes at 37°C. The collagen-coated 6-well plates were washed with 1x PBS. The trypsinized feeder cells were resuspended in FAD medium (low calcium), and the medium applied with the epidermal suspension to one well per mouse. The medium was adjusted to 2 ml with 0.5 ml of feeder cell suspension and everything incubated at 32°C, 5% CO₂.

Complete Primary Murine Keratinocyte Medium

Component	Comment	Concentration	Volume
DMEM/Ham's F12	50 μ M Ca ²⁺	-	460 ml
FBS Gold	Chelex 100-treated	-	40 ml
Pen/Strep	GibCo	100x	5 ml
Amphotericin	GibCo	100x	5 ml
Adenin	Warmed-up to 56°C	180 mM	500 μ l
Insulin	Dissolved in 5 mM HCl	5 mg/ml	500 μ l
Vitamin C	Dissolved powder by Sigma	-	250 μ l
EGF	Human	100 μ g/ml	50 μ l
Hydrocortison	Dissolved in 100% EtOH	5 mg/ml	50 μ l
Choleratoxin A	Dissolved in ddH ₂ O	10 ⁻⁵ M	5 μ l

2.29 TRYPSINIZATION

To detach adherent cells from culture dishes, media was taken off and cells were washed with PBS to remove rests of medium. Cells were then incubated in a small volume of trypsin/EDTA in the incubator until detachment was visible. The reaction was stopped by adding the same volume of media containing 10% FBS.

2.30 COUNTING

After trypsinization, cells were diluted with Trypan blue. Trypan blue is a vital stain, which selectively stains dead cells blue. 10 μ l of dilution were transferred

into a “Neubauer” chamber. Four squares were counted and an average was calculated. The number of cells (n) in one square equals $n \times 10^4$ per ml divided through dilution factor of Trypan blue.

2.31 FREEZING AND THAWING OF CELLS

Cells were grown to confluence, trypsinized and pelleted at 1,200 rpm for 5'. They were then resuspended in freezing medium containing 80% FBS and 20% DMSO. Aliquots were pipetted into cryotubes, and slowly frozen at -80°C in freezing containers. For long-term storage the cryotubes were transferred into a liquid nitrogen tank after 1-2 days.

For thawing cells, frozen vials were taken out of the liquid nitrogen tank, carefully thawed at 37°C in a water bath and immediately transferred into a 15 ml tube containing 5 ml of pre-warmed culture medium. Pelleting the cells by centrifugation at 1,200 rpm for 5' removes the toxic DMSO. After resuspension of the cells in fresh culture medium the cells were plated on a 10-cm dish.

2.32 PREPARATION OF CELL LYSATES

To detect the expression pattern of different proteins, they have to be separated on a gel.

Cell pellets were washed 2x with 1x PBS and then lysed in 100 μl RIPA buffer, sonicated with an ultrasound sonicator for 2x 10". The lysed proteins were spun down in a cooling centrifuge at 400 x g for 30'. After centrifugation the clear lysate was transferred into a new tube, and then the protein content determined.

RIPA Buffer

25 mM Tris HCl pH 7.6

150 mM NaCl

1% NP-40

1% Sodium deoxycholate

0.1% SDS

adjusted to volume of 1 l with ddH₂O

2.33 QUANTIFICATION OF PROTEINS

The protein concentration is determined by a Bradford assay, preparing a standard curve with BSA. Standard proteins and cell lysates are mixed with Roti-Nanoquant (Roth), which was diluted 1:5 in ddH₂O.

For the assay, 2 µl of protein lysate was mixed with 1 ml of Roti-Nanoquant. To prepare protein standards for calibration of the reader, 2, 4, 6, 8 and 10 µg of bovine serum albumin from a 1 mg/ml stock were diluted in Roti-Nanoquant. 200 µl of this dilution was pipetted into a 96-well plate, also the dilution of the protein samples. The determination of the protein concentration was measured at wavelengths of 450 nm and 590 nm as reference, using a spectrophotometer. The standard curve of absorbance minus micrograms protein was plotted (O.D.590/O.D.450) and the protein concentration of each sample was determined by linear regression.

2.34 SDS POLYACRYLAMIDE GEL ELECTROPHORESIS (SDS-PAGE)

In SDS polyacrylamide gel electrophoresis (SDS-PAGE), proteins are separated on the basis of their molecular weight.

Two sequential gels were casted, the top gel, so called stacking gel was slightly acidic (pH 6.8) and had a low polyacrylamide concentration, where the proteins were poorly separated but formed thin and sharply defined bands. The lower gel, the separating or resolving gel, was more basic (pH 8.8) and had a higher polyacrylamide content, which allowed the proteins to be separated according to their molecular sizes, where smaller proteins travelled faster than the larger proteins. Sodium dodecyl sulfate (SDS), an anionic detergent, denatured the protein and imparted a negative charge, while β -mercaptoethanol, a hybrid of ethylene glycol broke disulfide bonds in the proteins. In an electric field, the negatively charged proteins were attracted towards the anode and resolved solely on the basis of their sizes by the pores of the polyacrylamide gel.

Electrophoresis was carried out using a vertical apparatus Mini Protean II (BioRad, Munich, Germany). Protein samples for electrophoresis were prepared by adding 4x sample buffer and boiling the mixture at 95°C for 5'. Equal amounts of protein samples and the molecular weight marker were loaded in the slots of the stacking gel. Gels were run at 100 V, until the blue running front has traveled to the bottom of the separating gel.

Solutions for Casting SDS-Polyacrylamide Gels

Solutions	Stacking gel	Resolving gel	
		10 %	15 %
ddH ₂ O	2.5 ml	2.075 ml	2.075 ml
1.5 M Tris (pH 6.8)	1.25 ml	-----	
1.5 M Tris (pH 8.8)	----	0.825 ml	2.075 ml
30% Acrylamide	1.25 ml	0.33 ml	2.075 ml
10% SDS	50 µl	33 µl	33 µl
10% APS	13.3 µl	17 µl	33 µl
TEMED	6 µl	3.3 µl	33 µl

Electrophoresis Buffer

192 mM Glycin

25 mM Tris

0.1% SDS (v/v)

4x Sample Buffer

50 ml 1 M Tris pH 6.8

30 ml ddH₂O

20 ml Glycerol

4 g SDS

200 mg Bromophenol blue

prior to use, 200 µl of β-mercaptoethanol to 4.8 ml of stock were added

2.35 PROTEIN TRANSFER

For the detection of the protein of interest, the resolved protein bands on the gel are transferred on to blotting membranes by the process referred to as blotting. The blotting process was achieved by using the Trans-blot Cell Wet Transfer apparatus. Proteins were transferred onto nitrocellulose membranes. Membranes, filter paper and fiber pads were all pre-soaked in the transfer buffer.

The following is the order of assembly of the module (sandwich-blotting chamber):

Anode (white)

Fiber pad

Filter paper

Membrane

Gel

Filter paper

Fiber pad

Cathode (black)

Care should be taken to remove all the air bubbles in the assembly. The transfer was carried out at 100 V for 60'.

Transfer Buffer

250 mM Tris

200 mM Glycine

20% Methanol

2.36 IMMUNOBLOTTING AND DEVELOPMENT

Immunoblotting involves the detection of specific proteins on membranes using antibodies. The membranes were first blocked with blocking reagent (5% non-fat dry milk in PBS or 5% BSA in TBS-T) to prevent non-specific binding of antibodies. Then, primary antibodies that recognize specific proteins were allowed to bind to their targets. Respective primary antibodies were diluted in the blocking reagent and the membrane incubated o/n at 4°C on a shaker. After three washing steps, 10' each with 1x PBS or TBS-T to remove non-specific binding and excess antibody, secondary antibodies labeled with horseradish peroxidase (HRP) that recognize the primary antibodies were applied to the membrane. The secondary antibody was also diluted in the blocking reagent and incubated with the membrane for 60' at RT. Thereafter, the membrane was washed again three times with 1x PBS or TBS-T for 10' before detection of the protein by chemoluminescent visualization using the enhanced chemoluminescent (ECL) detection system. For the detection, mixing Solution A and B prepare 1 ml of freshly prepared ECL working solution in a ratio of 1:1 (v/v). The mixture was immediately spread on the membrane and incubated for 1'. Excess solution was drained off, and the membrane exposed to Hyperfilm in the dark for the appropriate time and developed in an X-ray film processor.

10x PBS Buffer

80 g NaCl

2 g KCl

26.8 g Na₂HPO₄·7H₂O

2.4 g KH₂PO₄

adjusted to volume of 1 l with ddH₂O, adjusted to pH 7.4

TBS Buffer

10 mM Tris-HCl, pH 8.0

150 mM NaCl

TBS-T Buffer

1% (v/v) Tween-20 in TBS

2.37 ANTIBODIES FOR IMMUNOBLOTTING

- β actin (1:10,000, 42 kD; clone AC-15, Sigma-Aldrich, St. Louis, Cat. No. A 1978)
- β -tubulin (1:1,000, 55 kD; clone 5H1, Becton Dickinson, Franklin Lakes, Cat. No. 556321)
- MIF (1:1,000, 12.5 kD; clone FL-115, Santa Cruz, Cat. No. sc-20121)
- MIF (1:1,000, 12.5 kD; clone Ka565, kindly provided by J. Bernhagen, RWTH Aachen)
- PARP (1:2,000, 113 kD; clone 42, Becton Dickinson, Franklin Lakes, Cat. No. 611038)
- secondary, HRP-labeled antibodies were purchased at DAKO

2.38 GENERATION OF CHEMICALLY COMPETENT CELLS

3 ml LB were inoculated with tip that had been dipped into glycerol stock of chemically competent bacteria and incubated on a shaker at 37°C with 120 rpm.

1 ml of o/n culture was taken into 25 ml LB solution and grown on a shaker until $OD_{600} = 0.6$. The cell suspension was chilled on ice. After chilling, the cell suspension was spun for 7 min at 4°C with 5,000 rpm. The pellet was resuspended in 8.5 ml TB1 and placed on ice for 5 min. The cell suspension was spun 7 min at 4°C with 5,000 rpm again and the pellet resuspended in 1 ml TB2 and placed on ice for 30 min. Volumes of 100 µl were aliquoted and aliquots deep-frozen in liquid nitrogen immediately.

Transformation Buffer 1 (TB1)

3 ml 1 M KoAc

10 ml 1 M KCl

1 ml 1 M $CaCl_2$

12 ml 87% Glycerol

volume was adjusted to 80 ml with ddH₂O and pH to 6.1 with NaOH or glacial acetic acid

5 ml 1 M $MnCl_2$ were added and volume adjusted to 100 ml with ddH₂O

pH was 5.8

solution was filter sterilized

Transformation Buffer 2 (TB2)

1 ml 0.2 M MOPS

0.2 ml 1 M KCl

1.5 ml 1M $CaCl_2$

2.4 ml 87% Glycerol

adjusted volume to 15 ml with ddH₂O

pH was 6.5 now; if not, pH was corrected by using KOH or HCl

volume was adjusted to 20 ml with ddH₂O and the solution filter sterilized

LB Medium (per liter)

10g Bacto-Tryptone
5 g Bacto-Yeast
10 g NaCl

2.39 TRANSFORMATION OF CHEMICALLY COMPETENT CELLS

A fresh vial with *E.coli* (Top10 = DH5 α strain) was thawed on ice. During this time a 1.5 ml Eppendorf tube was pre-chilled. The pre-chilled tube was filled with 100 μ l bacterial suspension. 1 μ l, containing 50 ng of the plasmid solution, was added to the bacterial suspension and incubated for 30 min on ice. During this time, a water bath was pre-heated to 42°C. The samples were incubated at 42°C in the water bath for exactly 45 sec. The samples were immediately transferred on ice, and left for 5 minutes. 400 μ l of SOC or LB medium (w/o antibiotics!) were added and incubated at 37°C for 60 min. The bacterial suspension was plated in dilutions from 1:100 to 1:10,000 on pre-warmed antibiotic agar plates (LB_{Amp150}). The plates were incubated o/n at 37°C.

SOC medium

2.0 g Bacto-Tryptone
0.5 g Bacto-Yeast Extract
1 ml 1 M NaCl
25 ml 1 M KCl
1 ml 2 M Mg stock (1 M MgCl₂-6H₂O, 1 M MgSO₄-7H₂O), filter sterilize
1 ml 2 M Glucose, filter sterilize
adjusted to volume of 100 ml with ddH₂O

LB plates (per liter)

10g Bacto-Tryptone
5 g Bacto-Yeast
10 g NaCl
15 g Agar

autoclaved and cooled to 50°C before antibiotics were added

2.40 AMPLIFICATION OF $\Delta NTP53R175H$

Volume [μ l]	Component
21	1x PCR-Mix
1	FOR [10 pmol]
1	REV [10 pmol]
1	50 ng Plasmid DNA (pREBNA_dntp53R175H)
1	Taq Polymerase (Fermentas)
25	Total volume

- program

2' 94°C
45'' 94°C
45'' 60-70°C } 36 x
90'' 72°C
10' 72°C
~ 4°C

- primer sequences

FOR	5'– ATC TAG AAT GGA GGA GCC GCA GTC AGA TCC – 3'
REV	5'– ACT CGA GTC AGT CTG AGT CAG GCC CTT CTG – 3'

- fragment size = 1274 bp

- agarose gel

1%, ca. 10' with 150V

- standard marker = MassRuler DNA ladder, Low and High Range (Fermentas)

The amplified sequence was purified with QIAquick Gel Extraction Kit and a double digestion with *Xba*I and *Xho*I for 5 h at 37°C performed.

Volume [μ l]	Component
43	Elution
5	10x Tango Buffer
1	<i>Xba</i> I [= 10 u]
1	<i>Xho</i> I [= 10 u]
50	Total volume

2.41 DIGESTION OF PSC_AEGFPFG2

Volume [μ l]	Component
2	Plasmid DNA (= 3 μ g)
5	10x Tango Buffer
1	<i>Xba</i> I [= 10 u]
1	<i>Xho</i> I [= 10 u]
41	ddH ₂ O
50	Total volume

The solution was incubated for 5 h at 37°C and the reaction heat-inactivated at 80°C for 20 min.

2.42 LIGATION OF DIGESTED PSC VECTOR AND $\Delta NTP53R175H$ INSERTION SEQUENCE

Volume [μ l]	Component
10	Backbone elution fluid (= 10 ng/ μ l)
25	Insert elution fluid (= 20 ng/ μ l)
4	T4 Ligase Buffer
1	T4 Ligase
40	Total volume

The Ligation solution was incubated o/n at 16°C. A transformation of the complete solution into chemically competent cells was performed and the plated bacteria incubated on antibiotic agar dishes o/n at 37°C. Clones were picked and analyzed for successful insertion by double and single digestions with *Xba*I and *Xho*I, respectively, as previously described for 5 h at 37°C. The reaction was heat-inactivated at 80°C for 20 min and everything loaded onto a 1% agarose gel supplied with ethidium bromide for analysis.

2.43 CONTROL DIGESTION OF CLONED PLASMIDS FOR ITR FUNCTIONALITY

As presented in Chapter 3.36, clon #3 after insertion of $\Delta Ntp53R175H$ into the psc vector was chosen, because sequence analyses confirmed correctness of the cloning sites flanking the insert. In the following, correct ITRs are necessary for guaranteed functionality of the rAAV2 vector. Therefore, specific digestions of the ITRs were performed with restriction enzymes *Ahd*I and *Sma*I.

Volume [μ l]	Component
34.8	ddH ₂ O
4	10x Unique Buffer
0.2	<i>AhdI</i>
1	cloned plasmid (= 1.3 μ g DNA)
40	Total volume

The solution was incubated on 37°C for 2 h.

Volume [μ l]	Component
34.8	ddH ₂ O
4	10x Tango Buffer
0.2	<i>SmaI</i>
1	cloned plasmid (= 1.3 μ g DNA)
40	Total volume

The solution was incubated on 30°C for 2 h.

The results of these digestions are presented in Chapter 3.36.

2.44 STATISTICAL ANALYSIS

Statistical analyses were done using a Student's *t*-test or the Pearson Chi² test as indicated. A *p* value < 0.05 or < 0.01, respectively, was considered significant.

3 RESULTS

3.1 GENOTYPING TO DETERMINE THE *MIF* STATUS WITH THREE PRIMERS WAS RELIABLE

To determine whether the experimental animals were *MIF*^{+/+} or *MIF*^{-/-} mice, and to verify their genetic status, genotyping by PCR was performed. A combination of three primers (A, B, C) was used to generate bands of either wildtype (544 bp, Fig. 11) or knockout (383 bp; Fig. 11) genomic tail DNA.

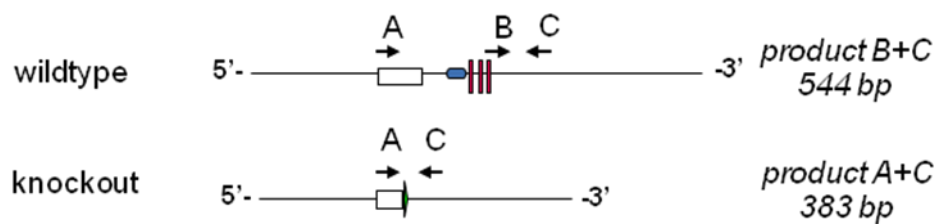


Fig. 11: Schematic overview about the primer design for genotyping mice to determine their mif status.

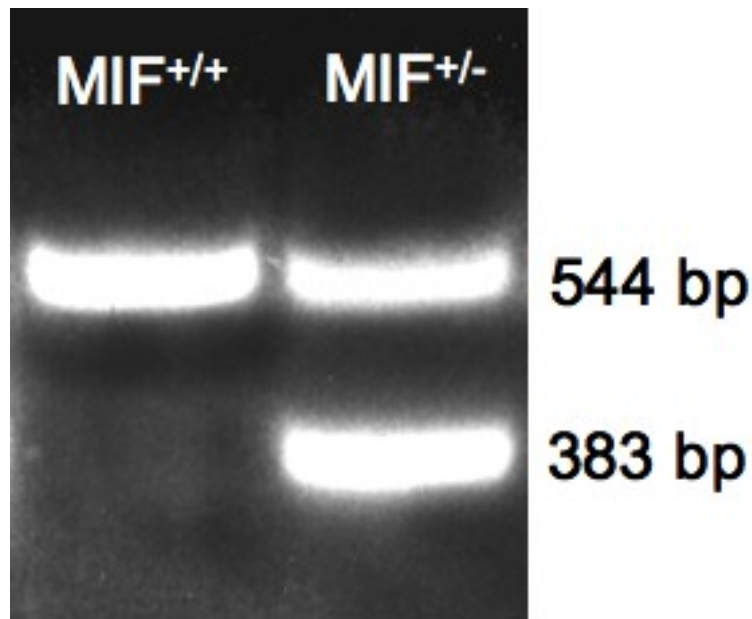


Fig. 12: Representative agarose gel showing the result of genotyping from a homozygous $mif^{+/+}$ and a heterozygous $mif^{+/-}$ mouse, respectively. DNA was visualized using ethidium bromide.

Mice, homozygously MIF wild-type or MIF knockout of the same age and sex were grouped. MIF-deficient mice were chosen as the experimental animals, MIF wild-type mice as the controls.

3.2 APPLICATION OF A CHEMICAL CARCINOGENESIS IN A CLASSICAL TWO-STAGE PROTOCOL WITH DMBA AND TPA SHOWS THAT MIF-DEFICIENCY IN MICE TURNS THEM PRONE TO INCREASED SKIN TUMOR FORMATION

The experimental series started with the chemical carcinogenesis protocols. A single topical application of the carcinogen DMBA on day 1, followed by repeated administration of the tumor-promoting compound TPA onto the shaved

dorsal skins of MIF-deficient mice resulted in tumors arising from week 7 on after the start of the experiment, while controls animals remained tumor-free at this time point.



Fig. 13: Representative picture of a MIF wild-type (left) and a MIF-deficient mouse (right) bearing skin tumors after chemical carcinogenesis with DMBA/TPA.

Tumors in control animals formed with a delay of 4 weeks starting in week 11. During the remaining 9 weeks of the observation period the number of tumors per mouse was always higher for MIF-deficient animals compared to their wild-type controls, reaching statistical significance levels from week 13 on. At the end of the experiment in week 20, when tumor incidence in both groups (MIF-deficient and wild-type control animals) had reached 100% (Fig. 15), MIF KO showed twice as many tumors than MIF WT animals (Fig. 14).

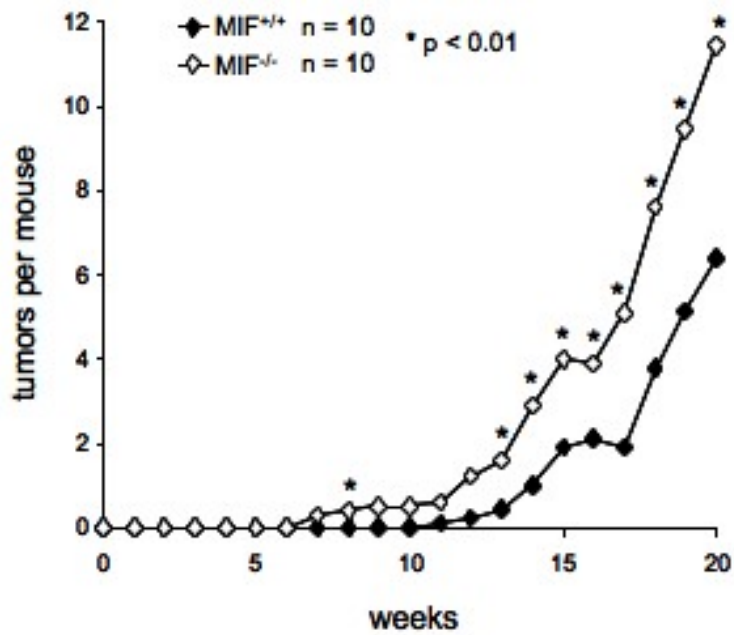


Fig. 14: Number of tumors per mouse during chemical carcinogenesis with DMBA/TPA in MIF-deficient and control mice. MIF-deficient mice started to develop tumors as of week 7, wild-type controls as of week 11. Tumor numbers per mouse differed significantly from week 13 on with the tumor number for MIF-deficient mice twice as high as for control mice at the end of the experiment in week 20. The asterisks indicate $p < 0.01$ (Pearson χ^2 test).

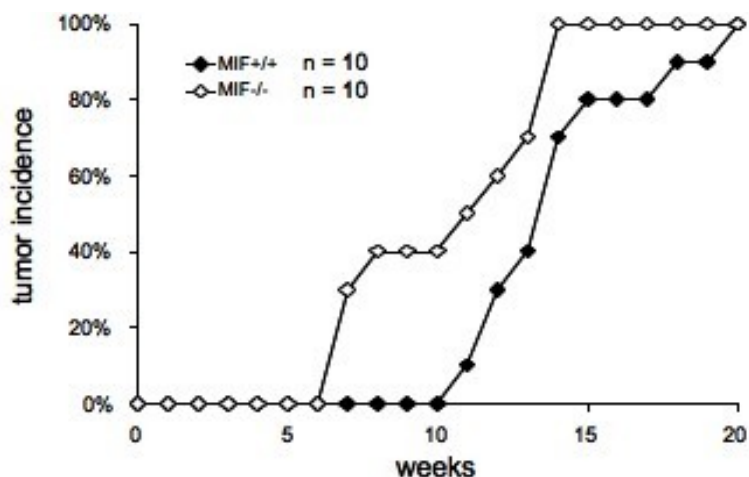


Fig. 15: Tumor incidence for the DMBA/TPA-treated animals. The group of MIF-deficient mice reached 100% tumor incidence already in week 14, whereas mice in the control animal group reached 100% tumor incidence only in week 20.

3.3 CHEMICAL SKIN CARCINOGENESIS WITH DMBA AND TPA INDUCES PREDOMINANTLY BENIGN TUMORS AND HAIR FOLLICLE NEOPLASIAS IN MIF-DEFICIENT 129S1 MICE

Histopathological examination of H&E stainings of the tumor material from the DMBA/TPA experiment was performed using the WHO classification (Heenan et al., Histological Typing of Skin Tumours [WHO. World Health Organization. International Histological Classification of Tumours], 1996). Most of the analyzed MIF KO (23/47) and MIF WT (9/21) tumors were keratoses with various subtypes (data not shown) occurring at comparable frequencies in both groups (MIF WT 43%, MIF KO 49%). One squamous cell carcinoma (SCC) and one keratoakanthoma were found in wild-type animals. Akanthoses, papillomas and cysts as well as sebaceous hyperplasia were found in both genetic backgrounds but more frequently in MIF-deficient mice. Interestingly, neoplasias of the hair follicle, like pilar tumor, trichoadenoma, and hair follicle hyperplasia were only found in MIF-deficient animals (Fig. 16).

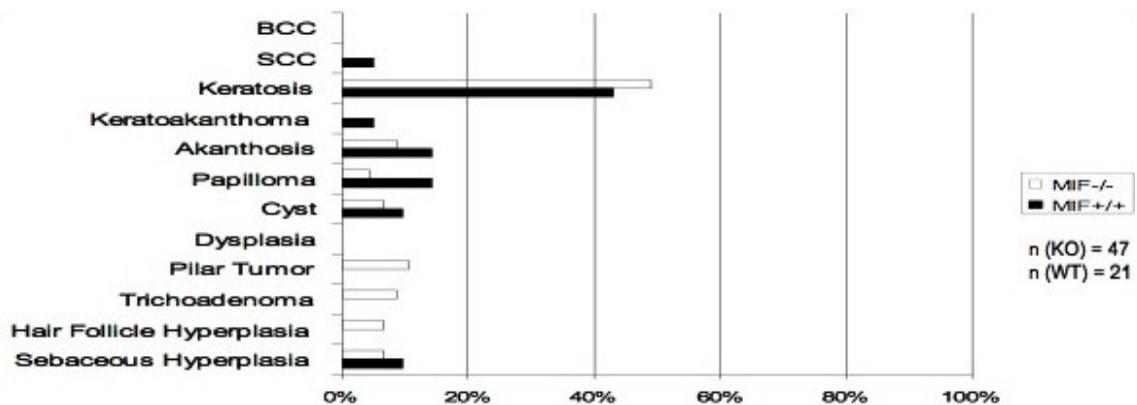


Fig. 16: Histopathological classification of tumor material obtained in the DMBA/TPA experiment according to the WHO classification of skin tumors. Most of the MIF KO and MIF WT tumors were keratoses, and there was no significant difference between the two groups. One squamous cell carcinoma (SCC) and one keratoakanthoma were found in wild-type animals. Akantoses, papillomas, cysts and sebaceous hyperplasias were more frequently present in MIF-deficient mice. Neoplasias of the hair follicle, like pilar tumor, trichoadenoma and hair follicle hyperplasia, were diagnosed only in MIF-deficient animals. BCC = basal cell carcinoma.

3.4 CHEMICAL SKIN CARCINOGENESIS WITH BENZO(A)PYRENE REVEALS A DISTINCT DIFFERENCE BETWEEN TUMOR NUMBERS IN MIF-DEFICIENT AND CONTROL MICE AND THEIR SEXES

During the second chemical carcinogenesis experiment, the repeated topical administration of B(α)P onto the shaved dorsal skins of 20 MIF KO and 20 MIF WT mice resulted in tumor formation in MIF-deficient mice from week 17 and in control animals from week 26 on.



Fig. 17: Representative picture of a MIF wild-type (left) and a MIF-deficient mouse (right) after topical treatment with the carcinogenic compound B(α)P.

Throughout this experiment, MIF-deficient animals developed more tumors at all time points after week 16 (statistically significant from week 20 on with $p < 0.01$). At the end of this chemical carcinogenesis protocol, the tumor frequency was 12.5-fold higher in MIF KO than in MIF WT mice (Fig. 18).

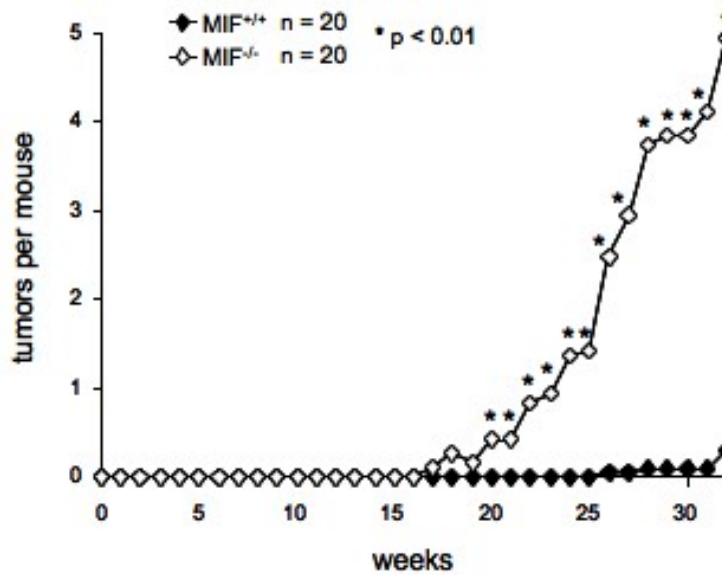


Fig. 18: Tumors per mouse during chemical carcinogenesis with B(α)P in MIF-deficient and control mice. MIF-deficient mice developed significantly more tumors than wild-type controls from week 20 on. At the end of the experiment, there was a 12.5-fold difference in the number of tumors per mouse between MIF KO and WT animals. The asterisks indicate $p < 0.01$ (Pearson χ^2 test).

A separate analysis for sex and genotype revealed that male mice were generally more prone to tumor formation than females. Male MIF-deficient mice developed first tumors in week 17, females with a delay of 9 weeks in week 26. In the control group, male mice were again the first to undergo tumor formation in week 26, whereas females displayed tumors in week 32 for the first time. Tumor numbers between male and female animals within the MIF KO group differed 5.4-fold at the end of the experiment in week 32 (Fig. 19).

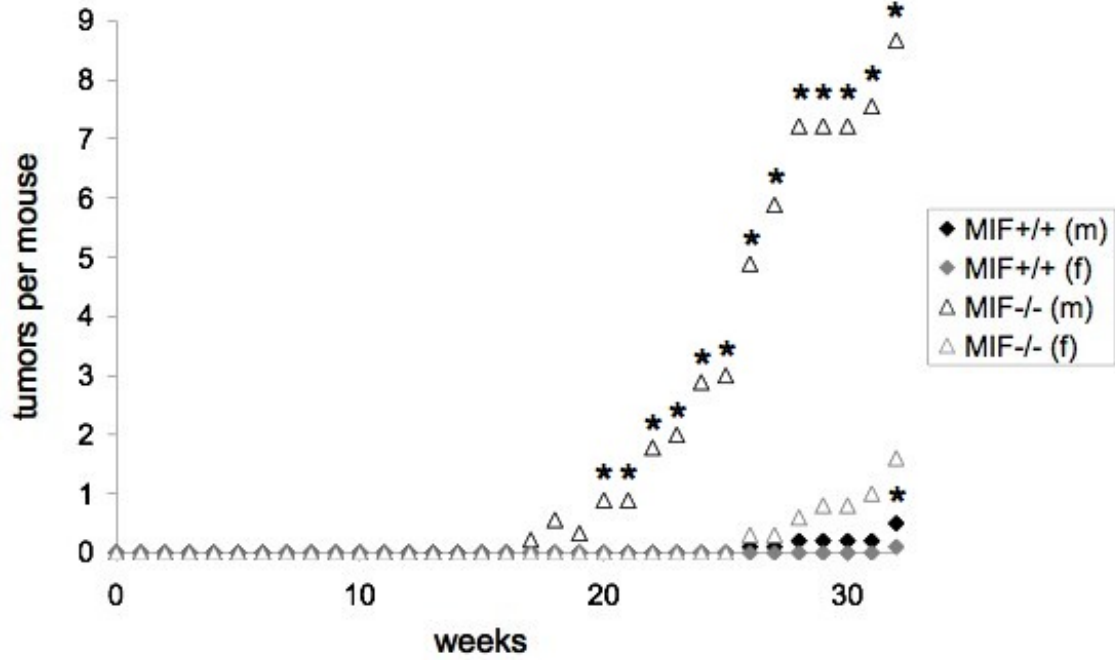


Fig. 19: Tumors per mouse during chemical carcinogenesis with B(α)P according to sex and genotype. MIF-deficient male mice developed tumors significantly earlier and in higher numbers than MIF-deficient females. Male MIF-deficient mice developed first tumors in week 17, females with a delay of 9 weeks in week 26. In the control group, male mice were again the first to undergo tumor formation in week 26, whereas females displayed tumors in week 32 for the first time. The asterisks indicate $p < 0.01$ (Pearson χ^2 test).

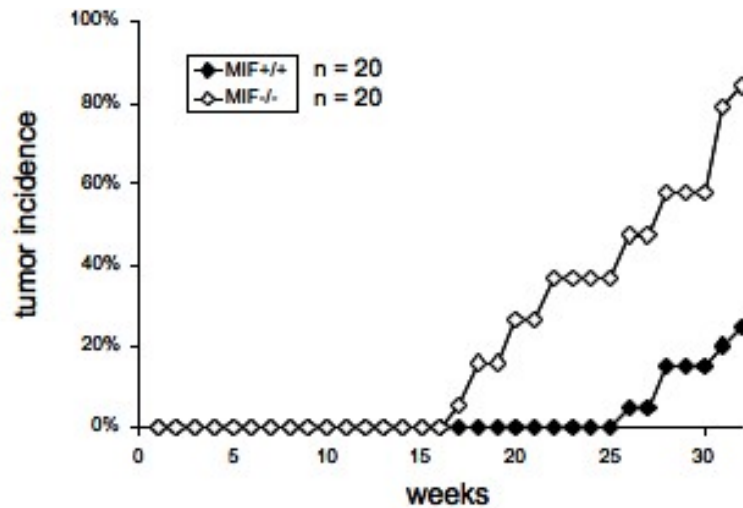


Fig. 20: Tumor incidence in carcinogenesis induced by B(α)P. From week 17 on, the group of MIF-deficient mice always reached a higher tumor incidence than control mice, which started to develop tumors as of week 26.

3.5 THE TUMOR SPECTRUM INDUCED BY CHEMICAL SKIN CARCINOGENESIS WITH BENZO(A)PYRENE DISPLAYS A SHIFT FROM BENIGN TO MALIGN ENTITIES, OF WHICH MOST OCCUR IN MIF-DEFICIENT MICE

As shown in Fig. 21, the spectrum of tumors induced by chemical carcinogenesis with Benzo(α)pyrene was different to the one induced with DMBA/TPA (Fig. 16). In this model, SCCs were the predominant tumor type and were seen in both genotypes at comparable frequencies. BCC and cysts were only found in MIF-deficient mice. Hair follicle tumors and sebaceous hyperplasias were completely absent. Dysplasias were only found in MIF WT mice, while keratoakanthomas were observed in MIF-deficient mice as well as in controls.

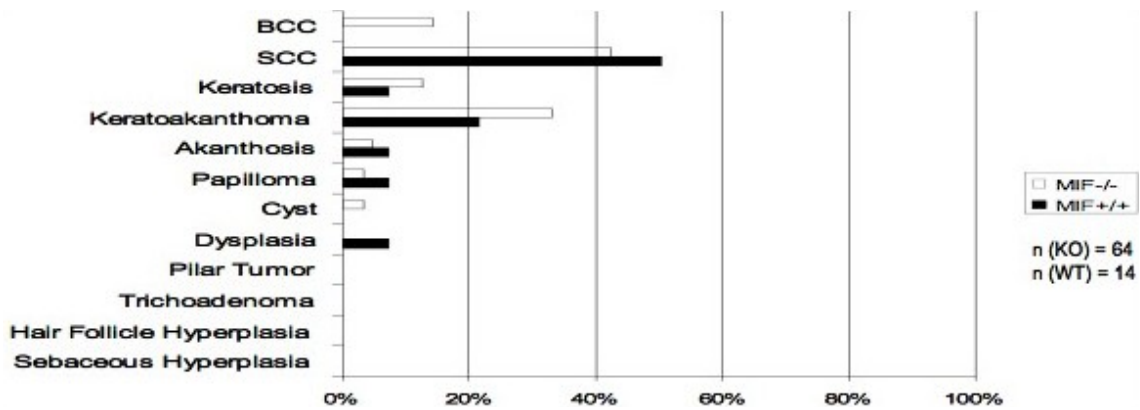


Fig. 21: Histopathological classification of skin tumors induced by chemical carcinogenesis with B(α)P according to WHO. SCCs were the predominant tumor type and were seen in both genotypes at comparable frequencies. BCC and cysts were only found in MIF-deficient mice. Hair follicle tumors and sebaceous hyperplasias were completely absent. Dysplasia was only found in MIF WT mice, while keratoakanthoma were observed in MIF-deficient mice as well as in controls. SCC = squamous cell carcinoma, BCC = basal cell carcinoma.

Taken together, both models of chemical skin carcinogenesis surprisingly, but reproducibly showed that MIF acts tumor-preventing in murine skin. Since this phenotype is opposite to what was observed in other tissues we sought to ascertain the tumor suppressor role of MIF by subjecting MIF WT and KO mice to other models of induced skin carcinogenesis such as UV irradiation or HPV8 transgenesis.

3.6 THE INDUCTION OF SKIN TUMORS BY IRRADIATION WITH UV-B COULD NOT BE COMPLETED DUE TO UNFORESEEN CIRCUMSTANCES, WHICH TERMINATED IN EUTHANASIA OF THE EXPERIMENTAL ANIMALS

Besides a chemical carcinogenesis, an UVB irradiation of MIF-deficient and control mice was performed to cover the most available means of skin tumor induction in mice.

The protocol for the induction of skin tumors with UV-B radiation as published by Loeser et al. [77] specifies a three-steps procedure, in which the shaved dorsal skins of the experimental animals were UVB-desensitized in two incremental steps (2.5 and 5 kJ/m²) for 4 weeks each to be finally irradiated with a constant dosage of 10 kJ/m² for a period of 6 months.

As described in the experimental set-up, an additional group of gene modified animals was used in this experiment, *mif*^{P1G/P1G} mice [73], to study whether the enzymatic activity of MIF with the prolin at position 1 of the protein sequence, which is a crucial part of the catalytic pocket, is important for a response of MIF to UV-B irradiation.

Unexpectedly, this protocol of UV-B irradiation caused such severe keratitis of the mice's eyes (Fig. 22) that this experiment had to be terminated for ethical considerations one month after the protocol had been completed. Mice developed massive inflammation of the cornea with thickening and neoangiogenesis. Therefore, the observation period for skin tumor development was only 4 weeks after the end of UV-B irradiation.

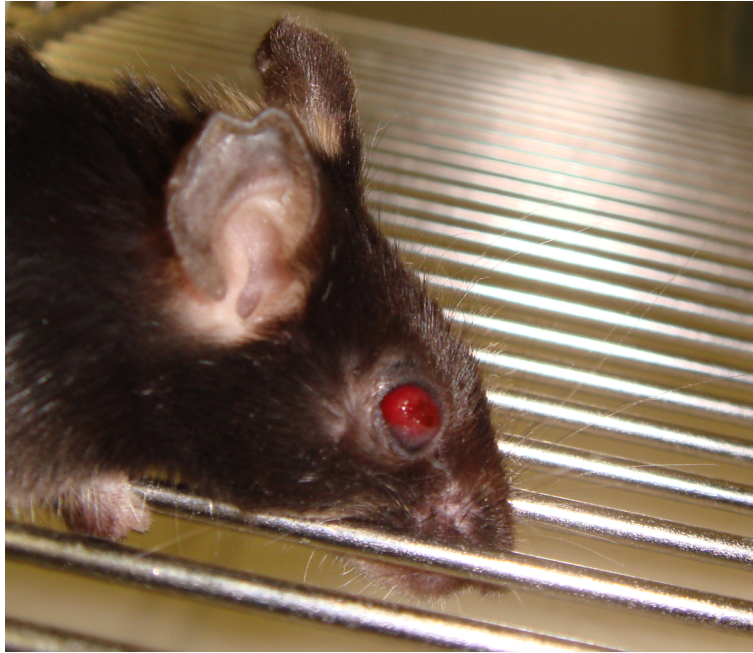


Fig. 22: An UVB-irradiated mouse prior to sacrifice, showing symptoms of a severe keratitis with massive neoangiogenesis in the cornea.

Severe inflammatory keratitis of the eye as defined by macroscopically visible neoangiogenesis within the cornea was more frequently observed in MIF WT mice than in MIF-deficient mice (Fig. 23).

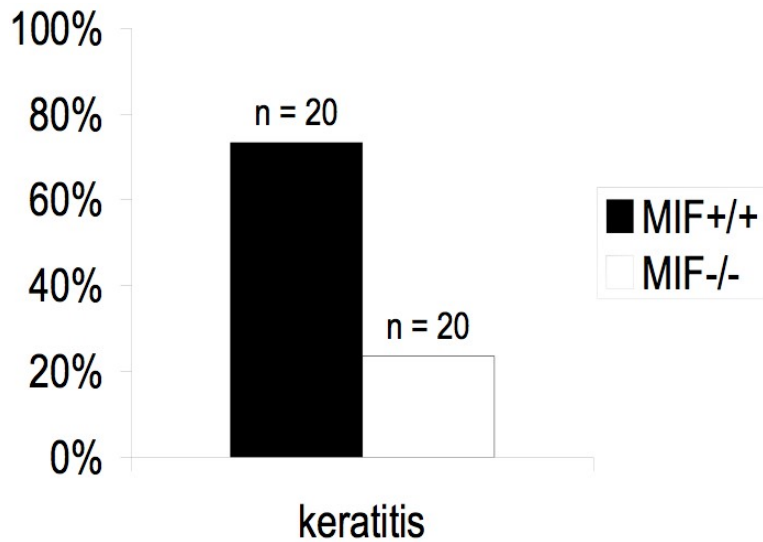


Fig. 23: Rate of severe keratitis following UVB irradiation in MIF KO and WT mice. Severe keratitis was defined by the presence of macroscopically visible neoangiogenesis within the cornea. Not significantly more MIF WT than MIF KO mice suffered from this disease of the eye ($p = 0.123$ in a Pearson χ^2 test).

At the time the experiment was terminated, 1 MIF^{+/+}, 3 MIF^{P1G/P1G}, and 1 MIF^{-/-} animal had developed visible tumors on their backs (Fig. 24).



Fig. 24: Representative example of a $MIF^{P1G/P1G}$ mouse bearing a large UVB-induced tumor on the back.

Histopathological study of these tumors indicated a mesenchymal origin with features of atypical fibroxanthomas (AFX), a superficial malign fibrous histiocytoma (MFH, Fig. 25).

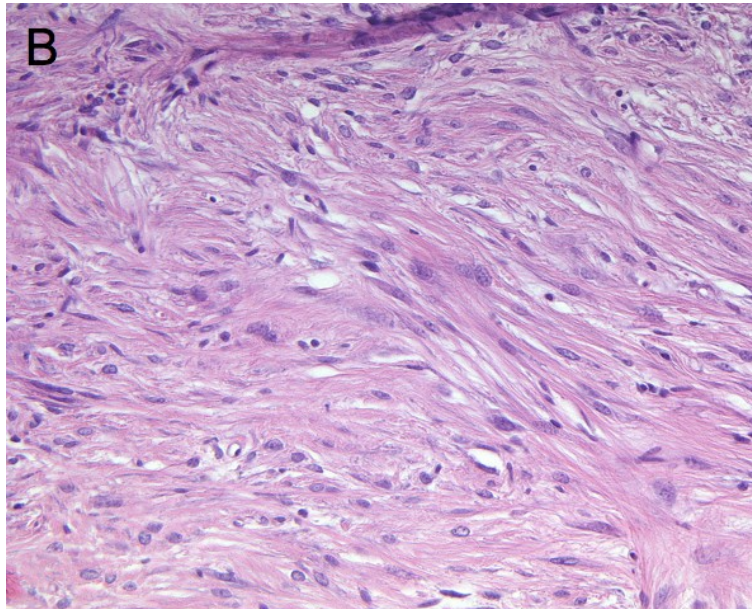
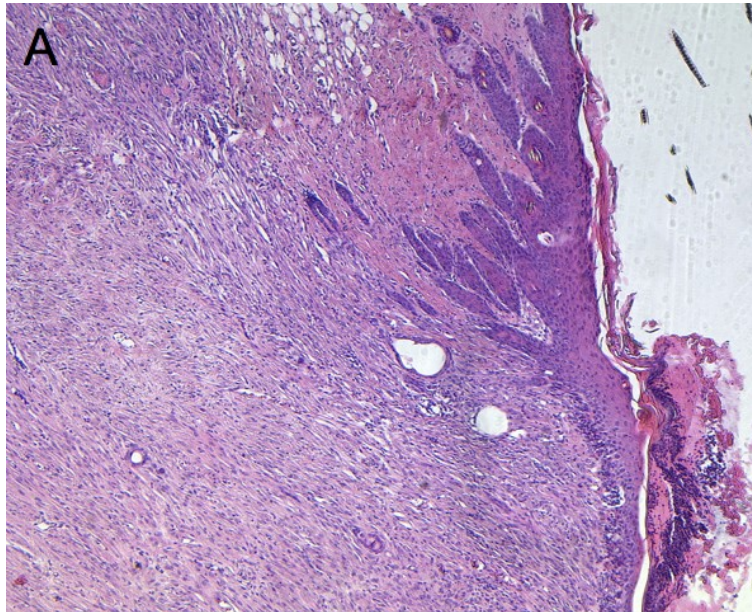


Fig. 25: H&E staining of the tumor sample of $MIF^{P1G/P1G}$ mouse displayed in Fig. 24. The tumor was classified as an atypical fibroxanthoma (AFX), which is a superficial malign fibrous histiocytoma (MFH), by pathological review.

A: The cutaneous tumor was large in size and the epidermis (right tissue edge) was of abnormal structure and increased thickness. Magnification 100x.

B: The typical pleomorphologic appearance of the nuclei within the tumor tissue is evidence for the malignant character of this tumor. Magnification 200x.

MIF's promoting role in neovascularization and inflammation is well established and our finding supports the notion that MIF acts as a pro-inflammatory mediator. Due to the limited number of tumors obtained and the short observation time, we did not draw any conclusions from this experiment with respect to MIF and UV-B induced tumorigenesis.

3.7 SKIN TUMOR DEVELOPMENT IN MICE WITH A *K14HPV8-CER*-TRANSGENIC BACKGROUND CONFIRMS THAT MIF PROTECTS THE MURINE SKIN FROM NEOPLASTIC EVENTS

In order to induce murine skin tumors in another way than by chemical carcinogenesis or UV-B irradiation, a viral induction of epithelial tumors was designed, making use of *K14HPV8-CER*-transgenic mice.

The *K14HPV8-CER*-transgenic mice spontaneously develop skin tumors due to the oncogenic action of the oncoproteins E2, E6 and E7 (corresponding to the complete early region) of the human papilloma virus isotype 8 (HPV8). In collaboration with Dr. Gian Paolo Marcuzzi from Prof. Pfister's research group, *K14HPV8-CER*-transgenic mice on a FVB/N background were crossed with *mif*^{-/-} mice on a 129S1/SvImJ background and *K14HPV8-CER*^{+tg} *mif*^{+/+} and *K14HPV8-CER*^{+tg} *mif*^{-/-} mice were generated in the F2 generation. Their transgenic status was confirmed by genotyping with *HPV8E6*-specific primers (Fig. 26), their MIF status as described in chapter 2.13.

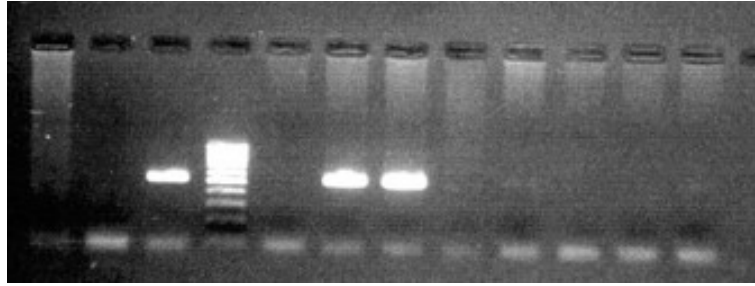


Fig. 26: Genotyping K14HPV8-CER mice for the virally induced skin tumor formation experiment. Primers designed for the detection of the E6 oncoprotein of the human papilloma virus isotype 8 (HPV8) were used to identify the K14HPV8-CER-transgenic animals. The animals, which genomic DNA was tested in lanes 6 and 7, were transgenic for K14HPV8-CER. The positive control was loaded into lane 3.

31 $K14HPV8-CER^{+tg} mif^{-/-}$ and 23 $K14HPV8-CER^{+tg} mif^{+/+}$ mice were subjected to a lifelong observation for tumor formation. $K14HPV8-CER^{+tg} mif^{-/-}$ mice (10/31 or 32.3%) developed epithelial tumors at a younger age and with a higher incidence compared to $K14HPV8-CER^{+tg} mif^{+/+}$ mice (2/22 or 8.7%). At the end of the experiment, there was a 3.7-fold difference between the curves (Fig. 28).

One of such a transgenic mouse bearing a typical papilloma is shown in Fig. 27.



Fig. 27: Picture of a papillomatous tumor in the neck region of a K14HPV8-CER^{+tg} mif^{-/-} mouse.

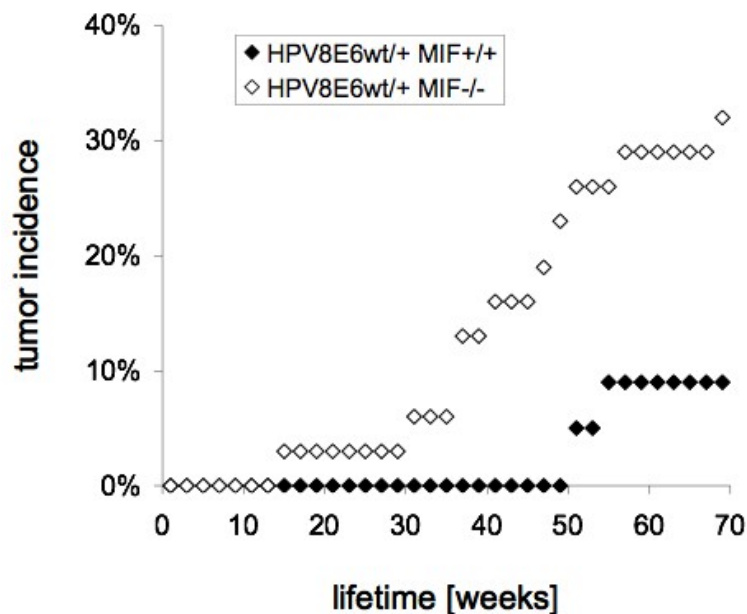
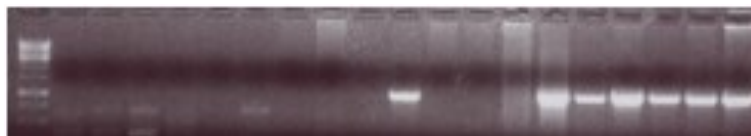


Fig. 28: Tumor incidence during HPV8-GFR-induced tumor formation. 31 K14HPV8-CER^{+tg} mif^{-/-} and 22 K14HPV8-CER^{+tg} mif^{+/+} mice were observed for a maximum of 70 weeks. K14HPV8-CER^{+tg} mif^{-/-} mice developed epithelial tumors earlier in age (week 16) and at higher incidence (32.3%) compared to the K14HPV8-CER^{+tg} mif^{+/+} control mice (week 52) (8.7%). At the end of the experiment, there was a 3.7-fold difference of tumor incidence between the two genotypes ($p < 0.0001$ in a Pearson χ^2 test).

Taken together, our results from both chemical carcinogenesis and HPV oncoprotein-induced tumorigenesis provide genetic proof that MIF acts as a tumor-preventing chemokine in the murine epidermis.

3.8 THE GENERATION OF MICE WITH EPIDERMIS-SPECIFIC DEFICIENCY OF WAS ONLY PARTIALLY SUCCESSFUL, AS IT WAS NOT POSSIBLE TO GENERATE A SUFFICIENT NUMBER OF AGE- & SEX-MATCHED MICE TO START A CHEMICAL SKIN TUMOR INDUCTION

MIF is ubiquitously expressed and therefore all cells of the skin such as keratinocytes, immune cells and fibroblasts are known to produce MIF. In order to determine whether the observed phenotype of MIF is due to keratinocytic MIF, the generation of mice with a keratinocyte-specific deletion of *mif* was started. To this end, *K14-cre^{+tg}* (Tg(KRT14-cre)1Amc/J, donated by Andrew McMahon, Harvard, through Prof. Carien Niessen and MD Dr. Axel Roers, Cologne) mice were cross-bred with floxed *mif* mice (*mif^{f/f}*). The *cre* transgene was kept in a heterozygous status in order to avoid any phenotype artifacts.



*Fig. 29: Genotyping offspring of the *K14-cre^{+tg} mif^{-/-}* breedings for its Cre status. A 1 kb ladder was used as standard and genomic DNA probes isolated from mouse tail biopsies were loaded on an 1.5% agarose gel. The size of the expected fragment was 1000 bp. The *K14 cre⁺* probes show a strong signal on the same level as the more intensive band of the ladder, which corresponds to 1000 bp. The other lanes are void meaning that the loaded probe was *K14-cre⁻*.*

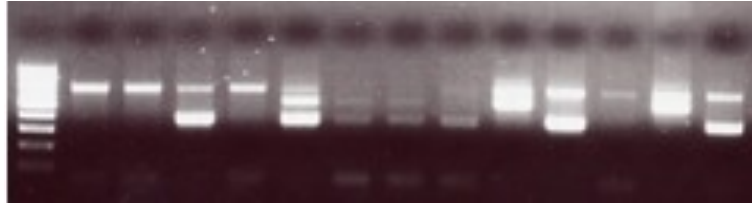


Fig. 30: Genotyping offspring of the K14-cre^{+tg} mif^{-/-} breedings for their mif status. A 1 kb ladder was used as standard and genomic DNA probes isolated from mouse-tail biopsies were loaded on an 1.5% agarose gel. The sizes of the expected fragments could be 383, 544 and 683 bp. Lane 2, e.g., the band representing a mif^{fl/fl} mouse. Lane 4 shows the genotyping result for a mif^{fl/+} mouse, lane 6 the one for a mif^{+fl/Δepi}, which is a mif WT mouse with epidermis-specific deletion of the mif gene. The last lane tells how the genotyping result for a mif^{fl/-} looked like.

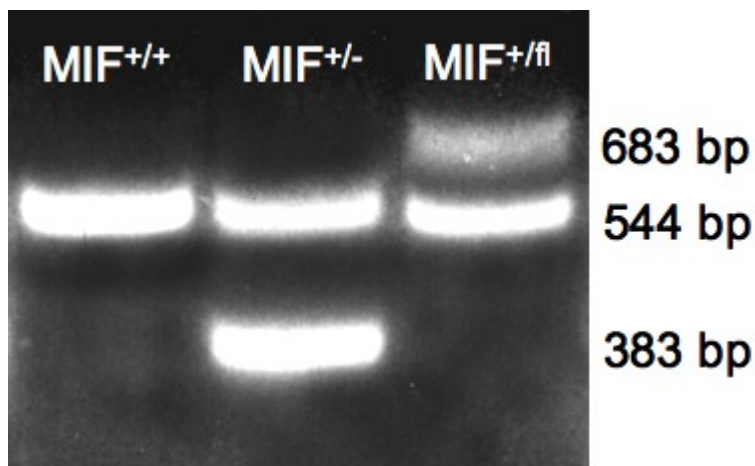


Fig. 31: Possible fragment sizes in an agarose gel after a PCR on murine genomic DNA with primers A, B and C for the determination of the mif status. Mice can be homozygous (lane 1) or heterozygous for mif (lane 2) or have a wild-type allele in combination with a floxed one (lane 3) when they are mif^{+fl}. The corresponding sizes to the fragments are indicated on the right.

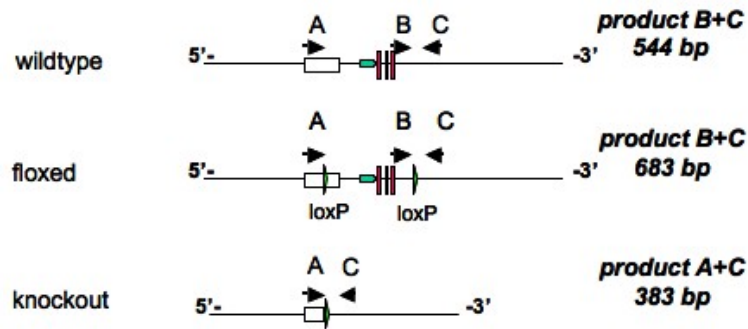


Fig. 32: Primer design for the determination of the mif status in experimental mice. The PCR mixture of reagents for genotyping such animals always contains three primers named A, B and C. A mif wild-type allele will generate a fragment of 544 bp size as result of the hybridization of primers B and C with the genomic DNA. A floxed mif allele will result in a larger fragment although primers B and C hybridize, too, but there is an additional loxP site in between. A mif knockout allele is identified by a fragment of 383 bp size, since primers A and C can hybridize with the genomic DNA where the part between the two loxP sites had been excised.

It was very difficult to breed these animals due to very low numbers of offspring and during the given time for this thesis, it was not possible to achieve sufficient numbers of animals to start a carcinogenesis experiment. Only after breeding support by Charles River, Inc mice numbers expanded, but starting time for any experiment with these mice was unfortunately too close to the deadline of the animal experiment protocol permission provided through the Animal Research Committee and to the end of this thesis.

3.9 EXPRESSION PATTERN OF MIF IN MURINE SKIN SHOWS HIGH PROTEIN LEVELS IN KERATINOCYTES COMPARED TO THOSE IN DERMAL CELLS

The detection of MIF in murine skin by immunofluorescence revealed a relatively strong expression by keratinocytes when compared to dermal fibroblasts (Fig. 34). The strong signal was not limited to the intrafollicular epidermis (IFE), but also found in follicular keratinocytes of the outer root sheath (ORS), the bulb, the matrix and in sebocytes of the sebaceous gland (Fig. 33).

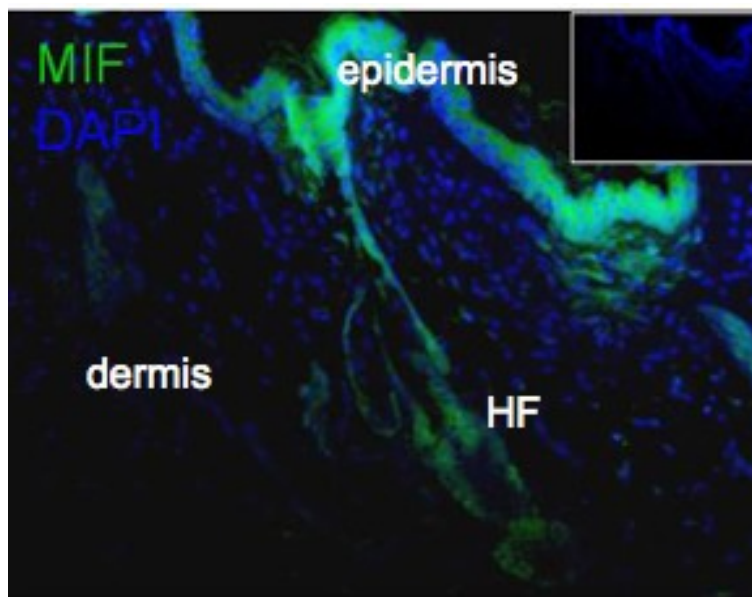


Fig. 33: Immunofluorescent detection of MIF. A paraffin-embedded tissue sample of murine normal wild-type skin was incubated with a full-length antibody against human and murine MIF. The secondary antibody was coupled to the fluorophore Alexa Fluor 488. DAPI was used as nuclear counterstain. Insert shows negative control in which the primary antibody was omitted. Magnification 200x.

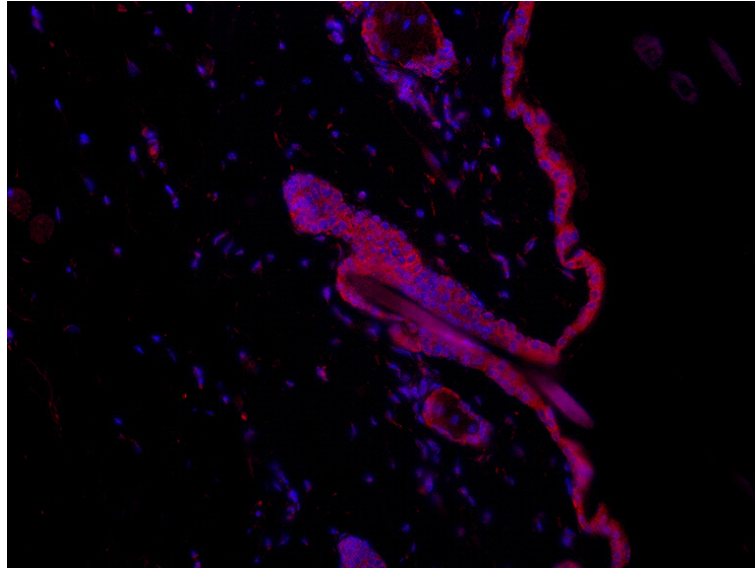


Fig. 34: Immunofluorescent detection of MIF in murine skin. The expression intensity of MIF in the epidermis is very strong compared to the signal in dermal cells. The MIF protein was detectable in keratinocytes of the interfollicular epidermis and the hair follicle. This time a secondary antibody emitting in the red spectrum was used for coupling to the first against MIF (Alexa Fluor 546). Magnification 200x.

3.10 IMMUNOHISTOCHEMICAL DETECTION OF MIF EXPRESSION IN MURINE SKIN REVEALS NUCLEAR SIGNALS IN KERATINO- AND SEBOCYTES OF DIFFERENT INTENSITIES

The analysis of MIF expression by immunohistochemistry in samples of dorsal and ventral skin from wild-type mice confirmed the expression pattern seen by immunofluorescence. In addition, it revealed a clear nuclear signal of MIF protein expression (Fig. 35). Nuclear expression of MIF was seen with three anti-MIF antibodies.



Fig. 35: Immunohistochemical detection of MIF in the normal murine skin. MIF expression in dermal fibroblasts is low (tissue layer underneath the epidermis). MIF expression intensity varies among the epidermal keratinocytes. Some cells are negative for any MIF signal, some show strong nuclear MIF expression (arrows), some a weaker nuclear, but cytoplasmic signal. Insert shows negative control in which the first antibody was omitted. Magnification 400x.

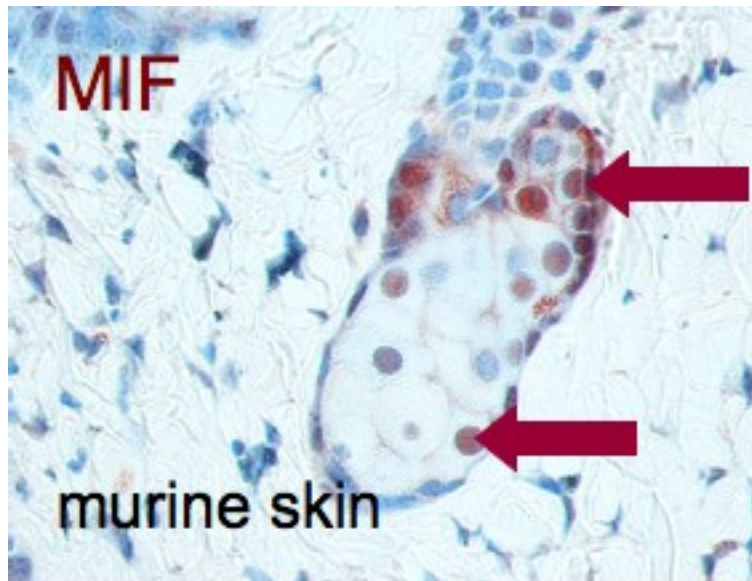


Fig. 36: Immunohistochemical detection of MIF. The sebocytes of the sebaceous gland, as adjacent structure of the hair follicle with their large cytoplasm containing sebum for secretion, show a strong nuclear MIF signal and the basaloid, quiescent and undifferentiated sebocyte precursor cells (upper arrow) display a cytoplasmic expression as well. Magnification 400x.

3.11 NUCLEAR MIF WAS DETECTED AND CONFIRMED BY WESTERN BLOT

In order to use another method than immunohistochemistry to verify the finding of nuclear MIF, cell lysates were prepared from HaCaT cells (a human immortalized keratinocyte cell line), as well as keratinocytes isolated from MIF-deficient and MIF^{+/+} mice. The nuclear fraction was separated from the cytoplasmic fraction and loaded onto a gradient gel. The Ponceau S staining in Fig. 37 confirmed successful semi-dry protein transfer.

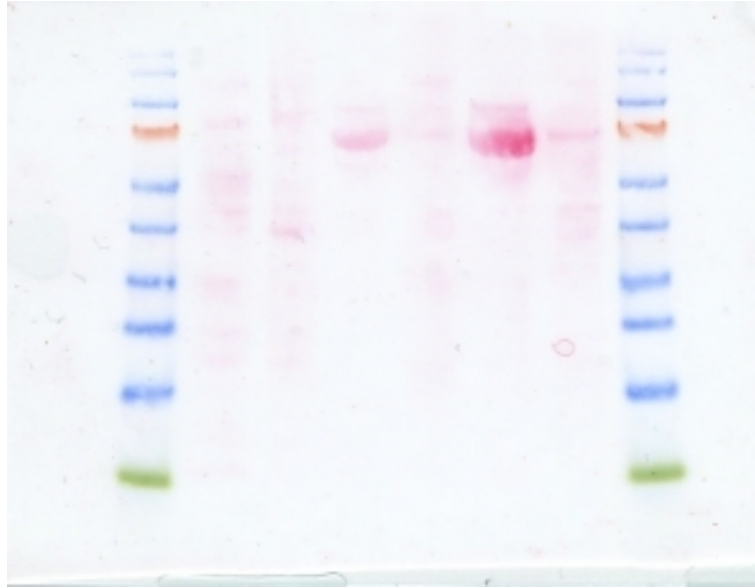


Fig. 37: Ponceau S staining after the semi-dry protein transfer of the cytoplasmic and nuclear fraction of a HaCaT cell lysate in lanes 2 & 3, the cytosolic and nuclear fraction of a MIF^{-/-} primary murine keratinocyte cell lysate in lanes 4 & 5 and the cytoplasmic and nuclear fraction of a MIF^{+/+} primary keratinocyte cell lysate in lanes 6 & 7. The protein standard was run in lanes 1 and 8. 20 µg protein of each fraction was loaded.

PARP, Poly(ADP-ribose) polymerase is constitutively expressed in the nucleus. β -Actin and β -tubulin as cytoskeleton components are expressed in the cytoplasmic compartment. Purity of nuclear and cytoplasmic fractions was confirmed by western blotting using antibodies against PARP and β tubulin (Fig.s 39 and 40).

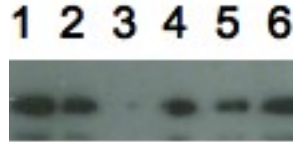


Fig. 38: Western blot for β actin in cytoplasmic and nuclear fractions of cell lysates of HaCaT cells, $MIF^{-/-}$ and $MIF^{+/+}$ keratinocytes. Anti-mouse β actin was used as loading control for all probes.



Fig. 39: Western blot for PARP in cytoplasmic and nuclear fractions of cell lysates of HaCaT cells, $MIF^{-/-}$ and $MIF^{+/+}$ keratinocytes. Incubation of the membrane with the antibody against human PARP shows a band in lane 2 and 6. There is no visible band in lane 4, although a nuclear cell lysate fraction had been loaded. The reactivity of this antibody on mouse tissue is undergoing a test phase, but it was said to cross-react with mouse protein. The reactivity could not be confirmed in the Western blots presented here.



Fig. 40: Western blot for β -tubulin in cytoplasmic and nuclear fractions of cell lysates of HaCaT cells, $MIF^{-/-}$ and $MIF^{+/+}$ keratinocytes. Incubation of the membrane with the antibody against human β -tubulin shows a band in lane 1. There are no visible bands in lane 3 and 5, though cytoplasmic fractions had been loaded. The antibody has been shown to react with mouse protein, but this could not be confirmed here.

The incubation with two different antibodies resulted in a strong signal for cytoplasmic MIF in HaCaT cells (lane 1 in Figures 41 and 42) and a weak band

for nuclear MIF in both cases (lane 2 in Figures 41 and 42). The cytoplasmic fraction of MIF WT keratinocytes displayed a weak band when incubated with the Ka565 antibody (kindly provided by J. Bernhagen, RWTH Aachen) (Fig. 42).



Fig. 41: Western blot for MIF in cytoplasmic and nuclear fractions of cell lysates of HaCaT cells, MIF^{-/-} and MIF^{+/+} keratinocytes. Incubation of the membrane with the antibody against MIF produced by Zymed shows a strong band in lane 1 and a weak band in lane 2, but not in lanes 5 and 6 though expected.



Fig. 42: Western blot for MIF in cytoplasmic and nuclear fractions of cell lysates of HaCaT cells, MIF^{-/-} and MIF^{+/+} keratinocytes. Incubation of the membrane with the Ka565 antibody against MIF, purified by Jurgen Bernhagen, RWTH Aachen, shows a band in lane 1. There are weak bands in lanes 2 and 5, but not in lane 6 although expected due to too little protein amounts of the murine lysates loaded.

The above Western blots show that the fractioning of cytoplasmic and nuclear protein lysates only worked for the HaCaT cell line (lanes 1 and 2), but not for the primary murine keratinocytes. The Ponceau S staining demonstrates very intense bands for the cytoplasmic murine lysates and that is why the protein estimation for these samples led to false values, resulting in too little protein amounts being loaded onto the gels. As the mere proof of nuclear MIF in any

keratinocytic cells was sufficient for a qualitative statement, no further immunoblottings were performed.

3.12 NUCLEAR MIF EXPRESSION IN HACAT CELLS, MURINE SKIN AND SKIN TUMORS WAS CONFIRMED BY CONFOCAL MICROSCOPY

To confirm the observation of a nuclear signal of MIF expression in keratinocytes, Z-stacks of HaCaT cells were collected with a confocal microscope. These cells are an immortalized human keratinocytic cell line derived from a cervical carcinoma. With three different antibodies applied, the detection pattern of MIF in HaCaT cells with DAPI as counterstain, intercalating with the genomic DNA, stayed the same (data not shown). The cyan color in the middle panel of Fig. 43 demonstrates the co-localization of MIF and DAPI within the nucleus.

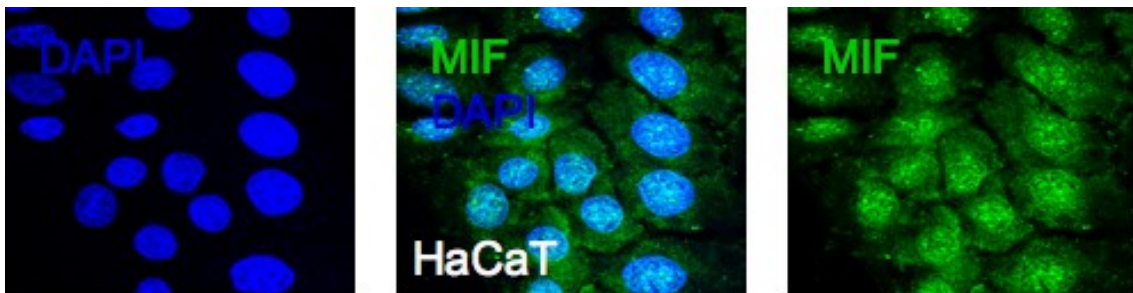


Fig. 43: MIF expression within the nucleus of HaCaT cells by immunofluorescence. HaCaT cells were incubated with DAPI (left and middle panel) and/or the antibody against MIF (middle and right panel). The Z-stacks confirm the nuclear localization of MIF, shown by the cyan color of the overlay of the blue color of DAPI and the green color of the secondary antibody coupled to the primary against MIF (Alexa Fluor 488). Magnification 400x. Pictures were taken with a confocal microscope.

Also in epidermal tumors from the chemical carcinogenesis experiments, it was possible to show that MIF was expressed within the nucleus of homeostatic and transformed keratinocytes (Fig. 44).

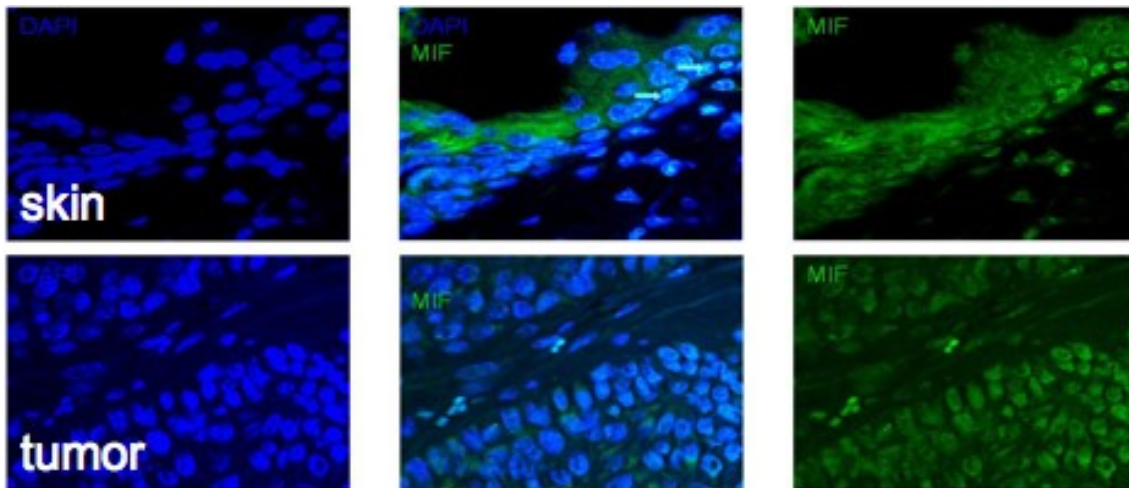


Fig. 44: Nuclear expression of MIF in normal murine skin and an epithelial tumor after chemical carcinogenesis. The tissues were incubated with DAPI (left and middle panel) and/or an antibody against MIF (middle and right panel). The small arrows indicate the cyan color of the overlay of the blue color of DAPI and the green color of the secondary antibody coupled to the primary against MIF (Alexa Fluor 488). Magnification 400x. Pictures were taken with a confocal microscope.

3.13 PRESENTATION OF THE METHOD HOW MIF EXPRESSION AT CYTOPLASMIC AND NUCLEAR LEVELS IN SINGLE CELLS OF HOMEOSTATIC AND NEOPLASTIC EPIDERMIS WAS HISTOPATHOLOGICALLY EVALUATED

Epidermal and dermal skin are comprised of several cell types with various expression levels of MIF in the cytoplasm and nucleus. Thus, scoring of MIF expression by Western blotting in total lysates is not likely to give clear and

relevant results with respect to MIF expression within tumor cells and intracellular compartments. Therefore, an immunohistopathological scoring system was developed and used to evaluate nuclear and cytosolic signal MIF expression levels of single cells. Expression levels were scored 'strong', 'medium', 'weak', or 'no expression' (Fig. 45).

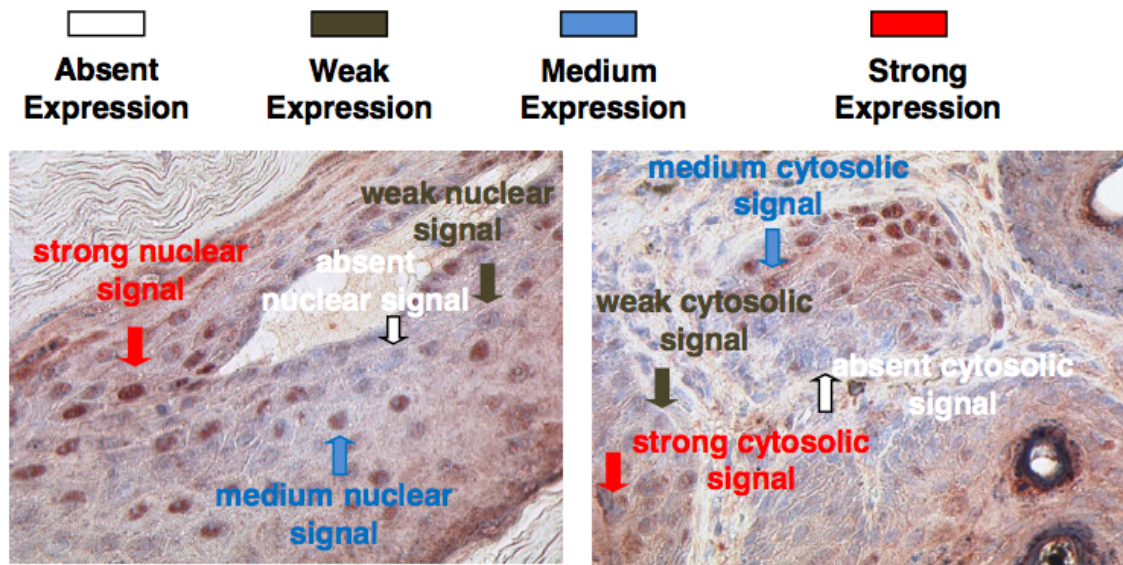


Fig. 45: Determination of the cytosolic and nuclear MIF expression intensity by immunohistochemical detection of the MIF protein. The arrows indicate a representative example for each classification. Left panel: nuclear signal intensities, right panel: cytosolic signal intensities. The tissue sample shows a tumor of a MIF WT mouse after chemical carcinogenesis.

3.14 HISTOPATHOLOGICAL SCORE OF MIF EXPRESSION AT CYTOSOLIC AND NUCLEAR LEVELS IN SINGLE CELLS OF HOMEOSTATIC AND NEOPLASTIC EPIDERMIS REVEALS THE DIMINISHMENT OF THE STRONG NUCLEAR MIF SIGNAL IN MURINE SKIN TUMOR TISSUE

The diagram in Fig. 46 reveals the signal strength of nuclear and cytosolic MIF expression in the homeostatic epidermis and the tumor tissue after chemical induction of skin tumors, as described in Chapter 2.17, on the basis of the defined score presented in the previous paragraph.

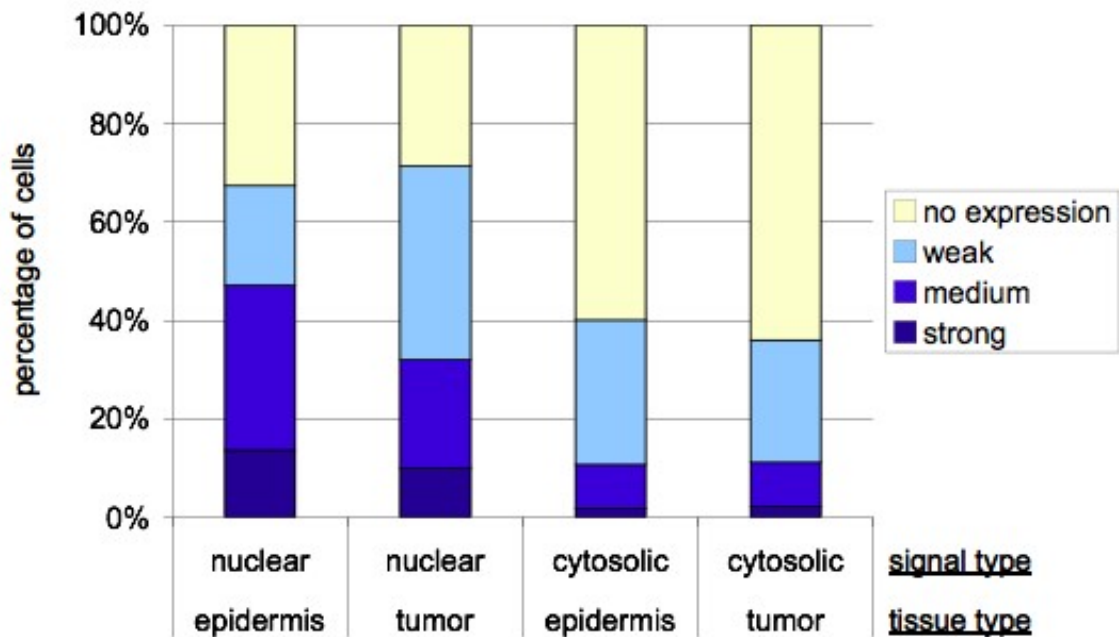


Fig. 46: Immunohistochemical signal intensity of nuclear and cytosolic MIF expression in homeostatic epidermis and tumor tissue after chemical induction of skin tumors with DMBA/TPA, as described in Chapter 2.17, on the basis of the defined score presented in Fig. 45. Nuclear MIF expression in epidermis vs. tumor has a p value of 0.036 in a Student's t test; cytosolic MIF expression in epidermis vs. tumor has a p value of 0.405 in a Student's t test.

Comparing non-tumoral epidermis and tumor tissue, a 4% reduction of strong, a 12% reduction of medium and a 4% reduction of the fraction of cells with no MIF expression was found in tumor tissue, while the fraction of cells with weak nuclear MIF expression was increased by 19%. The fractions of cells with strong and medium cytoplasmic MIF expression did not differ between normal and neoplastic tissues, while the fraction of malignant cells with weak cytoplasmic MIF expression was reduced by 5%. The percentage of malignant cells that did not show any signal of MIF expression was increased by 4%.

These findings show that nuclear MIF expression significantly diminishes within the tumor tissue ($p = 0.036$ in a Student's t test), whereas there is no significant change in MIF expression of cytosolic level upon/after tumorigenesis.

3.15 EXPRESSION OF JAB1, THE INTRACELLULAR BINDING PARTNER FOR MIF, IN MURINE SKIN IS MAINLY CYTOPLASMIC IN KERATINOCYTES, BUT ALSO OCCURS IN SEBACEOUS NUCLEI

To find out whether the distribution of MIF's intracellular binding partner JAB1 is the same as for MIF itself, JAB1 was immunohistochemically detected in murine wild-type skin. JAB1 is expressed predominantly within the cytoplasm of keratinocytes. A clear nuclear signal is completely absent in the interfollicular epidermis, but present in the nuclei of sebocytes (arrows in Fig. 47).

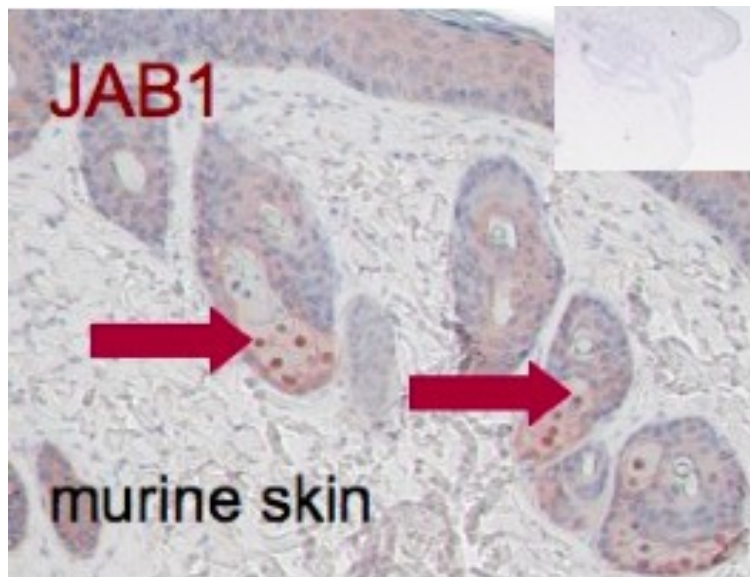


Fig. 47: Immunohistochemical detection of JAB1 expression in murine skin. JAB1 shows an ubiquitous, but weak expression in epidermal keratinocytes, but a strong nuclear expression in sebocytes of the sebaceous gland (arrows). Insert shows negative control in which the first antibody was omitted. Magnification 200x.

3.16 COMPARISON BETWEEN JAB1 AND MIF EXPRESSION IN EPIDERMAL TUMORS OF MICE TREATED WITH CHEMICAL CARCINOGENS REVEALS NO SIGNIFICANT CHANGES REGARDING THE EXPRESSION PATTERN OF JAB1 COMPARED TO HOMEOSTATIC SKIN

A comparison of the expression of MIF and its intracellular binding partner JAB1, at the magnification level used for Fig. 48, shows that the expression patterns of MIF and JAB1 are similar. The pattern of JAB1 distribution is not changed upon tumor initiation, formation, or development.

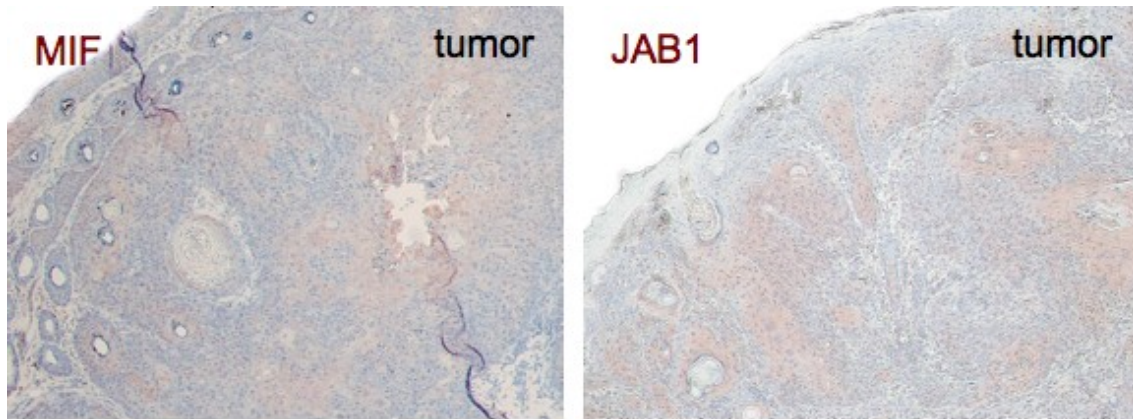


Fig. 48: Example of the expression patterns of MIF and its intracellular binding partner JAB1 in murine tumors after chemical carcinogenesis. The overall signal intensity is at the same level and weaker for MIF when compared to normal epidermis (see also Fig. 35), but similar to homeostatic conditions, as far as JAB1 is concerned. Magnification 100x.

3.17 CD44 EXPRESSION IN MURINE SKIN AND ITS TUMORS AFTER CHEMICAL CARCINOGENESIS IS UNCHANGED AND RESTRICTED TO THE BASAL EPIDERMAL LAYERS

As the expression of CD44, the co-receptor of CD74 (CD74 comprises the only surface receptor for MIF besides CXCR2/4) is known to be deregulated in many tumors, an immunohistochemical detection of its expression pattern in the tumor material after chemical skin tumor induction was performed to figure out any differences to normal epidermis. Fig. 49 shows that there is no difference in CD44 expression between homeostatic (normal) and neoplastic epidermis (tumor). The expression of the CD44 protein is limited to the basal layers and homogeneously distributed to all cells.

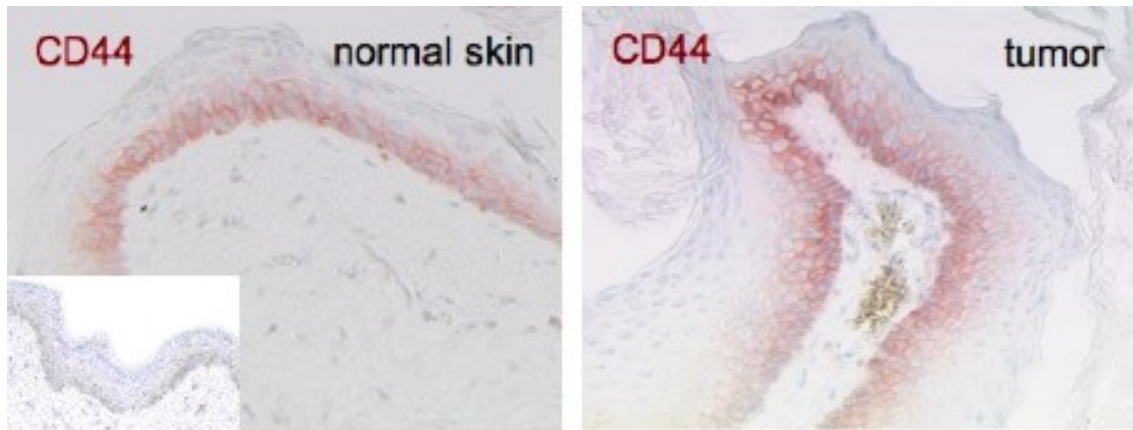


Fig. 49: Immunohistochemical detection of CD44 expression in normal murine skin and epithelial tumor tissue after chemical carcinogenesis. CD44 expression is limited to the basal layers of the epidermis. Insert shows negative control in which the first antibody was omitted. Magnification 200x.

3.18 THE MIF RECEPTOR CD74 IS EXPRESSED BY IMMUNE CELLS IN THE MURINE SKIN

CD74 is a known binding partner of MIF and primarily expressed on antigen presenting cells, including B cells, macrophages/monocytes and dendritic cells.

Fig. 50 shows how the CD74 protein is expressed in murine skin. Keratinocytes do not express CD74. There are few scattered dermal cells presenting CD74 on their surface, and only some cells embedded into the epidermis stain positive for CD74 (Fig. 50).

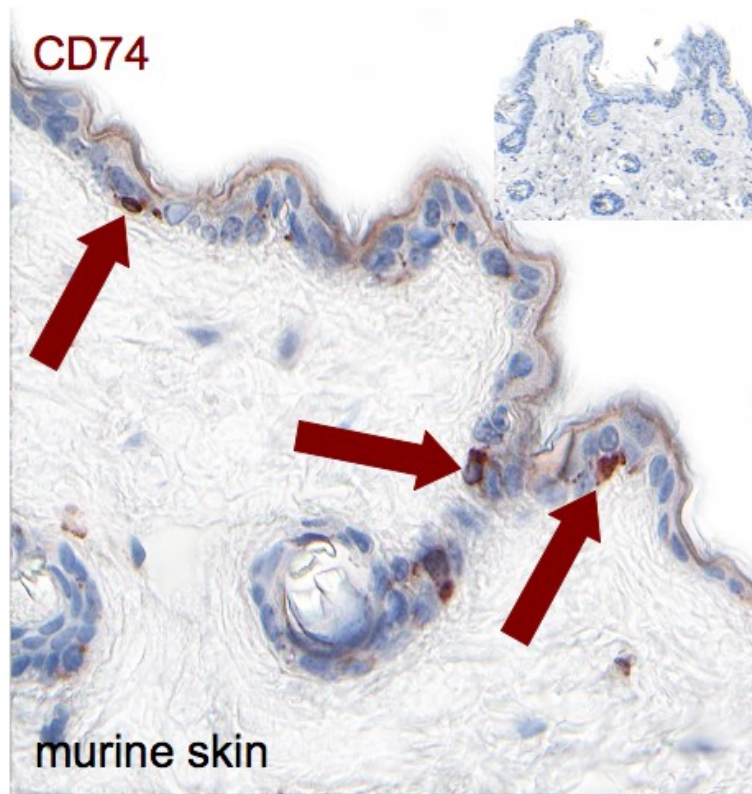


Fig. 50: Immunohistochemical detection of CD74 expression in normal murine skin. CD74 expression is only detectable in a few epidermal cells (arrows), potentially cells of the immune system. Insert shows negative control in which the first antibody was omitted. Magnification 400x.

3.19 IMMUNOHISTOCHEMICAL DETECTION OF CD74 EXPRESSION IN MURINE SKIN TUMORS AFTER CHEMICAL CARCINOGENESIS SHOWS LESS CD74-POSITIVE CELLS IN MIF-DEFICIENT TISSUE

A comparison of the left and right panel of Fig. 51 reveals that the number of CD74⁺ cells within the tumor tissue of wild-type mice after chemical carcinogenesis is higher than in MIF-deficient tissue samples (Fig. 51).

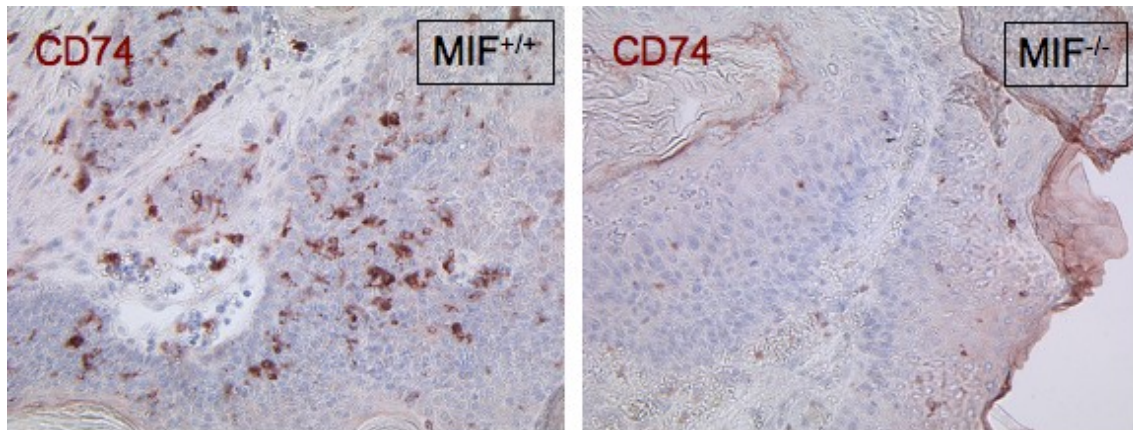


Fig. 51: Representative example of immunohistochemical detection of CD74 expression in epithelial tumor tissue after chemical carcinogenesis. The number of CD74⁺ cells in MIF WT tissue is larger than in MIF KO samples. Magnification 200x.

3.20 K14HPV8-CER-TRANSGENIC MIF-DEFICIENT MICE PRESENT A HIGHER NUMBER OF CD74-POSITIVE CELLS EMBEDDED INTO THE EPIDERMIS COMPARED TO NON-TRANSGENIC MIF KO MICE, AS UNRAVELED BY IMMUNOHISTOCHEMICAL DETECTION

The immunohistochemical detection of CD74-expressing cells in K14HPV8-CER-transgenic MIF-deficient tissue samples revealed that the number of such cells in these animals is higher compared to non-transgenic animals (33% to 6%). This finding will be discussed.

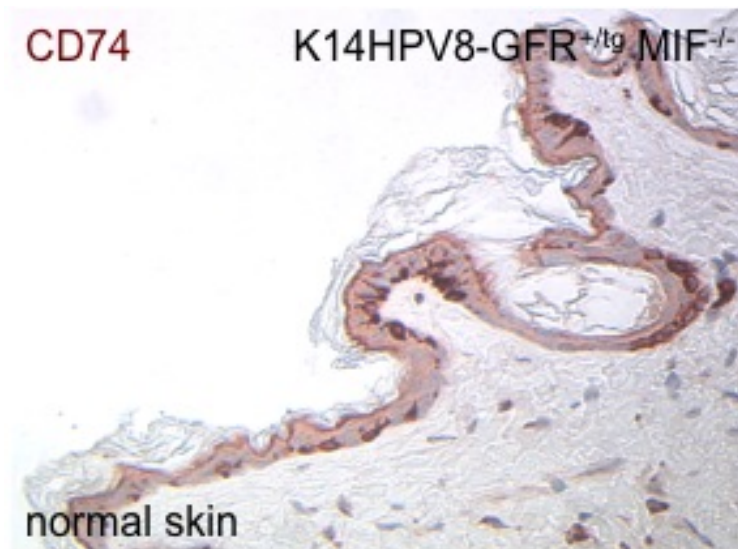


Fig. 52: Immunohistochemical detection of CD74 expression in the skin of K14HPV8-CER-transgenic MIF KO mice. Magnification 200x.

3.21 IMMUNOHISTOCHEMICAL DETECTION OF B CELLS BY B220 (CD45R) EXPRESSION IN MURINE SKIN AFTER CHEMICAL CARCINOGENESIS PRESENTS INCREASED INVASION OF B CELLS INTO MIF-DEFICIENT SKIN TUMOR TISSUE

B220 or CD45R is required for T cell activation through the antigen receptor. It is a receptor type protein tyrosine phosphatase (PTP) and its gene is specifically expressed in hematopoietic cells and a well-established marker for B cells.

The comparison between the left and the right panel of Fig. 53 reveals that there are more B cells leaving the tumor stroma and invading the MIF-deficient tumor tissue compared to wild-type control samples.

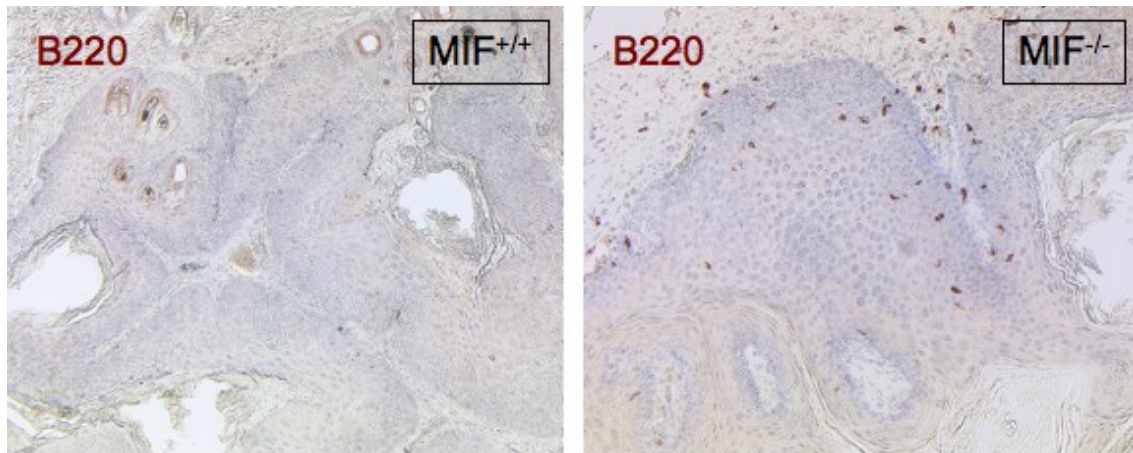


Fig. 53: Representative example for the immunohistochemical detection of B220 (CD45R)-expressing cells in epithelial tumor tissue after chemical carcinogenesis. The amount of B220⁺ cells in MIF-deficient tissue is higher than in MIF WT samples. Magnification 200x.

3.22 IMMUNOFLUORESCENT DETECTION OF F4/80-EXPRESSING CELLS IN MURINE SKIN BEFORE AND AFTER CHEMICAL CARCINOGENESIS IMPRESSES BY AUGMENTED ACCUMULATION OF F4/80-POSITIVE CELLS IN THE TUMOR STROMA

F4/80 is expressed on the surface of murine macrophages, but not by lymphocytes or polymorphonuclear cells. As seen in Fig. 54, few epidermal cells in murine skin are positive for F4/80 as well as some dermal cells.

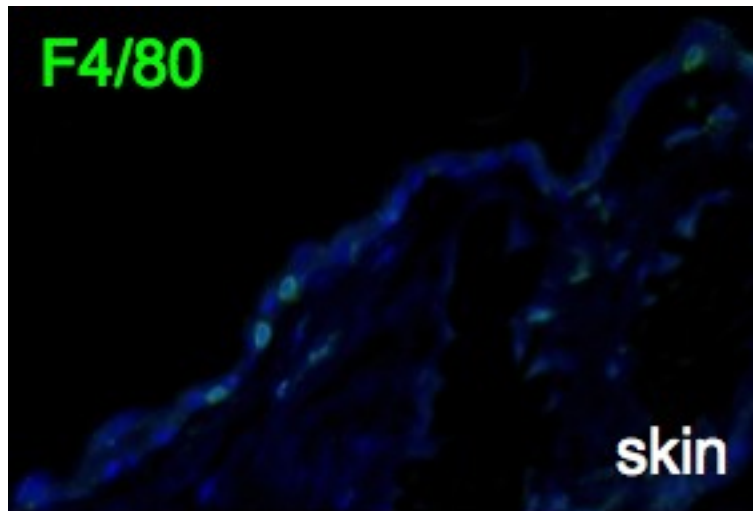


Fig. 54: Representative example for the detection of F4/80 expressing cells by immunofluorescence in murine skin. There are a few F4/80⁺ cells embedded into the epidermis as well as in the dermis. The secondary antibody was conjugated to Alexa Fluor 488 (emitting green light). Magnification 400x.

Consistent with the notion of an immune reaction to an epidermal tumor, the number of F4/80⁺ cells in the stroma surrounding a tumor, induced by chemical carcinogenesis, is increased, whereas the amount of F4/80⁺ cells within the tumor tissue seems unchanged (Fig. 55). A statistical analysis of the data can be found in Fig. 60.

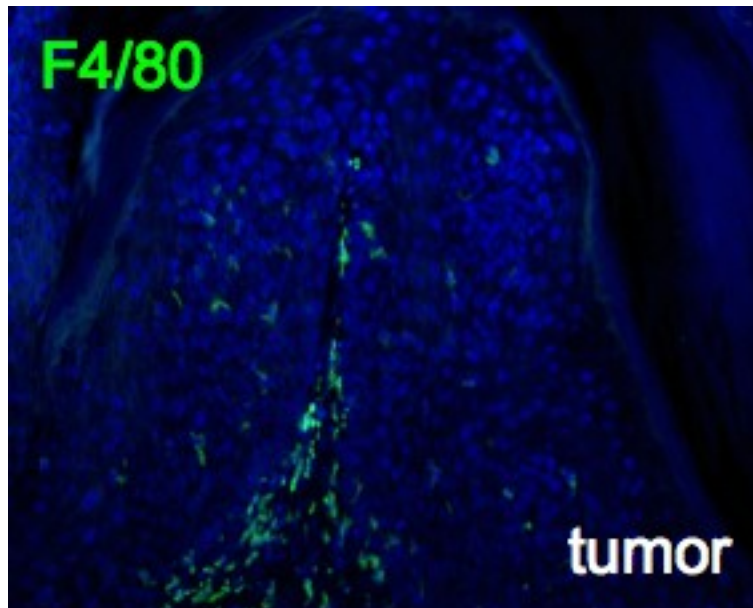


Fig. 55: Example for the spatial distribution of F4/80⁺ cells in murine skin tumors after chemical carcinogenesis. Most F4/80⁺ cells accumulate within the stroma surrounding the tumor and only few invade the tumor tissue. The secondary antibody was conjugated to Alexa Fluor 488 (emitting green light). Magnification 400x.

3.23 IMMUNOHISTOCHEMICAL DETECTION OF F4/80 EXPRESSION IN THE ASYMPTOMATIC SKIN OF K14HPV8-CER-TRANSGENIC MIF-DEFICIENT MICE AND ITS NEOPLASIA SHOWS SIMILAR AMOUNTS OF F4/80-POSITIVE CELLS RELATIVE TO COMPARABLE TISSUES OF NON-TRANSGENIC MIF KO MICE

Fig. 56 shows F4/80-expressing cells in the epidermis of K14HPV8-CER-transgenic mice on a MIF-deficient background. The number of F4/80⁺ cells in these animals is comparable to numbers in non-transgenic MIF wild-type mice (data not shown). But, it seems as if the percentage of F4/80-positive cells within the tumor tissue (Fig. 57) of these transgenic animals with MIF-deficient genetic background is comparable than in those, which are MIF-deficient, but

non-transgenic (K14HPV8-CER^{+tg} MIF KO epidermis: 7%; K14HPV8-CER^{+tg} MIF KO tumor: 11%; MIF KO epidermis: 12.4% ± 11.5%; MIF KO tumor: 1.4% ± 1.5%).

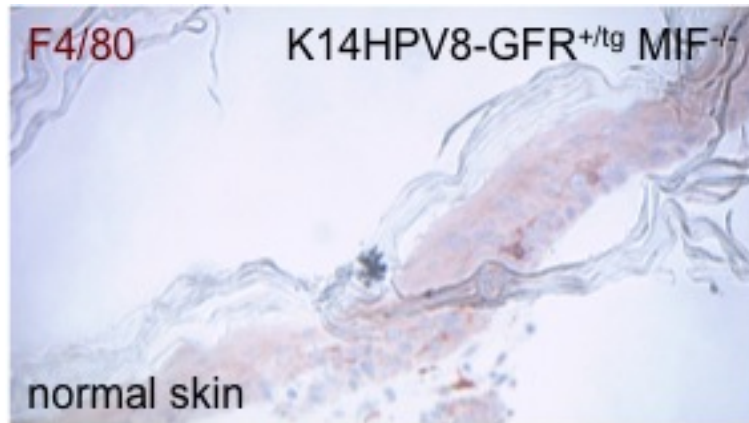


Fig. 56: Immunohistochemical detection of F4/80 expressing cells in the epidermis of K14HPV8-CER-transgenic MIF KO mice. Magnification 200x.

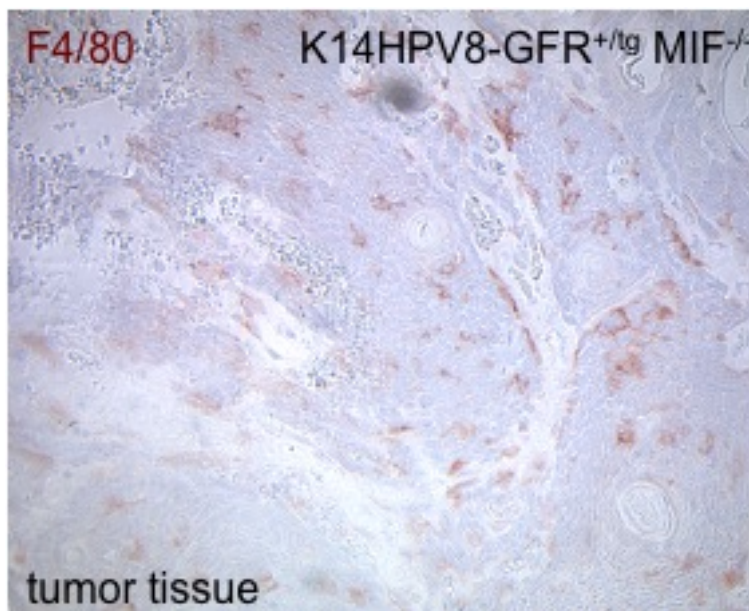


Fig. 57: Immunohistochemical detection of F4/80 expressing cells in an epithelial tumor of K14HPV8-CER-transgenic MIF KO mice. Magnification 100x.

3.24 IMMUNOFLUORESCENT DETECTION OF CD3 EXPRESSING T CELLS IN MURINE SKIN BEFORE AND AFTER CHEMICAL CARCINOGENESIS REVEALS NO APPARENT INCREASE OF T CELL NUMBERS IN TUMOR TISSUE

CD3 is specifically expressed on peripheral T lymphocytes. CD3⁺ cells were very rare in the epidermis, but a few were found in the dermal tissue (Fig. 58).

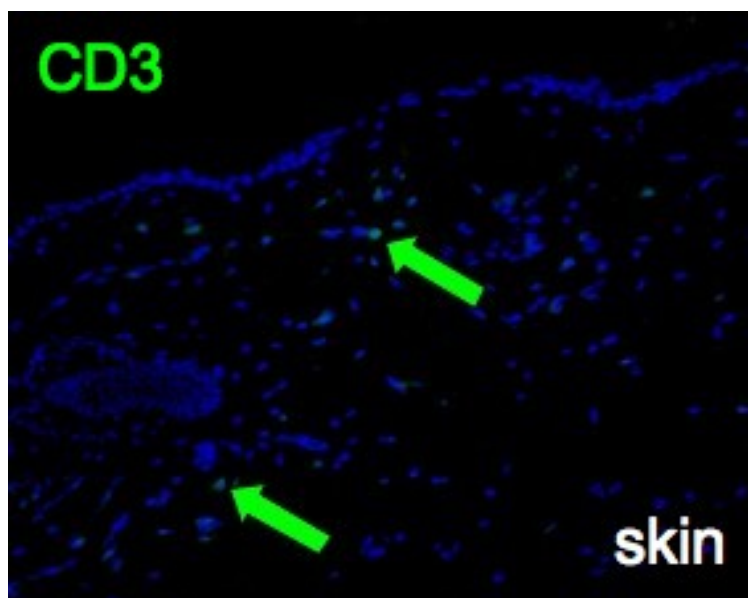


Fig. 58: Immunofluorescent detection of CD3 expressing T cells in murine skin. There are only very few CD3⁺ cells detectable in the dermis (arrows). The secondary antibody was conjugated to Alexa Fluor 488 (emitting green light). Magnification 200x.

No apparent increase in CD3⁺ cell numbers in the tumor or stromal tissue after chemical carcinogenesis (Fig. 59) was found at first sight.

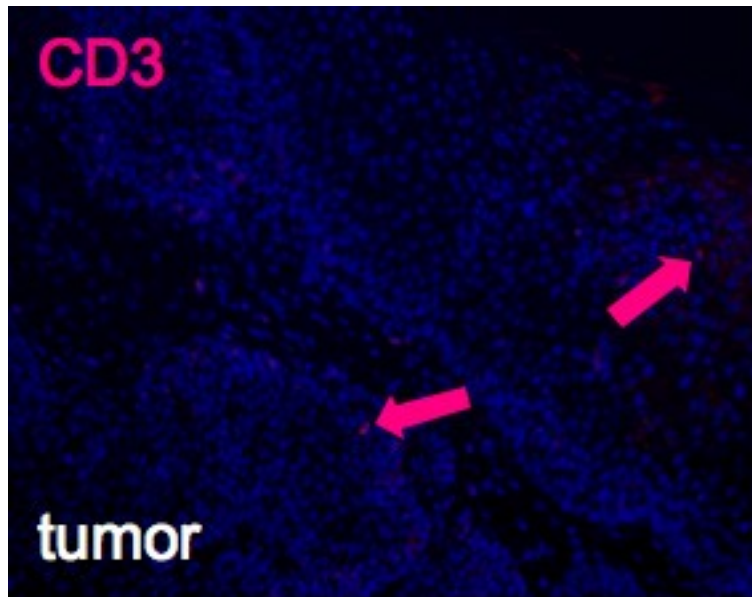


Fig. 59: Immunofluorescent detection of CD3 expressing cells in murine skin tumors after chemical carcinogenesis. There are very few CD3⁺ cells detectable in the tumor tissue (arrows). The secondary antibody was conjugated to Alexa Fluor 546 (emitting red light). Magnification 200x.

3.25 THE ANALYSIS OF THE PROPORTIONS OF IMMUNE CELLS IN HOMEOSTATIC EPIDERMIS AND DERMIS TO TUMOR AND STROMAL TISSUE IN COMPARISON REVEAL MASSIVE DIFFERENCES BETWEEN MIF-DEFICIENT AND WILD-TYPE CONTROL MICE

Since the immune system plays a pivotal role for the formation and development of skin tumors, and as MIF is well known as a pro-inflammatory mediator and regulator of innate and acquired immunity, it is possible that MIF deficiency impacts quantitatively on cell numbers of the immune system. Therefore, it was attempted to assess numbers of immune cells in normal and neoplastic tissue from chemical carcinogenesis experiments.

The next two figures demonstrate the percentage of macrophages, B and T lymphocytes relative to the total number of cells within the particular tissues.

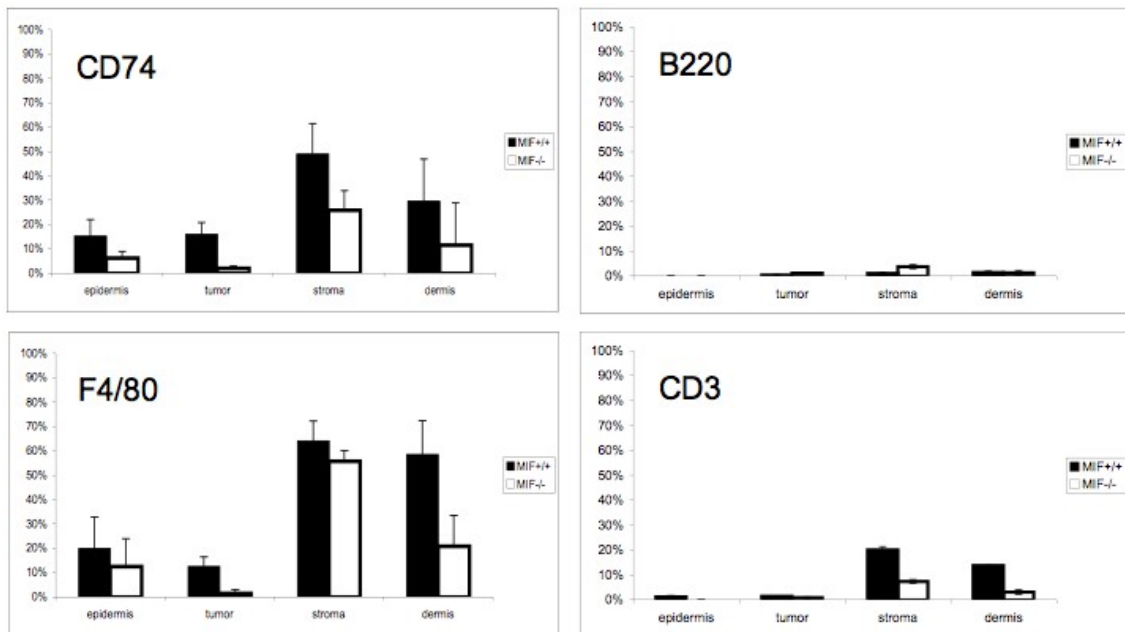


Fig. 60: Percentages of macrophages, B and T lymphocytes relative to total number of cells within particular tissues. Ordinates of panels are standardized to 100%. Percentages belonging to data of MIF wild-type mice are shown in black columns, data of MIF-deficient mice in blank columns. Epidermis = untreated, normal epidermis, tumor = epithelial part of the tumor induced by chemical carcinogenesis, stroma = dermal tissue surrounding the tumor, dermis = dermal tissue below untreated normal epidermis. Column pairs from left to right are arranged in a way epidermis and tumor are opposed and that dermis follows stroma.

The relative numbers of CD74⁺ cells (APCs) are decreased in MIF-deficient skin compared to MIF-wild-type skin. The induction of a tumor does not change this pattern. The amounts of CD74⁺ cells in the tumor stroma double those of the dermal tissue in MIF WT as well as in MIF KO samples.

The relative numbers of B220⁺ cells (B lymphocytes) are below 10% in all samples and tissues and thus a direct comparison is not possible due to low numbers.

The relative numbers of F4/80⁺ cells (macrophages) are nearly the same as the ones of CD74⁺ cells in epidermal and tumor tissue, but higher in stromal and dermal tissue. There is a slight difference between MIF WT and KO

percentages in the tumor stroma, but a statistically significant difference in the dermal tissue.

CD3⁺ cells (T lymphocytes) were two-times more frequent in stromal and dermal tissues of MIF WT animals than in tissues from than MIF-deficient mice.

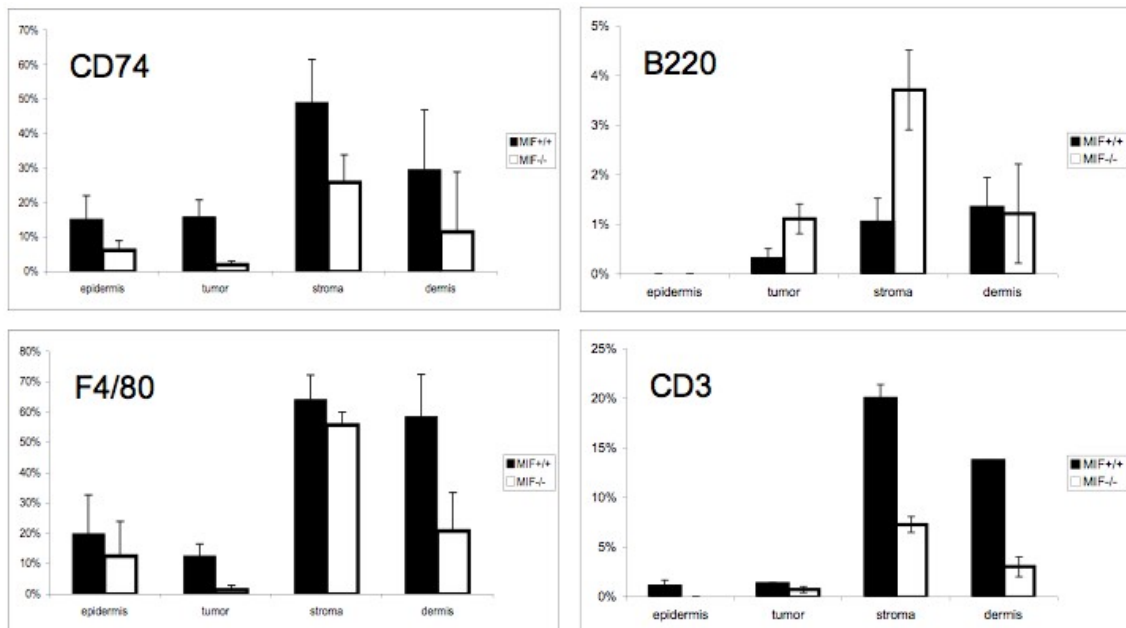


Fig. 61: Percentages of macrophages, B and T lymphocytes relative to total number of cells within particular tissues.

B220⁺ cells (B lymphocytes) are absent in the epidermis of both genotypes. There are more B cells in the tumor and stromal tissue of MIF-deficient mice than in wild-type controls, whereas the levels in the dermis are equal for both genotypes.

CD3⁺ cells (T lymphocytes) are absent in the epidermis of MIF-deficient mice, but a few are found within the tumor tissue. The levels of T cells in MIF WT mice in these two tissues remains unchanged. There is a huge difference between MIF WT and MIF KO samples of stromal and dermal tissue. Tissues of MIF WT animals bear more than twice as many T cells than MIF-deficient ones.

The upper left panels of figures 60 and 61 represent the content of CD74⁺ cells in the different tissues. The amount of CD74⁺ cells in the epidermis and tumor tissue of MIF WT mice did not differ (MIF WT epidermis: 15.1% ± 6.9%; MIF WT tumor: 15.8% ± 4.9%, $p = 0.416$), while tumor tissue from MIF KO mice showed a reduction of cell number by factor 3.2 compared to MIF WT (MIF KO epidermis: 6.1% ± 2.8%, MIF KO tumor: 1.9% ± 1.1%, $p = 0.002$). There were nearly twice as many CD74⁺ cells in the dermis and stromal tissue of MIF WT mice compared to MIF KO mice and numbers doubled upon neoplastic transformation.

The upper right panel of Fig. 60 conveys the impression that the amount of B cells in the examined tissues is very low. However, when looking at it more in detail (Fig. 61), more B cells were found in tumors and stromal tissue of MIF-deficient mice. The epidermis is generally lacking B cells and their number in the dermis of both genotypes is at same level (MIF WT epidermis: 0.0% ± 0.0%; MIF WT tumor: 0.3% ± 0.3%, $p = 0.014$; MIF KO epidermis: 0.0% ± 0.0%; MIF KO tumor: 1.1% ± 2.0%, $p = 0.104$).

The ratios between the numbers of CD74⁺ and F4/80⁺ cells in epithelial MIF WT and KO tissue are comparable. Any differences between the CD74 and F4/80 score in the dermis and tumor stroma are probably due to antibody specificities (MIF WT epidermis: 19.8% ± 12.9%; MIF WT tumor: 12.4% ± 4.0%, $p = 0.098$; MIF KO epidermis: 12.4% ± 11.5%; MIF KO tumor: 1.4% ± 1.5%, $p = 0.044$).

The percentages of CD3⁺ cells, which are shown in the lower right panels, confirm the existence of a small population of $\gamma\Delta$ T cells in the epidermis of MIF WT mice [97]. CD3⁺ cells were nearly absent in MIF KO mouse tissue specimens. MIF WT mouse tumors display double as many CD3⁺ T cells as MIF-deficient tissue samples. The cell numbers differed by a factor of 3 or 12.7% in the stromal and by a factor of 4 or 10.7% in the dermal tissue, respectively (MIF WT epidermis: 1.1% ± 1.3%; MIF WT tumor: 1.3% ± 1.0%, $p = 0.401$; MIF KO epidermis: 0.0% ± 0.0%; MIF KO tumor: 0.7% ± 1.1%, $p = 0.093$).

p values were calculated with a Student's t test each.

3.26 EPIDERMAL MOUSE KERATINOCYTES DO NOT EXPRESS CD74, BUT A SUBPOPULATION OF EPIDERMAL CELLS DOES, AND CD74-EXPRESSING CELLS INVADE THE EPIDERMIS UPON SKIN TUMOR FORMATION

It is known that keratinocytes do not express CD74 under normal conditions. Only when treated with 100 U/ml IFN- γ , CD74 mRNA was found in primary human keratinocytes (Freeman, Cardoso et al. 1998). Fig. 62 shows that epidermal CD74⁺ cells (in red) are not murine keratinocytes, because there is no co-localization with keratin 14 (in green) as keratinocyte marker. These CD74⁺ cells are embedded into the epidermis at the level of basal epidermal keratinocytes and possess morphological features of dendritic cells, as seen in the magnified excerpt.

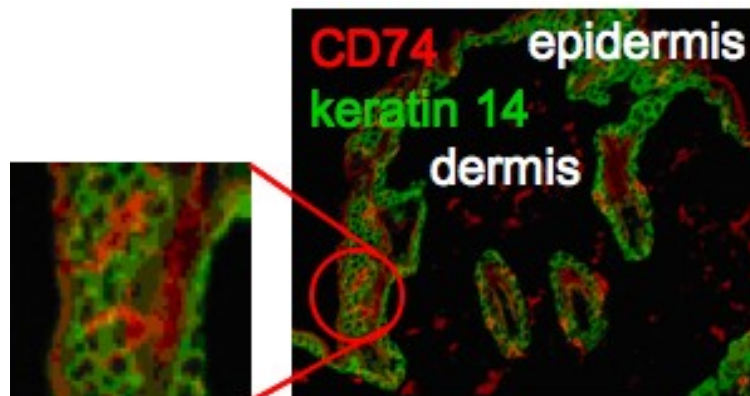


Fig. 62: CD74 expressing cells within the epidermis are negative for keratin 14 and possess features of dendritic cells in murine skin. CD74⁺ cells appear in red, keratin 14⁺ (K14) cells in green due to the choice of Alexa Fluor-coupled secondary antibodies. K14 is a marker for basal, undifferentiated keratinocytes. CD74-positive cells exhibit dendritic cell morphology (see magnified detail). Magnification 100x.

The analysis of untreated murine skin, in comparison with DMBA/TPA treated skin and the corresponding tumor material, showed that the content of CD74⁺ cells is quite low (left panel of Fig. 63), whereas there is a massive invasion of these cells into the treated skin areas and infiltration of the epidermis (middle panel of Fig. 63). The CD74⁺ cells are also able to invade the tumor tissue as shown in the right panel of Fig. 63.

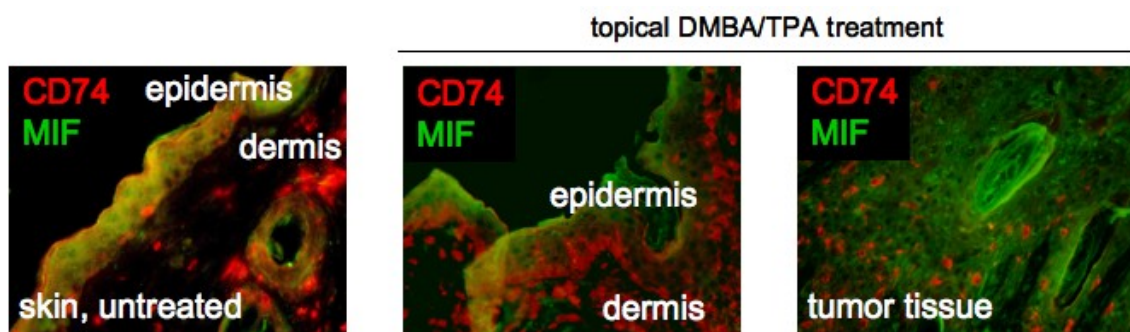


Fig. 63: Immunofluorescent analysis of CD74 and MIF expression in murine skin. CD74⁺ cells appear in red, the MIF protein in green due to the choice of Alexa Fluor-coupled secondary antibodies. There are no cells expressing CD74 and MIF, since there is no overlay of red and green, which would result in yellow (all panels). Left panel shows normal murine skin with high expression of MIF in the epidermis, few CD74-expressing epidermal cells and some in the dermis. Middle panel displays skin, topically treated with DMBA/TPA, within a neoplastic transition state. CD74⁺ cells accumulate in the dermis below the treated epidermis, and an invasion of such cells in high numbers into the epidermis is observed. Right panel shows a tumor sample after the chemical induction with DMBA/TPA where CD74⁺ cells are evenly spread within the tumor tissue. Magnification 100x.

3.27 EPIDERMAL DENDRITIC CELLS ARE POSITIVE FOR CD74 AND F4/80

As shown in Fig. 64, antibodies against CD74 and F4/80 recognize the same epidermal cell type, which differs from keratinocytes (see previous paragraph). Therefore, a double staining with both antibodies was done and analyzed. The sections show a clear overlay of both emission curves (red and green), resulting in a yellowish color in the case of double positivity.

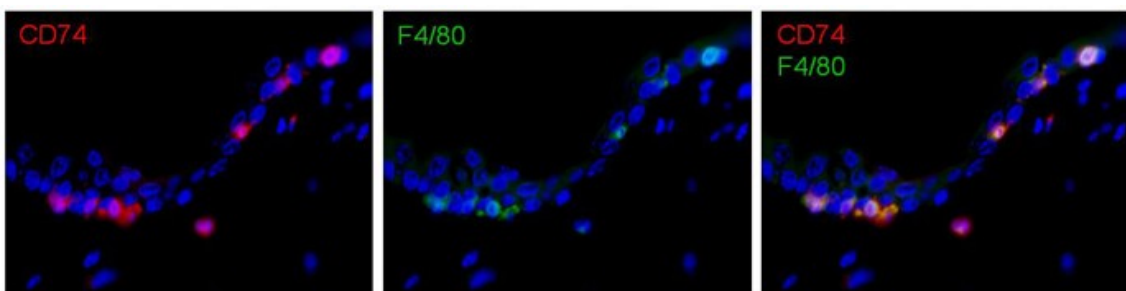


Fig. 64: Representative example for the double positivity of epidermal dendritic cells (DCs) for CD74 and F4/80 by immunofluorescence in murine epidermis. The secondary antibody for CD74 was conjugated to Alexa Fluor 546 (emitting red light), the one for F4/80 to Alexa Fluor 488 (emitting green light). A co-expression of CD74 and F4/80 by the same cell is therefore identified by the yellow color visible in the right panel. All cells, which express CD74, do express F4/80 as well. Magnification 200x.

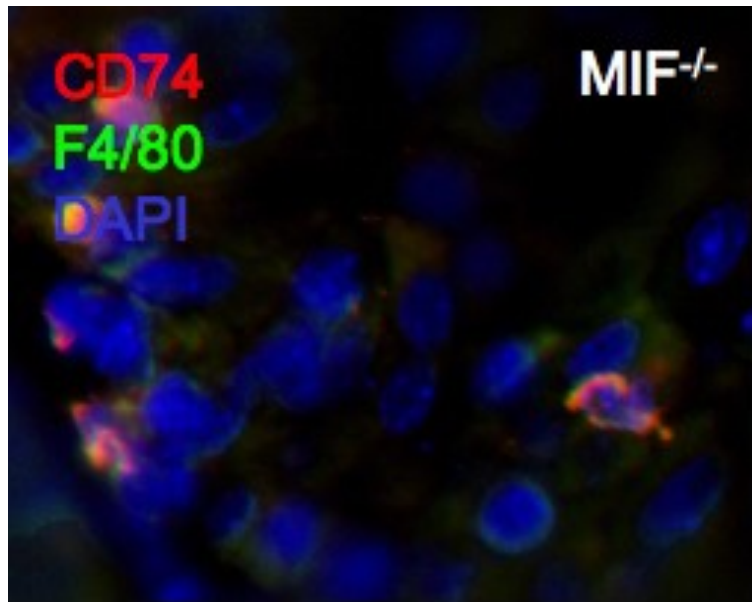


Fig. 65: Immunofluorescent analysis of CD74 and F4/80 expression in a murine skin tumor after chemical carcinogenesis at a higher magnification (400x).

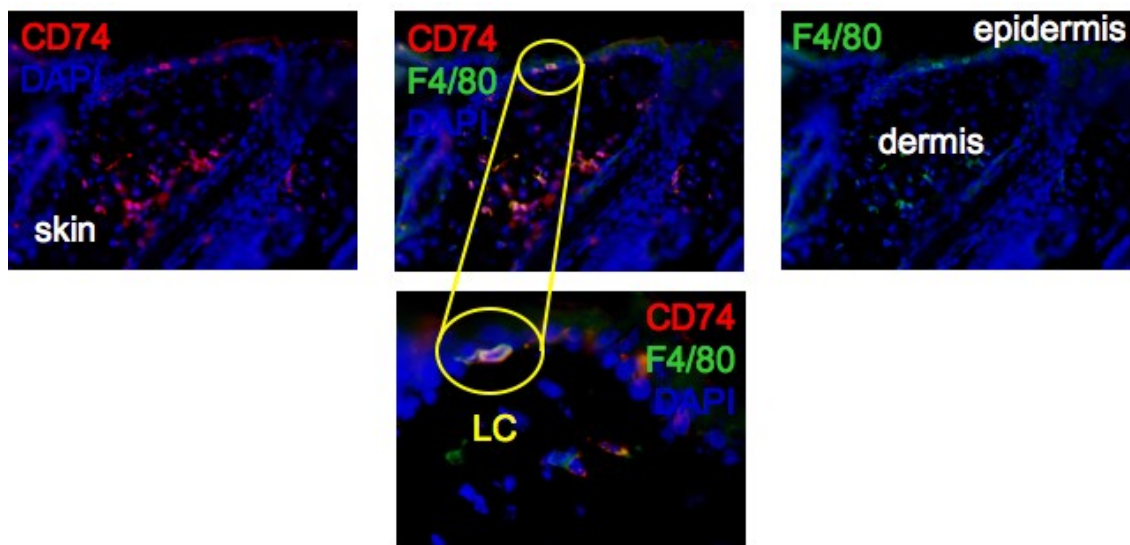


Fig. 66: Immunofluorescent analysis of CD74 and F4/80 expression in murine epidermis with emphasis on the morphology of the cell type that expresses both surface receptors. Magnification in upper panel: 200x. The magnified detail shows a highlighted CD74⁺/F4/80⁺ cell, embedded into the epidermis, and its typical morphology with dendritic extensions from the cellular body. Magnification 400x.

3.28 COMPARISON OF CD74⁺ CELL NUMBERS AFTER CHEMICAL SKIN CARCINOGENESIS WITH DMBA/TPA OR B(A)P REVEALS SIMILAR RELATIONS WITHIN MIF-DEFICIENT AND CONTROL TISSUES, AND HINTS AT A GENERAL TUMOR-PROTECTING FEATURE OF MIF IN MURINE SKIN TUMORIGENESIS AFTER CHEMICAL INDUCTION

To figure out whether there were differences in the percentages of CD74⁺ cells after chemical skin carcinogenesis with DMBA/TPA or B(α)P, two graphs, representing the DMBA/TPA and B(α)P results, were opposed for a better overview. The content of CD74⁺ cells in epidermis, dermis, tumor and stroma and the relations between the balances of such cells in wild-type and MIF-deficient tissues differ little, no matter whether the skin tumors had been induced with the combination of DMBA and TPA or B(α)P alone. The finding that MIF KO tissue contains less CD74⁺ cells both in epidermis and dermis of untreated skin or tumor is also true for the animals of B(α)P experiment.

The difference between the percentage of CD74⁺ cells in wild-type mice regarding DMBA/TPA vs. B(α)P was -4% in the epidermis, +16% in the tumor, -0.6% in the dermis and +9.5% in the stroma.

The difference between the percentage of CD74⁺ cells in MIF-deficient mice regarding DMBA/TPA vs. B(α)P was +3.4% in the epidermis, +2.6% in the tumor, +8.7% in the dermis and +20.6% in the stroma (Fig. 67).

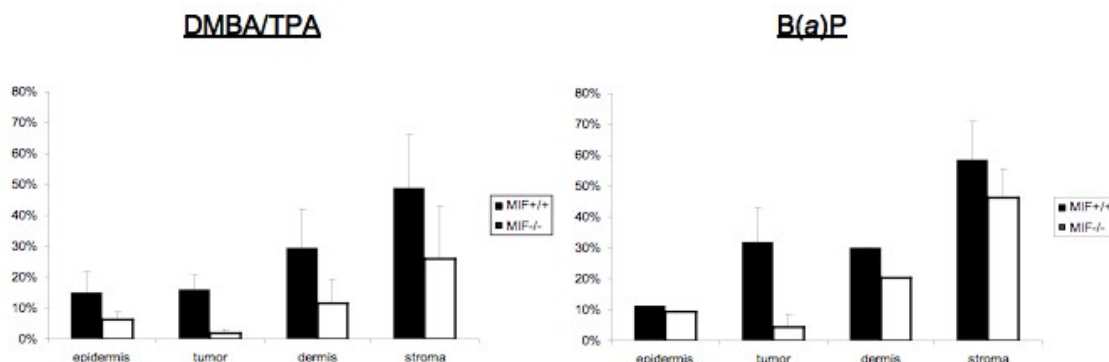


Fig. 67: Immunohistochemical evaluation of CD74-expressing cell contents in normal tissue and after skin tumor induction with the carcinogenic chemicals DMBA/TPA and B(α)P. Percentages of CD74⁺ cells of epidermis and tumor are paired as well as dermis and tumor stroma. The comparison between the left and the right panel shows that the levels of CD74-expressing cells in all tissues are nearly the same, as well as the relations between MIF WT and MIF KO numbers. Epidermis = untreated, normal epidermis, tumor = epithelial part of the tumor induced by chemical carcinogenesis, stroma = dermal tissue surrounding a tumor, dermis = dermal tissue below untreated, normal epidermis.

3.29 IMMUNOFLUORESCENT DETECTION OF THE HISTOCOMPATIBILITY ANTIGEN HLA I-A IN SKIN SAMPLES BEFORE AND AFTER CHEMICAL CARCINOGENESIS WITH DMBA/TPA REVEALS THAT MIF-DEFICIENT SKIN AND TUMORS HARBOR SIGNIFICANTLY LESS I-A⁺ CELLS THAN CONTROL TISSUES

As an additional control for the identification of Langerhans cells (LCs), an immunofluorescent analysis of carcinogen-treated and untreated skin samples with an antibody against I-A was performed. The alloprotein I-A identifies antigen-presenting cells such as macrophages, dendritic cells and Langerhans cells in the murine organism. The comparison of numbers of I-A-expressing cells between MIF WT and KO skin and tumors revealed that MIF-deficient skin and tumors harbor significantly less I-A⁺ cells than control tissues. (Fig. 68). These results are in agreement with the findings based on the macrophage marker F4/80 and suggest that loss of MIF decreases the number of LCs in murine skin.

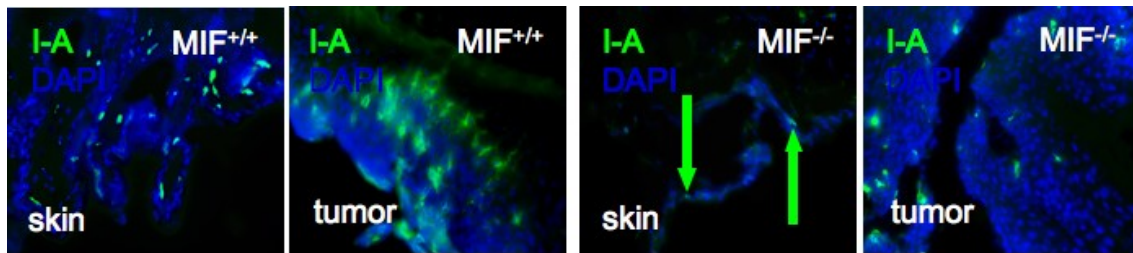


Fig. 68: Numbers of I-A expressing cells in murine wild-type and MIF-deficient skin in untreated skin and chemically induced epidermal tumors. I-A⁺ cells are in green, because the primary antibody has a FITC conjugate. There are less I-A⁺ cells within the tumor area in the MIF-deficient sample (right panel) compared to the wild-type control specimen (second panel from left). Magnification 400x.

3.30 CONTENT OF LCs IN THE EPIDERMAL SHEETS OF WILD-TYPE AND MIF-DEFICIENT MOUSE EARS IS THE SAME

The previous results suggested that MIF is required for maintaining the macrophage/LC population in murine epidermis. Since macrophages and LCs are able to mount immune responses against epidermal skin tumors, it is possible that a lower number of LCs in MIF-deficient animals leads to a diminished immune response towards chemically induced tumors. This would explain why MIF-deficient mice developed more tumors in the *in vivo* models. To answer the question whether MIF-deficient mice are prone to an increased tumor formation with chemical carcinogens because of a lower number of LCs in their epidermis compared to wild-type mice, numbers of LCs in epidermal sheets taken from ears of MIF WT and MIF KO mice were analyzed. Epidermal sheets provide an easy access to evaluate number of LCs, because relatively large pieces of epidermis separated from the dermis can be studied. After treatment with ammonium thiocyanate, the epidermis can be mechanically retrieved from the ear's cartilage and the epidermal sheets can be incubated with an antibody against langerin (CD207) on a glass slide. The successful immunofluorescent detection, e.g., of LCs lets these appear as an interstitial

network between the epidermal keratinocytes. Since LCs are dendritic cells with a soma-like cell body and dendrites arising from them, numbers of LCs can be counted from as locations from where the dendrites spread out (Fig. 69).

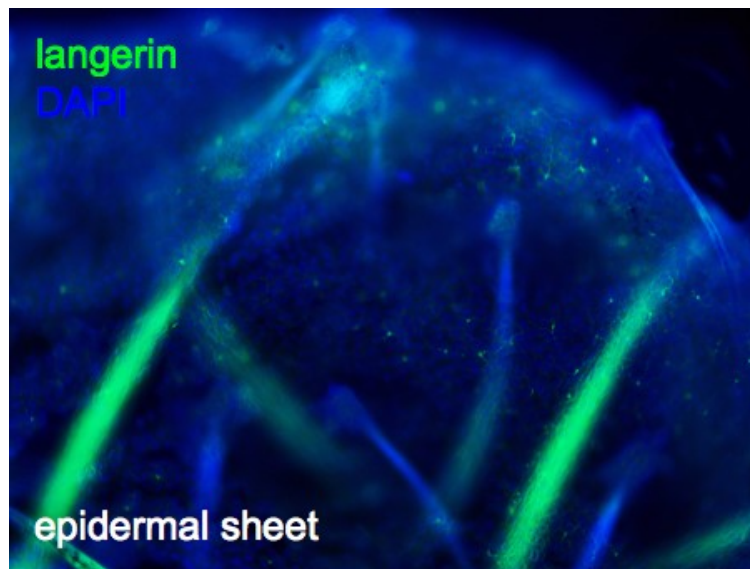


Fig. 69: Immunofluorescent detection of langerin (CD207) in murine epidermal sheets with an Alexa Fluor 488-conjugated primary antibody. DAPI was used as nuclear counterstain. LCs can be distinguished from keratinocytes by their dendritic extensions, which spread from the cellular body (green cells). Hair follicles with their autofluorescence appearing in green are to ignore as artifacts. Magnification 200x.

As shown in Fig. 70, the amount of LCs in the epidermis of MIF WT and MIF KO mice did not differ and was between $14\% \pm 1.2\%$ and $16\% \pm 0.2\%$, $p = 0.257$ in a Student's *t* test.

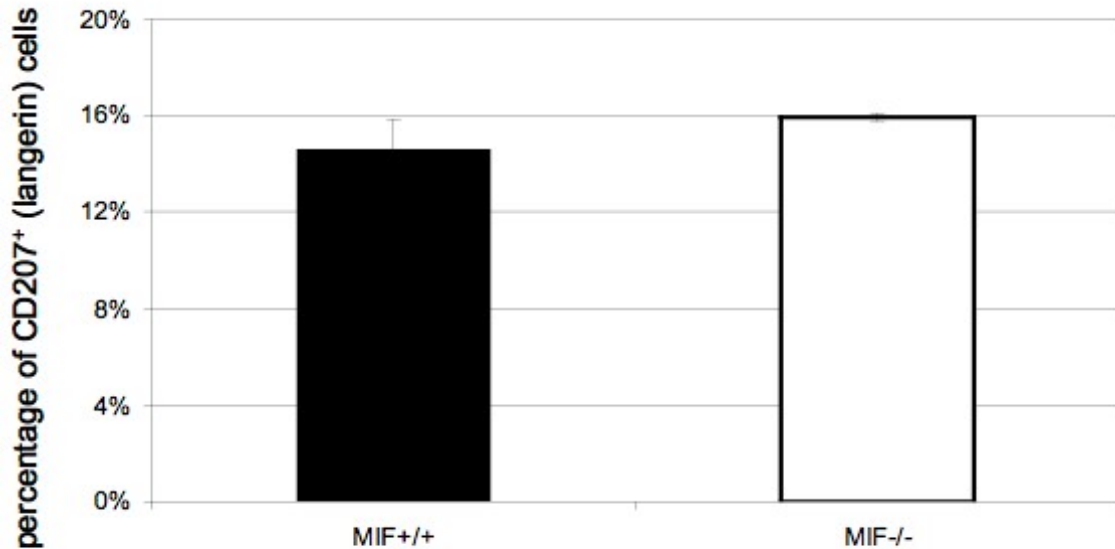


Fig. 70: Relative numbers of LCs in murine epidermal sheets of MIF WT and MIF KO mice, identified by immunofluorescent detection of CD207 (=langerin), relative to total number of counted, DAPI-stained cells in epidermal sheets taken from ears of MIF-deficient mice (right column) and wild-type controls (left column). The number of LCs in both genotypes is equal with 14% ± 1.2% and 16% ± 0.2%, $p = 0.257$ in a Student's t test.

3.31 LC NUMBERS IN UNTREATED AND NEOPLASTIC SKIN AFTER CHEMICAL TUMORIGENESIS WITH DMBA/TPA SHOW A DRASTIC DIMINISHMENT IN MIF-DEFICIENT TISSUE SAMPLES

As the percentages of LCs in the untreated epidermis in epidermal sheets of MIF-deficient and control mice does not differ, the dorsal skin and tumor tissues of MIF WT and KO mice was analyzed for LC numbers by immunofluorescent detection of langerin to find any differences in LC contents regarding the genetic background. Fig. 71 shows immunofluorescent staining of untreated skin and tumor tissue after chemical tumorigenesis in MIF-deficient and wild-type control mice. Tumors in MIF WT mice had a higher number of langerin⁺ cells (10.6% ± 3.9%) compared to MIF KO mice (2.0% ± 2.3%).

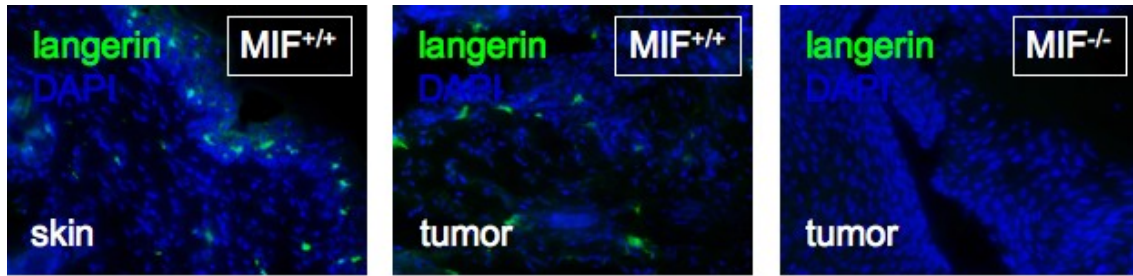


Fig. 72: Representative example of LC numbers in MIF WT and KO tumors. Immunofluorescent analysis of murine skin before (left panel) and after chemical carcinogenesis (middle and right panel) for langerin (CD207) expression. LCs appear in green due to the Alexa Fluor 488 conjugate of the antibody against langerin/CD207, DAPI was used as nuclear counterstain. The tumor tissue of MIF-deficient mice (right panel) bears hardly any LCs, whereas their amount, identified by their expression of langerin/CD207, in the tumor tissue of the wild-type controls is comparable to normal conditions (left panel). Magnification 400x.

Fig. 73 represents the score results of LC numbers in untreated epidermis, dermis, tumor, and stromal tissue before and after chemical tumorigenesis with DMBA/TPA.

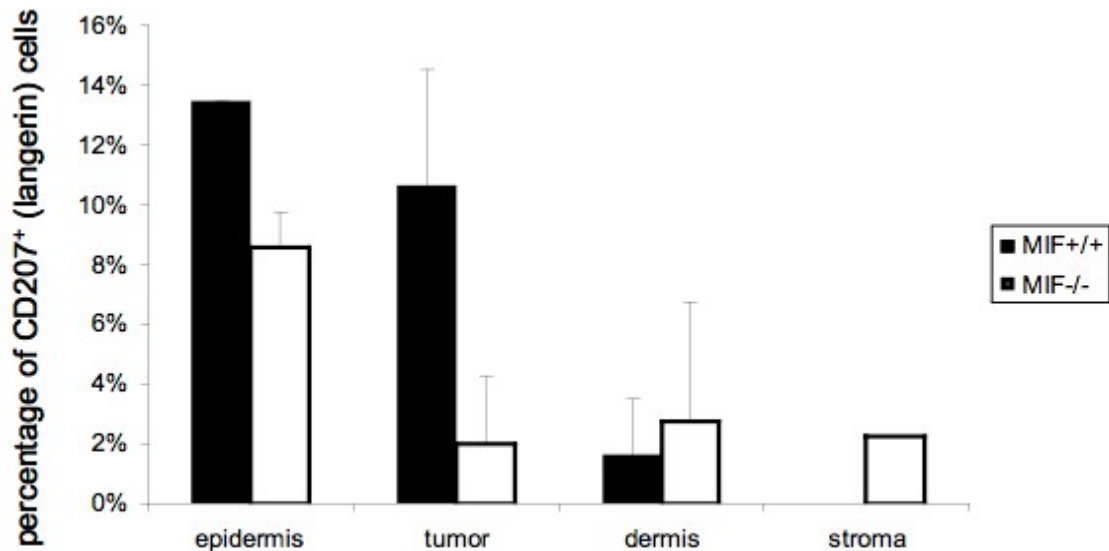


Fig. 73: Evaluation of the percentage of LCs in relation to total cells counted in the corresponding tissue. The score is based on the immunofluorescent analysis of the tissue as described shown in Fig. 72. The percentages of CD207⁺ cells within the epidermis differ significantly between MIF WT and MIF KO mice, as well as the numbers for the tumor tissue.

3.32 LANGERIN AND CD74 DISPLAY CO-EXPRESSION IN EPIDERMAL SHEETS

To prove that LCs also express CD74, epidermal sheets were taken and stained for both langerin and CD74 by immunofluorescence. Double positivity results in a yellowish appearance of the cell. LCs in epidermal sheets can be identified by their dendrites building an interstitial network. Since CD74 and langerin are both transmembrane proteins, the cell body of LCs appears as a ring (arrow in Fig. 74). Artifacts, deriving from prominent hair shafts, which could not be completely removed, should be ignored (star in Fig. 74).

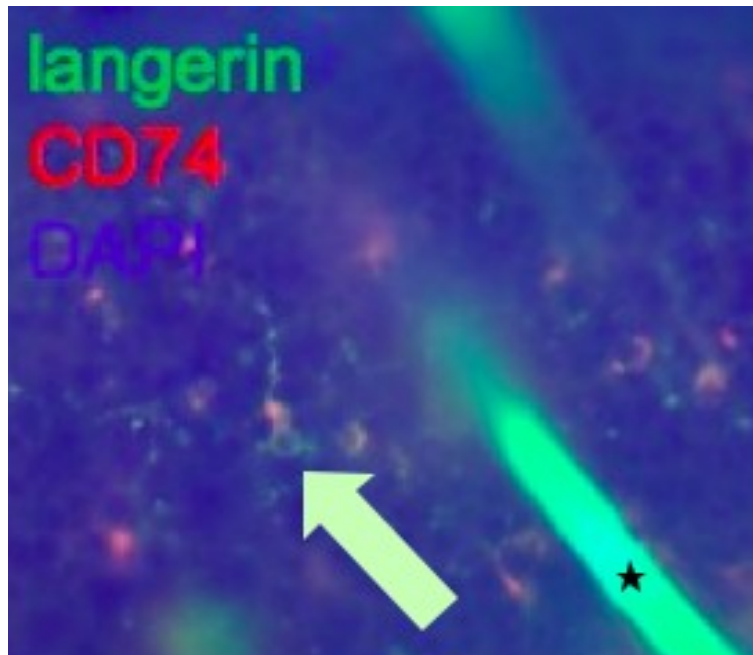


Fig. 74: Langerhans cells are positive for CD74. Immunofluorescent analysis of langerin/CD207 and CD74 expression in epidermal sheets. The antibody against langerin/CD207 has an Alexa Fluor 488 conjugate (emitting green light). The antibody against CD74 was detected by a secondary antibody conjugated with Alexa Fluor 546 (emitting red light). The yellowish color of such cells, like the one indicated with the arrow, confirm co-expression of both proteins by the same cell, since emissions curves overlay. The LCs can be distinguished from other cell types, such as keratinocytes, by their ring-like cellular body with dendritic extensions. Magnification 400x.

3.33 LCs DO NOT EXPRESS DETECTABLE AMOUNTS OF MIF IN EPIDERMAL SHEETS

To answer the question whether LCs also produce MIF, double staining of epidermal sheets for langerin and MIF was performed. As shown in Fig. 75, there was no overlay of green and red emission wavelengths, suggesting that LCs do not express detectable amounts of MIF. This confirms the result

presented in chapter 3.26, where also CD74⁺ cells were found to be negative for MIF.

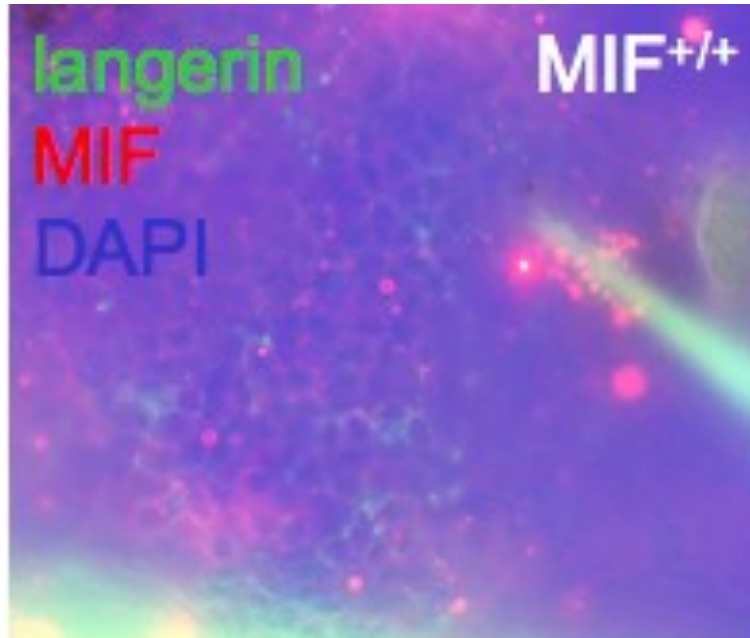


Fig. 75: Immunofluorescent analysis of langerin/CD207 and MIF expression in epidermal sheets. The antibody against langerin/CD207 has an Alexa Fluor 488 conjugate (emitting green light), the antibody against MIF was detected by a secondary antibody conjugated with Alexa Fluor 546 (emitting red light). There is no visible overlay, so no co-expression of the two proteins. Magnification 400x.

3.34 INTRA-EPIDERMAL INJECTIONS OF MIF RECONSTITUTE THE LC POPULATION IN MIF-DEFICIENT MICE TO NORMAL WILD-TYPE LEVELS

To investigate whether the tumor-suppressive features of MIF are keratinocyte-specific, a rescue experiment in which MIF-deficient mice received intradermal injections of recombinant murine MIF (rmuMIF), heat-inactivated MIF (hiMIF), a buffer control (NaPP) and a structural mutant of MIF (D44A-MIF) was

developed. The idea was to find out whether intra-epidermal injections of recombinant murine MIF could induce a reconstitution of the epidermal LC population to normal, aka wild-type, levels. As controls, heat-inactivated recombinant murine MIF was introduced to generate an immune response, and a mutated murine MIF protein, called D44A-MIF.

D44A-MIF was chosen, because the archaic cytokine macrophage migration inhibitory factor (MIF) was recently identified as a non-canonical ligand of the CXC chemokine receptors CXCR2 and CXCR4 in inflammatory and atherogenic cell recruitment [25]. Because the structure-function analysis demonstrated that mutation of residue D44 preserves proper folding and the intrinsic catalytic property of MIF, but severely compromises its binding to CXCR2 and abrogates MIF/CXCR2-mediated functions in chemotaxis and arrest of monocytes on endothelium under flow conditions, the effect of this MIF mutant (D44A) in the epidermal rescue experiment was also tested.

Intra-epidermal injections of recombinant murine MIF, D44A-MIF led to weak presence of MIF in KO tissue as demonstrated by immunohistochemistry (Fig. 76).

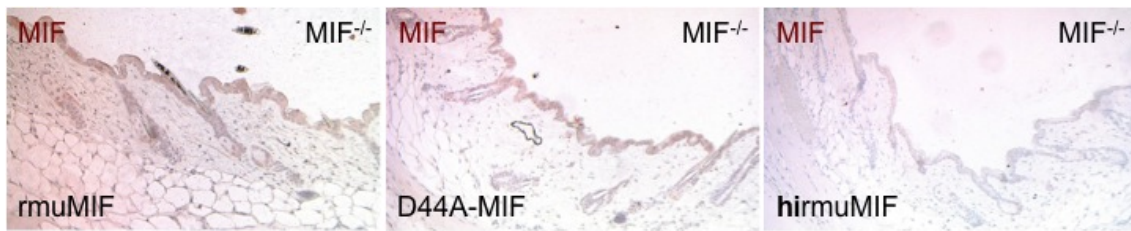


Fig. 76: Immunohistochemical detection of MIF after an intra-epidermal injection of 100 ng recombinant murine MIF (rmuMIF), structural mutant MIF protein (D44A-MIF) or heat inactivated, recombinant murine MIF protein (hirmuMIF) into the epidermis of MIF-deficient mice.

Left panel: A reddish signal comparable to a weaker normal staining of the murine wild-type skin is apparent. The staining pattern is similar to that of the normal wild-type epidermis. Magnification 200x.

Middle panel: A faint red signal comparable to a weak normal staining of the murine wild-type skin is visible. Magnification 200x.

Right panel: The applied antibody did not detect the denatured protein. Therefore, this staining served as negative control. Magnification 200x.

The immunohistochemical enumeration of CD74⁺ cell numbers demonstrated that rmuMIF as well as mutant MIF (D44A) was able to increase the numbers of infiltrating CD74⁺ cells (Fig. 77). The values obtained for NaPP, the buffer solution for the various MIF proteins, served as controls. 6% ± 2% and 25% ± 3% CD74⁺ cells were found in the epidermis and in the dermis, respectively. The injection of rmuMIF resulted in a 1.8-fold augmentation of CD74⁺ cells in the epidermis and a 1.6-fold increase in the dermis (11% ± 3% and 40% ± 9%). The percentage of CD74⁺ dermal cells doubled after injection of D44A-MIF, the structural mutant of MIF presumably devoid of chemotactic activity (11% ± 1% and 49% ± 14%). The value for the epidermal percentage of CD74⁺ cells was the same as after injection of the non-mutated recombinant murine MIF. The injection of heat-inactivated (hiMIF) lead to a slightly increased level of 50 % for

epidermal and dermal CD74⁺ cells compared to solvent-treated controls (9% ± 1% and 34% ± 9%) (Fig. 77).

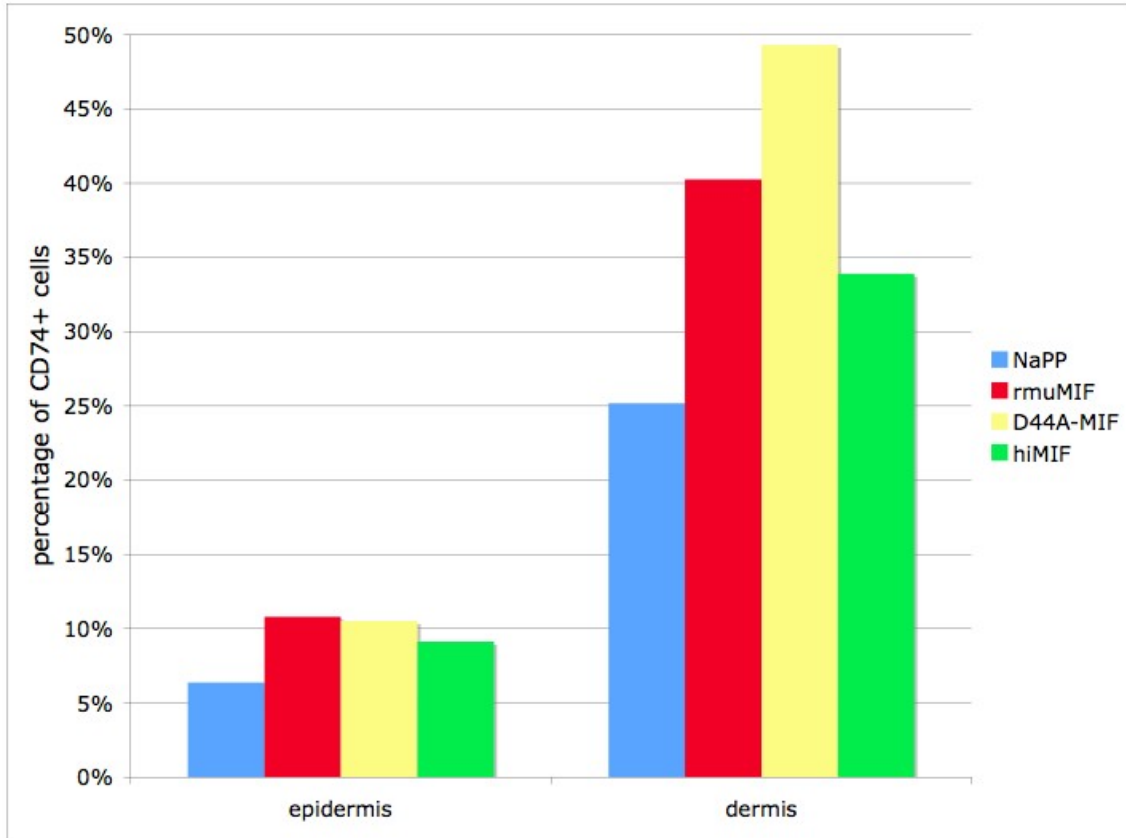


Fig. 77: Evaluation of CD74⁺ cells in epidermal and dermal tissues after intra-epidermal injection of 100 ng of recombinant murine MIF (rmuMIF), a structurally mutated MIF (D44A-MIF), heat-inactivated MIF (hiMIF) and NaPP (buffer control) into the dorsal epidermis of a MIF-deficient mouse, based on an immunohistochemical scoring. p values are 0.274 for rmuMIF, 0.320 for D44A-MIF and 0.081 for hiMIF against NaPP control in a Student's t test each.

3.35 ISOLATED PRIMARY MURINE KERATINOCYTES OF MIF-DEFICIENT AND WILD-TYPE MICE DISPLAY NO MORPHOLOGICAL DIFFERENCES

Next, primary murine keratinocytes were isolated to find out whether there are morphological or growth behavior differences between wild-type and MIF-deficient cells. During initial cultures, no morphological differences between MIF^{+/+} and MIF^{-/-} keratinocytes (Fig. 78), or a significantly different proliferative behavior were noted. However, a detailed characterization of growth and immortalization patterns was not possible due to time constraints.

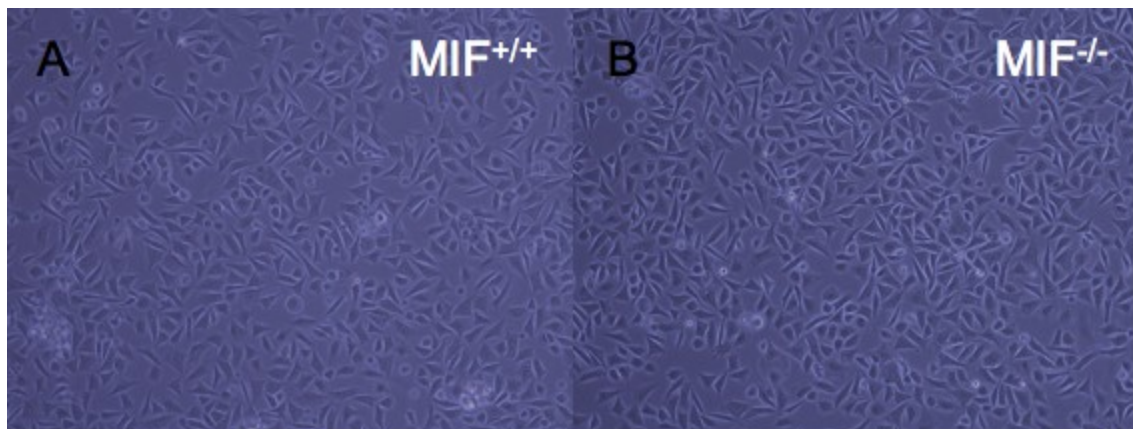


Fig. 78: Isolation of primary murine keratinocytes

A: MIF^{+/+} keratinocytes in passage 7, after having been stored in liquid nitrogen, without feeder cells.

B: MIF^{-/-} keratinocytes in passage 7, after having been stored in liquid nitrogen, without feeder cells.

There is no difference to MIF wild-type keratinocyte morphology in MIF-deficient primary murine keratinocytes.

3.36 SUCCESSFUL DEVELOPMENT OF AN AAV2-MEDIATED TRANSFORMATION OF PRIMARY MURINE KERATINOCYTES WITH GFP AND PRESENTATION OF THE DESIGN FOR A MALIGNANT TRANSFORMATION

To be better able to analyze MIF deficiency in keratinocyte cell lines, a new method to immortalize or transform murine keratinocytes was developed in collaboration with Jessica Sallach and PD Dr. Hildegard Buning, Internal Medicine I, University Hospital Cologne based on adeno-associated virus 2 (AAV2) technology.

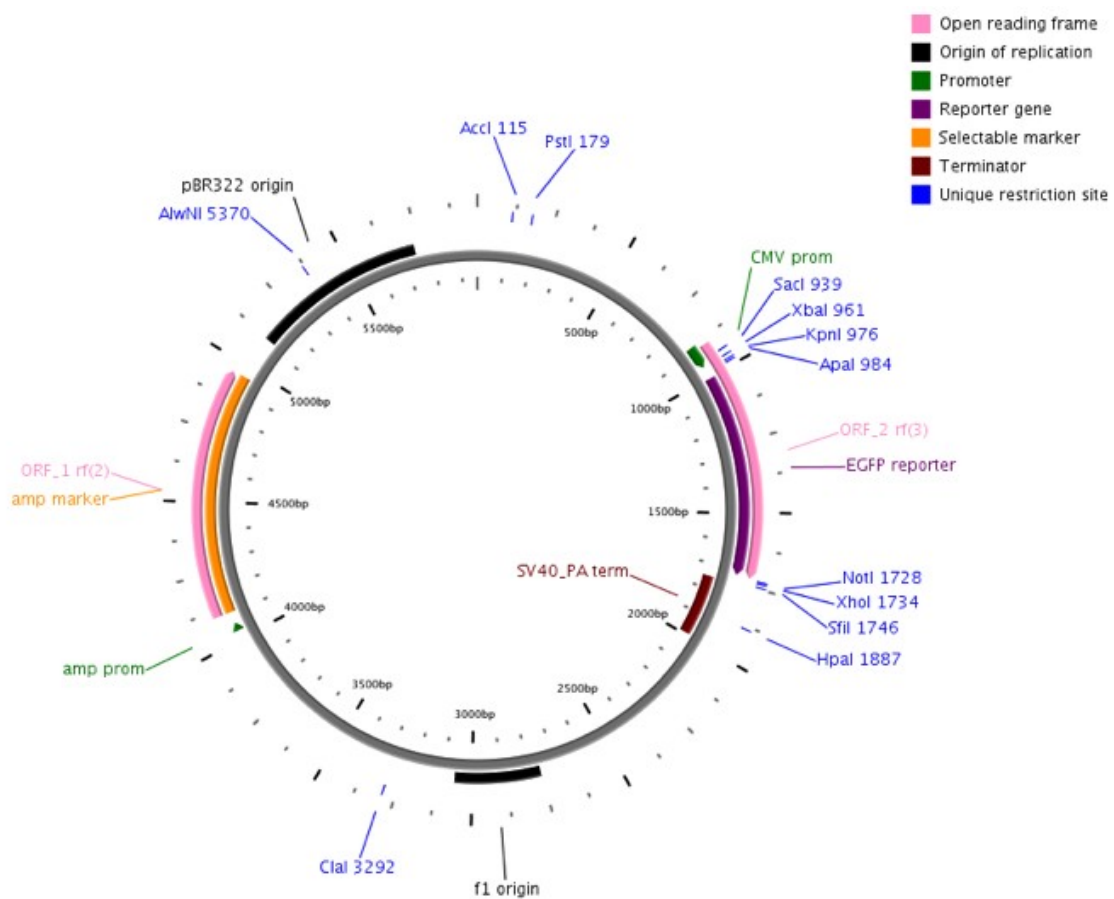


Fig. 79: Self-complimentary rAAV2 vector (psc_A) with the EGFP reporter gene designed by D. Grimm, Heidelberg. Generated with PlasMapper.

Different mutants of the HSPG- and integrin-ligating receptor mutants were tested for their ability to enable an infection of NIH-3T3 J2 cells with rAAV particles. Fig. 80 depicts how these mutants were generated and purified. NIH-3T3 J2 cells are fibroblasts and are standard feeder cells for the culture of murine primary keratinocytes. This study was necessary to test whether the particles would not only infect the isolated primary keratinocytes with MIF wild-type or MIF-deficient background, but also the feeder cells, too, and if the treatment of the NIH-3T3 J2 cells with mitomycin C would block their proliferation while being used as feeders.

Preliminary results of our experiments showed that the AAV2 receptor mutant H1 was the best choice, since the level of transduced feeder cells was the lowest with 50% (Fig. 80), and the transduction of keratinocytes second highest with 40% (Fig. 81). GFP expression was tested first.

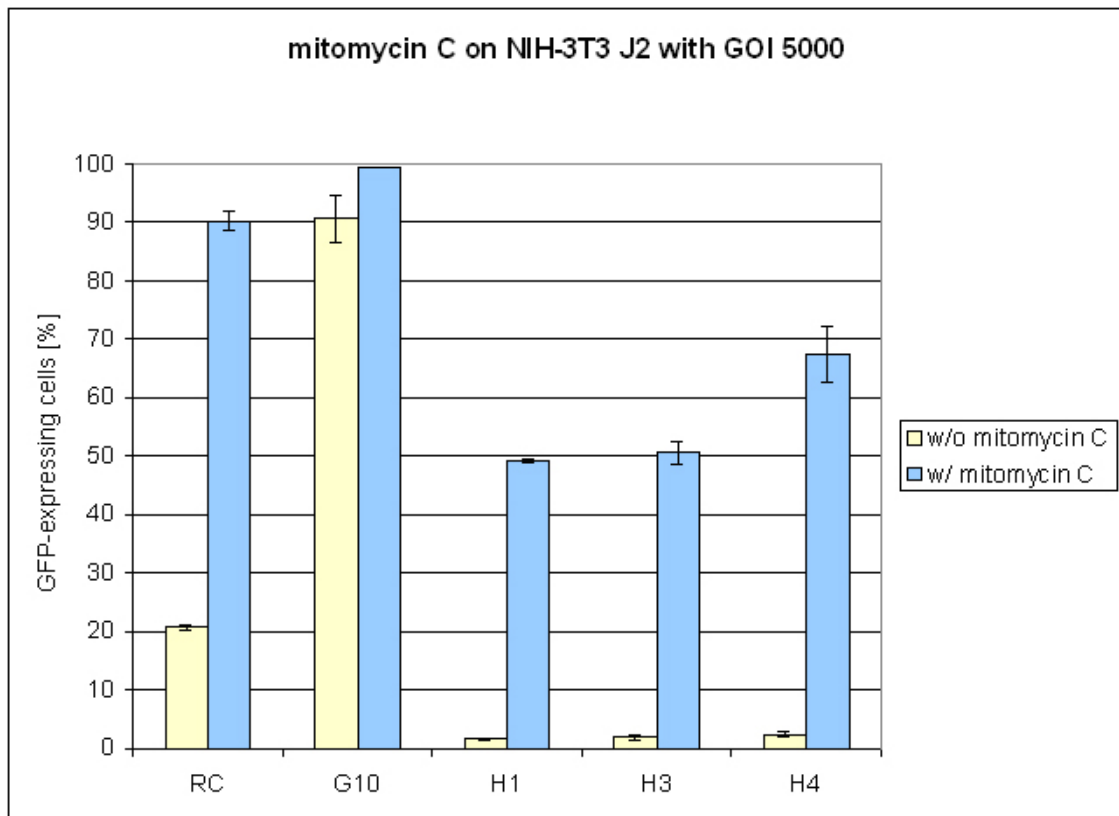


Fig. 80: GFP expression of NIH-3T3 J2 fibroblasts, which are normally used as feeder cells for primary murine keratinocytes, transfected with different rAAV2 receptor mutants (GOI [gene of interest ratio] was 5000). In these mutants, the HSPG or integrin receptor binding sequence was altered. RC is the AAV2 wild-type. Mitomycin C-treated cells were compared to cells, for which the treatment had been omitted. Mitomycin C treatment facilitates the entry of rAAV2 particles into the feeder cells (yellow vs. blue columns), but their treatment is a must for the culture of murine primary keratinocytes. Therefore, a low expression of GFP is preferred in mitomycin C-treated NIH-3T3 J2 cells, which was observed in the H1 mutant rAAV2.

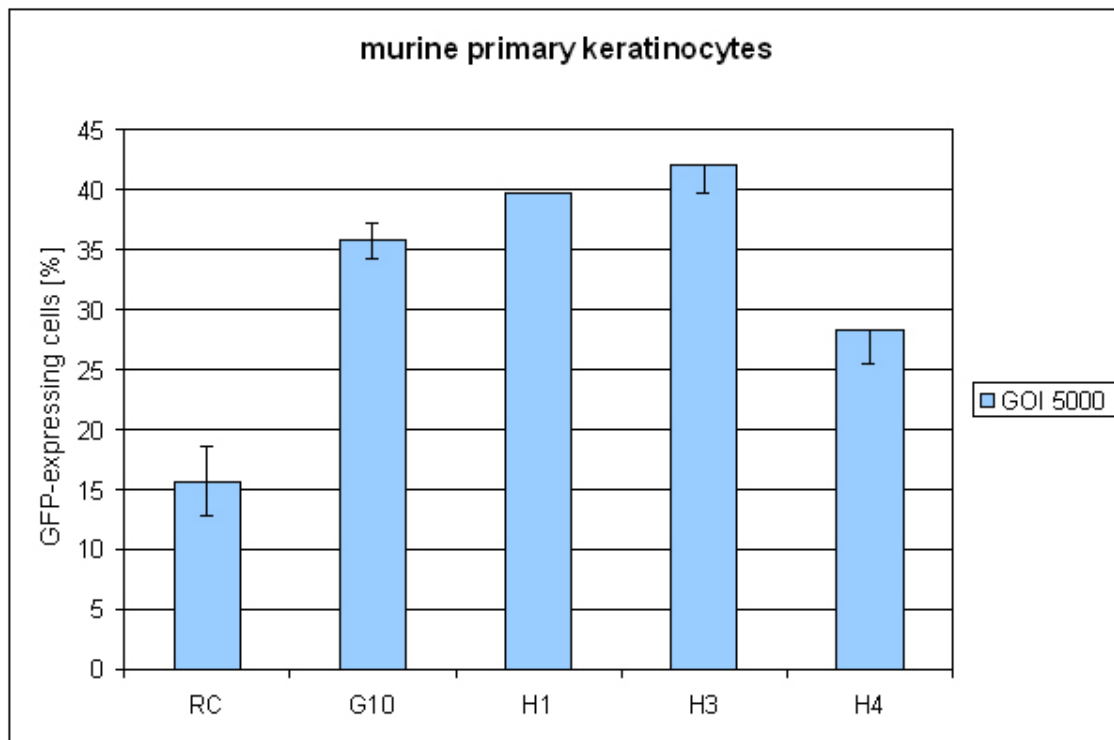


Fig. 81: GFP expression of murine primary keratinocytes, transfected with different rAAV2 receptor mutants (GOI [gene of interest ratio] was 5000). In these mutants, the HSPG or integrin receptor binding sequence was altered. RC is the AAV2 wild-type. The infection with rAAV2 H3 particles was most successful, but H1 was given first priority due to lower infection rate in NIH fibroblasts. 40% transfection efficiency in primary keratinocytes was achieved for rAAV2 H1.

It was planned to induce a malignant transformation with activated H-ras, E1A, and $\Delta Ntp53R175H$ in order to test whether the presence or absence of MIF affected the transformation properties of keratinocytes. Due to time limitations, it was not possible to realize these goals fully.

Cloning $\Delta Ntp53R175H$ into the viral vector psc_AEGFPFG2 was started. Sequence analysis was correct for the inserted gene, but unfortunately a restriction site for *SmaI* got lost during all cloning attempts, and one for *AhdI*

had been missing from the beginning, which meant that self-complementation was not possible any more.

Fig. 82 shows how the final, correct vector should have looked like.

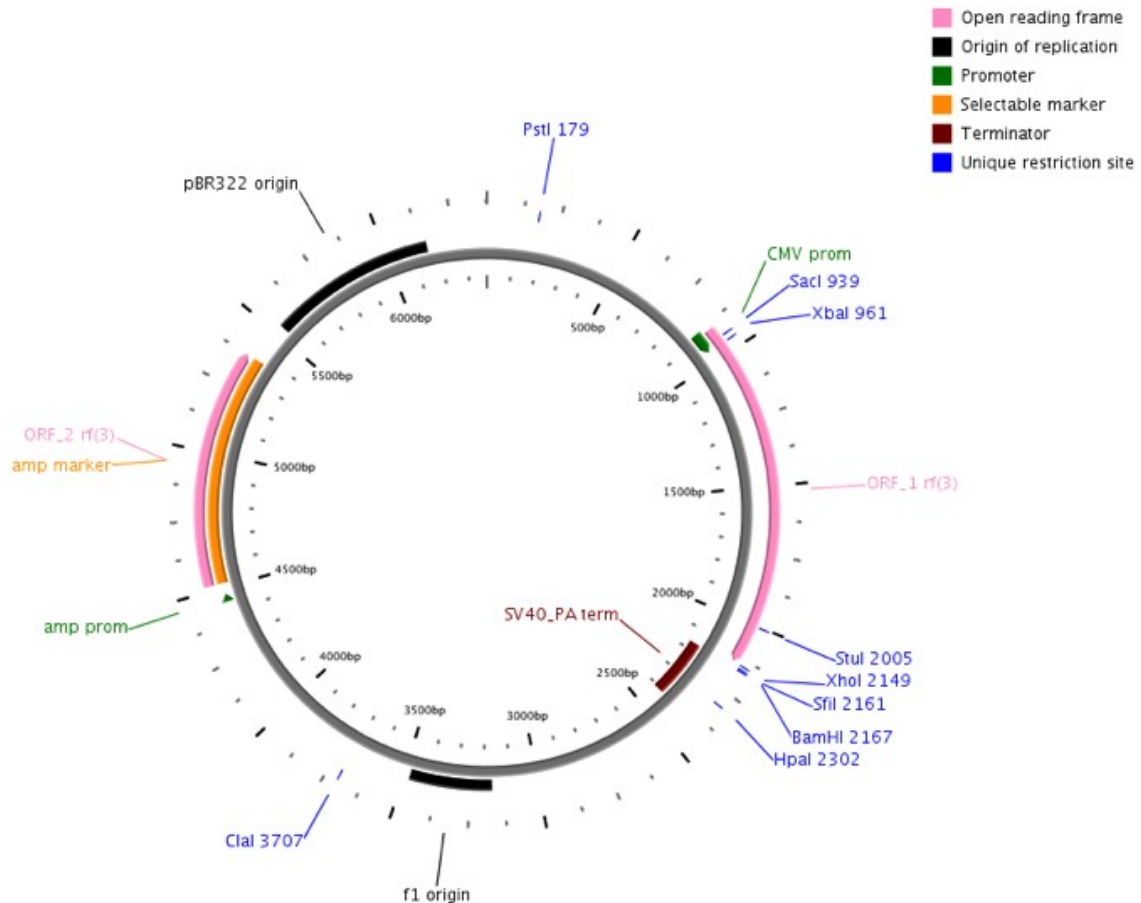
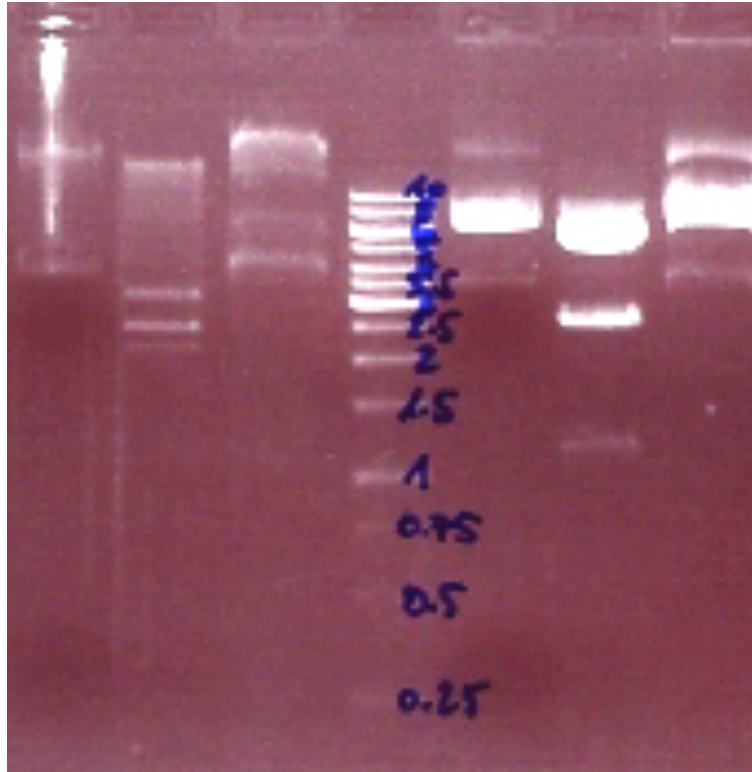


Fig. 82: Self-complementary rAAV2 vector (*psc_A*) with $\Delta Ntp53R175H$ insert (*ORF_1 rf(3)*, right side of the circle). Generated with *PlasMapper*.

Fig. 83 shows a test after the last cloning step to see whether the ITRs of the rAAV2 are intact to guarantee its correct self-completion. The expected bands after the digestion with *AhdI* (=Eam1105I) should be of 2629, 2207 and 1128 bp size for the *psc_AEFGPFG2* vector, and 2629 and 2648 bp for the plasmid after insertion of the $\Delta Ntp53R175H$ sequence. For *SmaI*, the expected, detectable fragments after the digestion with *AhdI* (=Eam1105I) are supposed to run at

3674, 1295 and 995 bp for the *psc_AEFGPFG2* vector, and 3702, 1736 and 945 bp for the plasmid after insertion of the $\Delta Ntp53R175H$ sequence.



*Fig. 83: Digestion gel as documentation of the cloning results for the generation of *psc_A_ΔNtp53R175H*.*

*Lane 1: undigested *psc_AEFGPFG2**

*Lane 2: *psc_AEFGPFG2* digested with *AhdI* (=Eam1105I)*

*Lane 3: *psc_AEFGPFG2* digested with *SmaI**

Lane 4: 1 kb standard

*Lane 5: undigested *psc_A_ΔNtp53R175H**

*Lane 6: *psc_A_ΔNtp53R175H* clone #3 digested with *AhdI**

*Lane 7: *psc_A_ΔNtp53R175H* clone #3 digested with *SmaI**

Table 1 provides an overview about the expected and real fragments as seen on the agarose gel after digestion of the original and cloned plasmid.

Plasmid	Fragment size [bp]			Status	RE
<i>psc_AEFGPFG2</i>	2629	2207	1128	expected	<i>AhdI</i>
<i>psc_AEFGPFG2</i>	2629	2207	3000-3500 (?)	real	<i>AhdI</i>
<i>psc_AEFGPFG2</i>	3674	1295	995	expected	<i>SmaI</i>
<i>psc_AEFGPFG2</i>	3674	1295	995	real	<i>SmaI</i>
<i>psc_A_ΔNtp53R175H</i>	2629	2648	-	expected	<i>AhdI</i>
<i>psc_A_ΔNtp53R175H</i>	2629	1648 (?)	-	real	<i>AhdI</i>
<i>psc_A_ΔNtp53R175H</i>	3702	1736	945	expected	<i>SmaI</i>
<i>psc_A_ΔNtp53R175H</i>	3702	(?)	945	real	<i>SmaI</i>

Table 1: Expected and real fragment sizes as seen on the agarose gel after digestion of the original vector (psc_AEFGPFG2) and cloned plasmid (psc_A_ΔNtp53R175H) and the corresponding restriction enzymes. The question marks (?) indicate unexpected results.

Although the sequence analysis for the insert was correct and the cloning sites impeccable (data not shown), a fragment of large size appeared after digestion of the original vector with *AhdI*. After cloning, one fragment of the plasmid digested with *AhdI* was too small (~1 kb) and one fragment, which should have been of 1736 bp size, was completely missing.

4 DISCUSSION

MIF FUNCTIONALLY PREVENTS MURINE SKIN FROM TUMOR FORMATION.

In 2007, Fingerle-Rowson and Petrenko presented first data claiming that MIF deficiency would lead to increased tumor formation in a model of chemically (B[a]P) induced skin carcinogenesis [33]. This observation was unexpected, because the same authors had also previously published data showing that MIF acted to increase tumor formation when subcutaneously treated with the same substance [66]. Furthermore, a tumor-suppressing role for MIF stood in contrast to several results, which showed that the presence of MIF rather enhanced tumor formation and led to increased metastatic potential. Overexpression of MIF is observed in various tumors compared to normal tissues. High expression levels of MIF are correlated with poor prognosis in malignancies such as prostate, colon and hepatocellular carcinoma [57-59]. MIF supports the malignant potential of transformed cells via several mechanisms such as increased neoangiogenesis [61, 64], augmented activation of pro-survival pathways (NF- κ B, Akt, MAPK) [98], higher metalloproteinase production [99]. Thus, the initial hypothesis of this thesis, namely that MIF suppressed skin tumor formation, was in contrast to the current way of thinking about MIF in tumor biology. We therefore tested this hypothesis extensively in different models of skin tumorigenesis in order to exclude that the initial observation was an experimental artifact.

Our experimental results and analyses, based on *in vivo* models of chemically and HPV-induced skin tumors in genetically defined mice, unequivocally demonstrate that MIF protects the murine skin from tumor formation. This observation was significant and reproducible, and the extent of protection might be of medical importance in the future. Polymorphisms of the *mif* promoter, which affect gene expression strength, are known to correlate with the Gleason score of prostate adenocarcinomas [57] and it is possible that certain individuals

with high MIF expression might be better protected from skin tumor formation than others with lower MIF protein levels.

Tumor formation occurs often on the basis of chronic inflammation. Excellent examples for this basic observation are gastric adenocarcinomas due to *Helicobacter pylori* infection, bladder cancer due to schistosomiasis or colorectal cancer in colitis ulcerosa [100]. Also skin carcinogenesis contains a very strong element of chronic inflammation in its pathogenetic process as can be seen by the presence of a cellular infiltrate at the tumor-stroma interface in our samples. MIF is a well-characterized regulator of innate and acquired immunity. Many of its biologic actions are of pro-inflammatory nature, but some effects of MIF have been identified, which essentially suppress immune reactions. One example for this is the action of MIF in immunoprivileged sites such as the eye and the testis in which MIF may act to suppress immune reactions [44]. Our experiments suggest an essential role of MIF in the function of immunosurveillance in the skin: MIF appears to be required for the population of the epidermis by Langerhans cells (LCs), since their number was significantly reduced in the tumor tissue of MIF-deficient mice. In addition, MIF may be required for the homing of macrophages to dermal tissues, since also numbers of dermal macrophages were found to be diminished both in homeostatic and tumor-bearing skin.

Initial proof for the concept that extracellular MIF might have chemotactic properties for macrophages and LCs was obtained by intra-epidermal injections of recombinant murine MIF into the back skins of MIF knockout mice. Recombinant MIF was able to raise the number of epidermal LC levels and dermal CD74⁺ cells in MIF-deficient mice.

Taken together, our results lead to the hypothesis that MIF is responsible for epidermal immunosurveillance and that MIF functionally act as a chemoattractant during the remigrational and reconstititional processes of dermal macrophages or LCs. Impaired epidermal immunosurveillance in the absence of MIF in turn facilitates tumor formation in the presence of DNA-damaging agents or oncoproteins. Our proposed model of MIF action in skin homeostasis is depicted in Fig. 84:

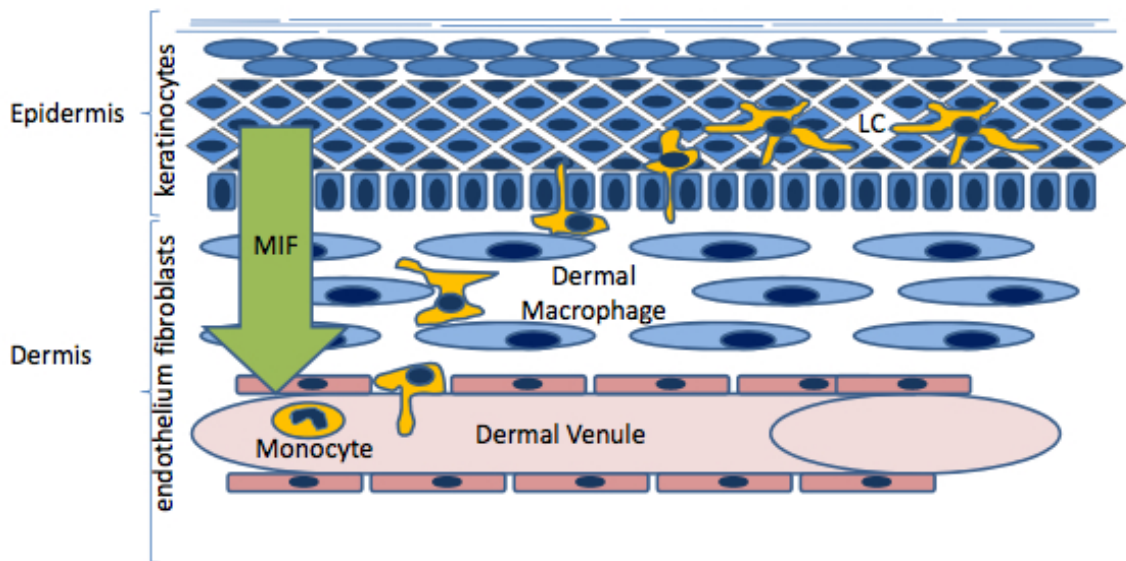


Fig. 84: MIF secreted by keratinocytes acts as a chemoattractant gradient for the reconstitution of the Langerhans cell (LC) population in the epidermis through recruitment of peripheral blood mononuclear cells (monocytes/PBMCs).

Currently, we do not know whether these effects are also due to MIF/CXCR2-mediated functions in chemotaxis and arrest of monocytes/macrophages since the chemotaxis-deficient structural mutant MIF (D44A-MIF) still induced the same immune reconstitution as the wild-type recombinant murine MIF.

Further experiments are ongoing to demonstrate that the observed phenotype is due to keratinocyte-derived MIF (by testing an epidermis-specific MIF KO in chemical tumorigenesis). In addition we try to obtain proof for the concept that lower numbers of LCs/dermal macrophages facilitate skin tumor formation by testing chemically induced skin carcinogenesis in mice depleted of LCs.

Besides the hypothesis of MIF as regulator of LC homeostasis, other effects of MIF in skin biology are conceivable. It is possible that intracellular or extracellular MIF may regulate growth and differentiation of murine keratinocytes via interaction with JAB1 since JAB1 is also expressed in keratinocytes. A prominent finding pointing towards this direction is our

observation that MIF is frequently expressed within the nucleus of primary murine keratinocytes and of the immortalized human epidermal cell line HaCaT. Since nuclear and cytosolic expression of MIF diminishes during malignant transformation, it is possible that nuclear MIF exerts a tumor-antagonistic function. Alternatively, it is conceivable that MIF is increasingly secreted upon tumorigenesis to support the chronic inflammatory process at the tumor-stroma interface.

4.1 MIF IN THE HUMAN EPIDERMIS

Little is known about the expression of MIF in the murine epidermis, but Shimizu et al. performed several analyses in the human skin. Their immunohistochemical studies demonstrated that MIF is expressed especially in the basal layer of the human epidermis [54]. In 1999, they could show that UVB irradiation induced an increased release of MIF by human keratinocytes [55] and that PBMCs should be an important source of increased serum MIF in atopic dermatitis (AD) [101]. They also evaluated MIF serum levels in psoriasis vulgaris and found an elevation due to the upregulation of MIF production by PBMCs [53]. The latest publication by the Shimizu group stated that DNA vaccination against MIF improves atopic dermatitis in mice [102]. MIF as mediator of innate cellular immunity is believed to play a role in the pathogenesis of vitiligo [103], and vitiligo is associated with autoimmune and inflammatory diseases and with mutations of the NALP1 gene. This gene is on a cascade that regulates inflammation and cell death, including myeloid and lymphoid cells. The NALP1 protein is expressed in T cells and LCs [104].

Currently, there are two publications available, dealing with MIF in murine skin. Martin et al. published increased epidermal thickness in UVB-irradiated MIF^{-/-} mice on BALB/c background and a diminished acute inflammatory response

[72]. The group of Martin et al. demonstrated that estrogen inhibited the local inflammatory response by downregulating MIF *in vitro* [105]. They presented data showing that MIF was upregulated in a distinct spatial and temporal pattern during wound healing and its expression was markedly elevated in wounds of estrogen-deficient mice as compared with intact animals. Wound-healing studies in mice rendered null for the MIF gene had revealed that in the absence of MIF, the excessive inflammation and delayed-healing phenotype associated with reduced estrogen was reversed. Moreover, *in vitro* assays showed a striking estrogen-mediated decrease in MIF production by activated murine macrophages, a process involving the estrogen receptor. Our observation that female (MIF-deficient and wild-type) mice generally developed fewer tumors than their male counterparts suggests that additional factors besides MIF must be operative in the process of skin tumorigenesis. Another publication [106] is very relevant since Ito et al. discovered a strong expression of MIF in the murine hair follicle. Hair follicles (HFs) in the growth stage of the hair cycle (anagen) are a recognized site of immune privilege (IP), and collapse of this IP is thought to initiate the loss of hair as seen in patients with the autoimmune disease alopecia areata (AA). Like its classical counterparts, HF-IP is characterized by downregulation of MHC class I expression, dysfunction of Langerhans cells (LCs), and strong local expression of immunosuppressants (for example, α -MSH, TGF- β) and may serve mainly to sequester anagen- and/or melanogenesis-associated autoantigens from immune recognition by autoreactive CD8⁺ T cells. In addition to NK cell receptors and their ligands, other secreted factors should be considered. In the anterior chamber of the eye, MIF suppresses NK cell activity and contributes to IP. MIF as a pleiotropic cytokine that is also present in the aqueous humor and potently inhibits NK cell-mediated cytotoxicity *in vitro*. However, any contribution of MIF to HF-IP and the connection between NK cell activity and HF-IP currently is speculative and remains to be investigated. But our observation that tumor types originating from the hair follicular in the DMBA/TPA carcinogenesis arose only in MIF-deficient mice provides support for the hypothesis that MIF could act as a potential protector of the HF-IP.

4.2 THE POTENTIAL ROLE OF THE MIF RECEPTOR CD74 IN MURINE SKIN CARCINOGENESIS

It has been reported that IFN- γ induced CD74 expression in human keratinocytes [107]. In our observation, both in homeostatic and chemically challenged skin murine keratinocytes do not express the MIF surface receptor CD74. In contrast to the complete absence of CD74 in keratinocytes, immune cells within the epidermis and dermis are strongly positive for surface CD74. Thus, there is a clear spatial distribution between the main MIF producer cells (i.e. keratinocytes) and the probable MIF effector cells (i.e. immune cells). This concept is strongly supported by significant reduction of the numbers of CD74⁺ immune cells within the epidermis, dermis or epidermal tumors in MIF-deficient mice compared to wild-type controls. Our results demonstrate that the LC expresses the MIF receptor CD74 on its surface. Due to its location within the epidermis surrounded by MIF-producing keratinocytes, obviously these cells may be regulated by MIF.

4.3 LANGERHANS CELLS AND SKIN IMMUNITY

In the last few years, although research on LCs has grown immensely, still we are far away from understanding the role of LCs in skin immunity. Studies demonstrating that LCs are dispensable for immune responses against viral and parasitic infection of the skin [108, 109] shook the basic beliefs of the scientific LC community and started the discussion whether LCs are involved at all in immune responses against pathogens invading the skin. The definition of langerin as a specific marker for LCs [110] accelerated the speed of discoveries dramatically, as it was possible for the first time to identify LCs beyond the skin, for instance in lymph nodes. Moreover, three different groups initiated the

generation of mouse models in which LCs can be depleted. These tools are instrumental in defining the functional role of LCs nowadays [111-113].

The early hopes that these models will instantly clarify the important role of LCs in skin immunity were soon shattered by initial findings that in the three mouse models contact hypersensitivity responses were different. The discovery of a novel subset of langerin-positive DCs in the dermis [114-116] further complicated matters. Now, 4 years later, some of the discrepancies between the mouse models have been resolved, yet there is still a hot debate about the specific role of LCs in the skin immune system. The research on the ontogeny of LCs has made major progress in recent years and we have begun to understand how precursors of LCs seed the epidermis during embryogenesis, and that they form the typical network in the epidermis within the first few days or weeks after birth by vigorous proliferation. Ginhoux [117] summarized the current knowledge on LC development in mouse and humans: The situation in humans is in some aspects quite similar to that in the mouse, yet differs in some aspects, such as acquisition of the LC phenotype, which occurs after birth in mice but already *in utero* in humans.

The specific role of the diverse skin DC populations in the induction of immunity and tolerance is currently under discussion, and there is some indication that dermal DCs and LCs might have different roles in the induction of immune responses in skin-draining lymph nodes. LCs appear to be important for the induction of T cell responses and dermal DCs for humoral responses. This division of tasks by the various cutaneous DCs is discussed in more detail in the review by Ueno [118]. The number of dermal DC subsets is still growing and Malissen and co-workers successfully disentangled the complex network of dermal DCs. Currently, five subsets of DCs in the dermis can be distinguished; however, whether they all exert different functions remains to be determined [119]. What becomes clear is that the recently discovered langerin-positive dermal DC subsets gains importance and seems to exert many functions that were so far attributed to LCs.

The notion that LCs might have a regulatory function is discussed for several tolerogenic situations by Lutz [120]. Surprisingly, LCs are not required for the

induction of peripheral tolerance against a self-antigen expressed in the keratinocytes of the epidermis. The langerin⁺ dermal DCs are the major antigen-presenting DC population in the lymph node [119, 121]. Thus, LCs can exert a dual function, that is, induce either tolerance or immunity, depending on the specific situation in the skin. Besides LCs, a subset of langerin-positive dermal DCs can take over the role of inducing peripheral tolerance and immunity when they gain access to the antigen.

The complex network of cutaneous DCs clearly impairs our understanding of the functional properties of LCs *in vivo*. Although the definite function of LCs is still elusive, it is becoming clear that similar to other DC subsets, LCs can exert manifold functions depending on the situation in the skin.

4.4 INFLUENCE OF CHEMICAL CARCINOGENS ON LANGERHANS CELLS

Epidermal LCs are an integral component of the skin immune system as they initiate immune responses to a variety of antigens, including tumor antigens. When skin is exposed to carcinogenic doses of UV-B irradiation, chemical carcinogens or tumor promoters one typically finds a significant reduction of LC density. This causes the skin to be immunocompromised thus providing an opportunity for aberrant cells to escape immune detection and to further develop into tumors. Consequently, LC depletion is a key event associated with the pathogenesis of skin cancer. It was proposed that LC depletion contributes to tumor promotion and therefore any agents that reduce LC number, e.g. the contact sensitizing antigen 2,4,6-trinitrochlorobenzene may also contribute to tumor promotion. This concept was evaluated in cutaneous carcinogenesis by treating mouse skin with a tumor initiating dose of the carcinogen 7,12-dimethylbenz[*a*]anthracene (DMBA) followed by a tumor promoter [122]. The initiating dose of DMBA did not cause LC depletion or tumor development. However, if the DMBA-treated skin was then exposed to a concentration of TNCB that caused LC depletion, skin tumors developed. This is analogous to

the classical initiator/promoter system with an LC-depleting dose of TNCB contributing to tumor promotion. Further, this promotion effect was independent of the commencement time of the promoter application, as 2% TNCB applied either 1 or 12 weeks after DMBA initiation induced tumor development. Analysis of the association of LC depletion with immunosuppression and tumor promotion showed that these events were linked, irrespective of the agent that caused the depletion. It was therefore concluded that LC depletion and local immunosuppression are important aspects of tumor promotion in cutaneous carcinogenesis and non-carcinogenic agents may have tumor promoter activities.

The ability of the chemical carcinogen DMBA to deplete LCs from murine skin is crucial to the development of antigen-specific suppression. This depletion is a consequence of the LCs recognizing the DMBA as antigenic and migrating to the draining lymph nodes to attempt to elicit T cell activation. This is exactly what we observed in our experiments: lower numbers of LCs and CD3⁺ T cells in the homeostatic epidermis, skin tumors, the dermis and stromal tissue of MIF-deficient mice relative to wild-type controls. This supports our hypothesis that MIF is required for a functional immune system in the skin.

The exposure of murine skin to potent chemical carcinogens induced distinctive effects on the distribution of epidermal LCs. In 1989, Ruby et al. [123] presented the following findings: Weekly applications of the tobacco-derived carcinogen, benzo[a]pyrene (B[a]P), caused a significant increase in I-A⁺ LC density within 2 weeks and elevated levels were maintained for up to 6 months with continuous treatment. The LCs in carcinogen-treated epidermis were morphologically abnormal; after B(a)P treatment LCs appeared smaller with shorter dendrites. Application of the contact sensitizing agent, dinitrofluorobenzene, to skin treated with B(a)P induced hyporesponsiveness in the Ruby et al. paper rather than contact sensitivity upon subsequent antigen challenge. Hence, the function of the large number of morphologically altered LC in B(a)P treated skin was impaired. They concluded that carcinogen-induced alterations of LCs were

associated with impaired immunocompetence, although different carcinogens probably operate via different mechanisms to induce such phenomena.

4.5 LANGERHANS CELLS AND HPV

Through the establishment of a transgenic mouse model with the complete early region of HPV8, it could be demonstrated that the expression of viral genes *in vivo* is sufficient for the development of non melanoma skin cancer in mice [124]. The HPV genes were controlled by the human keratin-14 promoter, which allows a targeted expression of these genes in the *stratum basale* and *s. spinosum* of the adult epidermis and developing hair follicles in the mouse embryo [125-127]. The HPV8-transgenic mice were crossed into the FVB/N background, because previous work showed that this inbred strain displays a predisposition to epidermal tumorigenesis (hennings 1993, brown 1995, coussens 1996). The early HPV genes become transcribed as polycistronic mRNA and alternatively spliced (fuchs 1994, haller 1995). The relative expression levels of the HPV8 genes E2, E6 and E7 are similar, as well as the absolute levels of β actin RNA. This contrasts the observation that E6 and E7 are much stronger expressed in keratin-14 HPV16-transgenic mice than E2 (Sethi 2004). In our model, incidence of multifocal papilloma formation was much lower than reported on the FVB/N background, but this may be due a lesser tumor sensitivity in our on the mixed FVB/N 129S1/SvImJ background. We can therefore postulate that the 129S1/SvImJ strain is highly responsive to chemical carcinogenesis, but seemingly not for tumor induction through viral oncoprotein expression.

In 12 human adenocarcinoma cases with HPV infection, Miyagi et al. showed a considerable variation in the amount of cytoplasm, with abundant eosinophilic cytoplasm [128]. The marked LC infiltration in the adenocarcinoma tissue was possibly a reaction to HPV infection in those cases. The type of adenocarcinomas, papillary or bronchioloalveolar did not influence the number

of infiltrating LCs. The HPV-infected squamous cell carcinoma cases also showed intense LC infiltration. The degree of infiltration did not vary between the types of HPV. As seen in that study, the unusual HPV infection in adenocarcinomas might have caused the intense infiltration of LCs. Episomal form HPV was frequently observed in the presented adenocarcinoma cases. The physical state of HPV DNA in the adenocarcinoma cells might also influence the number of infiltrating LCs. Unlike the adenocarcinoma cases, squamous cell carcinoma cases showed nearly equal numbers of both the episomal and integrated forms of HPV. The physical states of HPV were not strictly related to the degree of Langerhans cell infiltration in the squamous cell carcinoma cases. Miyagi et al. consider that the HPV infection in cancer cells might cause the intense Langerhans cell infiltration. LCs could react to the HPV and initiate the immune reaction, and thus serve a significant prognostic factor for squamous cell carcinomas. Furthermore, the lymphocytes infiltration in HPV-positive cases was stronger than that in HPV-negative cases. Histologically well-differentiated tumors were also considered to be a favourable prognostic factor. Furukawa et al. reported the good prognosis of lung tumors (adenocarcinomas) with high LC infiltration (about 20 per high-power field). In the Miyagi et al. study, HPV-infected and highly LC-infiltrated adenocarcinomas tended to have a better prognosis.

In conclusion, our work demonstrates that the mediator MIF plays an important regulatory role for skin immunity and tumorigenesis. The concept of MIF as a molecular link between chronic inflammation and tumorigenesis originally is strongly supported by our observations. Our data suggest that any systemic intervention with MIF for therapeutic purposes should be carefully balanced against the potential risk of increased skin tumorigenesis. On the other hand, our insight into the complex biology of MIF in skin opens many novel avenues of therapeutic intervention for inflammatory skin diseases.

5 SYNOPSIS

Tumor formation occurs often on the basis of chronic inflammation. Excellent examples for this basic observation are gastric adenocarcinomas due to *Helicobacter pylori* infection, bladder cancer due to schistosomiasis or colorectal cancer in colitis ulcerosa [100]. Also skin carcinogenesis contains a very strong element of chronic inflammation in its pathogenetic process as can be seen by the presence of a cellular infiltrate at the tumor-stroma interface in our samples.

MIF is a well-characterized regulator of innate and acquired immunity. Many of its biologic actions are of pro-inflammatory nature, but some effects of MIF have been identified, which essentially suppress immune reaction.

In 2007, Fingerle-Rowson and Petrenko presented first data claiming that MIF deficiency would lead to increased tumor formation in a model of chemically (B[a]P) induced skin carcinogenesis [33]. This observation was unexpected, because the same authors had also previously published data showing that MIF acted to increase tumor formation when subcutaneously treated with the same substance [66]. Furthermore, a tumor-suppressing role for MIF stood in contrast to several results, which showed that the presence of MIF rather enhanced tumor formation and led to increased metastatic potential. High expression levels of MIF are correlated with poor prognosis in malignancies such as prostate, colon and hepatocellular carcinoma [57-59].

Thus, the preliminary data published in 2007 by Fingerle-Rowson and Petrenko stood in contrast to the current way of thinking about MIF in tumor biology. We therefore analyzed the role of MIF in murine skin tumorigenesis in different models of skin tumor induction.

Our experimental results and analyses, based on *in vivo* models of chemically and HPV-induced skin tumors in genetically defined mice, unequivocally demonstrate that MIF protects the murine skin from tumor formation. Furthermore, our experiments suggest an essential role of MIF in the function of immunosurveillance in the skin: MIF appears to be required for the population of

the epidermis by Langerhans cells (LCs), since their number was significantly reduced in the tumor tissue of MIF-deficient mice. In addition, MIF may be required for the homing of macrophages to dermal tissues, since also numbers of dermal macrophages were found to be diminished both in homeostatic and tumor-bearing skin.

Initial proof for the concept that extracellular MIF might have chemotactic properties for macrophages and LCs was obtained by intra-epidermal injections of recombinant murine MIF into the back skins of MIF knockout mice. Recombinant MIF was able to raise the number of epidermal LC levels and dermal CD74⁺ cells in MIF-deficient mice.

Taken together, our results lead to the hypothesis that MIF is responsible for epidermal immunosurveillance and that MIF functionally act as a chemoattractant during the remigrational and reconstititional processes of dermal macrophages or LCs. Impaired epidermal immunosurveillance in the absence of MIF in turn facilitates tumor formation in the presence of DNA-damaging agents or oncoproteins.

Currently, we do not know whether these effects are also due to MIF/CXCR2-mediated functions in chemotaxis and arrest of monocytes/macrophages since the chemotaxis-deficient structural mutant MIF (D44A-MIF) still induced the same immune reconstitution as the wild-type recombinant murine MIF.

Further experiments are ongoing to demonstrate that the observed phenotype is due to keratinocyte-derived MIF (by testing an epidermis-specific MIF KO in chemical tumorigenesis). In addition we try to obtain proof for the concept that lower numbers of LCs/dermal macrophages facilitate skin tumor formation by testing chemically induced skin carcinogenesis in mice depleted of LCs.

6 REFERENCES

1. Bloom, B.R. and B. Bennett, *Mechanism of a reaction in vitro associated with delayed-type hypersensitivity*. Science, 1966. **153**(731): p. 80-2.
2. David, J.R., *Delayed hypersensitivity in vitro: its mediation by cell-free substances formed by lymphoid cell-antigen interaction*. Proc Natl Acad Sci U S A, 1966. **56**(1): p. 72-7.
3. Nathan, C.F., M.L. Karnovsky, and J.R. David, *Alterations of macrophage functions by mediators from lymphocytes*. J Exp Med, 1971. **133**(6): p. 1356-76.
4. Nathan, C.F., H.G. Remold, and J.R. David, *Characterization of a lymphocyte factor which alters macrophage functions*. J Exp Med, 1973. **137**(2): p. 275-90.
5. Churchill, W.H., Jr., et al., *Macrophages activated as suspension cultures with lymphocyte mediators devoid of antigen become cytotoxic for tumor cells*. J Immunol, 1975. **115**(3): p. 781-6.
6. Weiser, W.Y., et al., *Molecular cloning of a cDNA encoding a human macrophage migration inhibitory factor*. Proc Natl Acad Sci U S A, 1989. **86**(19): p. 7522-6.
7. Bozza, M., et al., *Structural characterization and chromosomal location of the mouse macrophage migration inhibitory factor gene and pseudogenes*. Genomics, 1995. **27**(3): p. 412-9.
8. Mitchell, R., et al., *Cloning and characterization of the gene for mouse macrophage migration inhibitory factor (MIF)*. J Immunol, 1995. **154**(8): p. 3863-70.
9. Budarf, M., et al., *Localization of the human gene for macrophage migration inhibitory factor (MIF) to chromosome 22q11.2*. Genomics, 1997. **39**(2): p. 235-6.
10. Paralkar, V. and G. Wistow, *Cloning the human gene for macrophage migration inhibitory factor (MIF)*. Genomics, 1994. **19**(1): p. 48-51.
11. Maleszka, R. and P. Ratka, *Clinical and epidemiological aspects of various forms of fungal infections caused by Trichophyton tonsurans*. Rev Iberoam Micol, 1998. **15**(4): p. 286-9.
12. Bernhagen, J., et al., *Purification, bioactivity, and secondary structure analysis of mouse and human macrophage migration inhibitory factor (MIF)*. Biochemistry, 1994. **33**(47): p. 14144-55.
13. Sugimoto, H., et al., *Crystal structure of macrophage migration inhibitory factor from human lymphocyte at 2.1 Å resolution*. FEBS Lett, 1996. **389**(2): p. 145-8.
14. Sun, H.W., et al., *Crystal structure at 2.6-Å resolution of human macrophage migration inhibitory factor*. Proc Natl Acad Sci U S A, 1996. **93**(11): p. 5191-6.
15. Muhlhahn, P., et al., *NMR characterization of structure, backbone dynamics, and glutathione binding of the human macrophage migration inhibitory factor (MIF)*. Protein Sci, 1996. **5**(10): p. 2095-103.
16. Sugimoto, H., et al., *Crystal structure of human D-dopachrome tautomerase, a homologue of macrophage migration inhibitory factor, at 1.54 Å resolution*. Biochemistry, 1999. **38**(11): p. 3268-79.

17. Nishibori, M., et al., *Affinity purification of macrophage migration inhibitory factor/glycosylation inhibiting factor (MIF/GIF) from bovine brain by using a peptide ligand derived from a novel serpin*. Jpn J Pharmacol, 1996. **71**(3): p. 259-62.
18. Watarai, H., et al., *Posttranslational modification of the glycosylation inhibiting factor (GIF) gene product generates bioactive GIF*. Proc Natl Acad Sci U S A, 2000. **97**(24): p. 13251-6.
19. Lolis, E. and R. Bucala, *Crystal structure of macrophage migration inhibitory factor (MIF), a glucocorticoid-induced regulator of cytokine production, reveals a unique architecture*. Proc Assoc Am Physicians, 1996. **108**(6): p. 415-9.
20. Leng, L., et al., *MIF signal transduction initiated by binding to CD74*. J Exp Med, 2003. **197**(11): p. 1467-76.
21. Stumptner-Cuvelette, P. and P. Benaroch, *Multiple roles of the invariant chain in MHC class II function*. Biochim Biophys Acta, 2002. **1542**(1-3): p. 1-13.
22. Shi, X., et al., *CD44 is the signaling component of the macrophage migration inhibitory factor-CD74 receptor complex*. Immunity, 2006. **25**(4): p. 595-606.
23. Gore, Y., et al., *Macrophage migration inhibitory factor induces B cell survival by activation of a CD74-CD44 receptor complex*. J Biol Chem, 2008. **283**(5): p. 2784-92.
24. Bernhagen, J., et al., *MIF is a noncognate ligand of CXC chemokine receptors in inflammatory and atherogenic cell recruitment*. Nat Med, 2007. **13**(5): p. 587-96.
25. Weber, C., et al., *Structural determinants of MIF functions in CXCR2-mediated inflammatory and atherogenic leukocyte recruitment*. Proc Natl Acad Sci U S A, 2008. **105**(42): p. 16278-83.
26. Kleemann, R., et al., *Intracellular action of the cytokine MIF to modulate AP-1 activity and the cell cycle through Jab1*. Nature, 2000. **408**(6809): p. 211-6.
27. Bech-Otschir, D., et al., *COP9 signalosome-specific phosphorylation targets p53 to degradation by the ubiquitin system*. EMBO J, 2001. **20**(7): p. 1630-9.
28. Chamovitz, D.A. and D. Segal, *JAB1/CSN5 and the COP9 signalosome. A complex situation*. EMBO Rep, 2001. **2**(2): p. 96-101.
29. Glickmann, E., et al., *Auxin production is a common feature of most pathovars of Pseudomonas syringae*. Mol Plant Microbe Interact, 1998. **11**(2): p. 156-62.
30. Henke, W., et al., *Comparison of human COP9 signalosome and 26S proteasome lid*. Mol Biol Rep, 1999. **26**(1-2): p. 29-34.
31. Hershko, A. and A. Ciechanover, *The ubiquitin system*. Annu Rev Biochem, 1998. **67**: p. 425-79.
32. Tomoda, K., Y. Kubota, and J. Kato, *Degradation of the cyclin-dependent-kinase inhibitor p27Kip1 is instigated by Jab1*. Nature, 1999. **398**(6723): p. 160-5.
33. Fingerle-Rowson, G. and O. Petrenko, *MIF coordinates the cell cycle with DNA damage checkpoints. Lessons from knockout mouse models*. Cell Div, 2007. **2**: p. 22.

34. Nemajerova, A., et al., *Macrophage migration inhibitory factor coordinates DNA damage response with the proteasomal control of the cell cycle*. Cell Cycle, 2007. **6**(9): p. 1030-4.
35. Bernhagen, J., et al., *MIF is a pituitary-derived cytokine that potentiates lethal endotoxaemia*. Nature, 1993. **365**(6448): p. 756-9.
36. Bernhagen, J., T. Calandra, and R. Bucala, *Regulation of the immune response by macrophage migration inhibitory factor: biological and structural features*. J Mol Med, 1998. **76**(3-4): p. 151-61.
37. Bae, M.K., et al., *Jab1 interacts directly with HIF-1alpha and regulates its stability*. J Biol Chem, 2002. **277**(1): p. 9-12.
38. Suzuki, H., H. Kanagawa, and J. Nishihira, *Evidence for the presence of macrophage migration inhibitory factor in murine reproductive organs and early embryos*. Immunol Lett, 1996. **51**(3): p. 141-7.
39. Kobayashi, S., et al., *Expression pattern of macrophage migration inhibitory factor during embryogenesis*. Mech Dev, 1999. **84**(1-2): p. 153-6.
40. Lan, H.Y., et al., *The pathogenic role of macrophage migration inhibitory factor in immunologically induced kidney disease in the rat*. J Exp Med, 1997. **185**(8): p. 1455-65.
41. Bernhagen, J., T. Calandra, and R. Bucala, *The emerging role of MIF in septic shock and infection*. Biotherapy, 1994. **8**(2): p. 123-7.
42. Bacher, M., et al., *An essential regulatory role for macrophage migration inhibitory factor in T-cell activation*. Proc Natl Acad Sci U S A, 1996. **93**(15): p. 7849-54.
43. Takahashi, A., et al., *Antisense macrophage migration inhibitory factor (MIF) prevents anti-IgM mediated growth arrest and apoptosis of a murine B cell line by regulating cell cycle progression*. Microbiol Immunol, 1999. **43**(1): p. 61-7.
44. Apte, R.S., et al., *Cutting edge: role of macrophage migration inhibitory factor in inhibiting NK cell activity and preserving immune privilege*. J Immunol, 1998. **160**(12): p. 5693-6.
45. Chen, H., et al., *Characterization of gene expression in resting and activated mast cells*. J Exp Med, 1998. **188**(9): p. 1657-68.
46. Rossi, A.G., et al., *Human circulating eosinophils secrete macrophage migration inhibitory factor (MIF). Potential role in asthma*. J Clin Invest, 1998. **101**(12): p. 2869-74.
47. Waeber, G., et al., *Insulin secretion is regulated by the glucose-dependent production of islet beta cell macrophage migration inhibitory factor*. Proc Natl Acad Sci U S A, 1997. **94**(9): p. 4782-7.
48. Benigni, F., et al., *The proinflammatory mediator macrophage migration inhibitory factor induces glucose catabolism in muscle*. J Clin Invest, 2000. **106**(10): p. 1291-300.
49. Kudo, T., *[Identification of macrophage migration inhibitory factor (MIF) in rat gastrointestinal tract and its role in rat stomach]*. Hokkaido Igaku Zasshi, 1998. **73**(4): p. 317-25.
50. Abe, R., et al., *Enhancement of macrophage migration inhibitory factor (MIF) expression in injured epidermis and cultured fibroblasts*. Biochim Biophys Acta, 2000. **1500**(1): p. 1-9.
51. Meinhardt, A., et al., *Local regulation of macrophage subsets in the adult rat testis: examination of the roles of the seminiferous tubules,*

- testosterone, and macrophage-migration inhibitory factor. *Biol Reprod*, 1998. **59**(2): p. 371-8.
52. Mizue, Y., et al., *Quantitation of macrophage migration inhibitory factor (MIF) using the one-step sandwich enzyme immunosorbent assay: elevated serum MIF concentrations in patients with autoimmune diseases and identification of MIF in erythrocytes*. *Int J Mol Med*, 2000. **5**(4): p. 397-403.
 53. Shimizu, T., et al., *High macrophage migration inhibitory factor (MIF) serum levels associated with extended psoriasis*. *J Invest Dermatol*, 2001. **116**(6): p. 989-90.
 54. Shimizu, T., et al., *Identification of macrophage migration inhibitory factor (MIF) in human skin and its immunohistochemical localization*. *FEBS Lett*, 1996. **381**(3): p. 199-202.
 55. Shimizu, T., et al., *Ultraviolet B radiation upregulates the production of macrophage migration inhibitory factor (MIF) in human epidermal keratinocytes*. *J Invest Dermatol*, 1999. **112**(2): p. 210-5.
 56. Shimizu, T., *Role of macrophage migration inhibitory factor (MIF) in the skin*. *J Dermatol Sci*, 2005. **37**(2): p. 65-73.
 57. Meyer-Siegler, K.L., M.A. Bellino, and M. Tannenbaum, *Macrophage migration inhibitory factor evaluation compared with prostate specific antigen as a biomarker in patients with prostate carcinoma*. *Cancer*, 2002. **94**(5): p. 1449-56.
 58. Legendre, H., et al., *Prognostic values of galectin-3 and the macrophage migration inhibitory factor (MIF) in human colorectal cancers*. *Mod Pathol*, 2003. **16**(5): p. 491-504.
 59. Hira, E., et al., *Overexpression of macrophage migration inhibitory factor induces angiogenesis and deteriorates prognosis after radical resection for hepatocellular carcinoma*. *Cancer*, 2005. **103**(3): p. 588-98.
 60. Mitchell, R.A., et al., *Macrophage migration inhibitory factor (MIF) sustains macrophage proinflammatory function by inhibiting p53: regulatory role in the innate immune response*. *Proc Natl Acad Sci U S A*, 2002. **99**(1): p. 345-50.
 61. Chesney, J., et al., *An essential role for macrophage migration inhibitory factor (MIF) in angiogenesis and the growth of a murine lymphoma*. *Mol Med*, 1999. **5**(3): p. 181-91.
 62. Amin, K., et al., *Dietary glycine inhibits angiogenesis during wound healing and tumor growth*. *Cancer Biol Ther*, 2003. **2**(2): p. 173-8.
 63. Martin, D., R. Galisteo, and J.S. Gutkind, *CXCL8/IL8 stimulates vascular endothelial growth factor (VEGF) expression and the autocrine activation of VEGFR2 in endothelial cells by activating NFkappaB through the CBM (Carma3/Bcl10/Malt1) complex*. *J Biol Chem*, 2009. **284**(10): p. 6038-42.
 64. Shimizu, T., et al., *High expression of macrophage migration inhibitory factor in human melanoma cells and its role in tumor cell growth and angiogenesis*. *Biochem Biophys Res Commun*, 1999. **264**(3): p. 751-8.
 65. Hudson, J.D., et al., *A proinflammatory cytokine inhibits p53 tumor suppressor activity*. *J Exp Med*, 1999. **190**(10): p. 1375-82.
 66. Fingerle-Rowson, G., et al., *The p53-dependent effects of macrophage migration inhibitory factor revealed by gene targeting*. *Proc Natl Acad Sci U S A*, 2003. **100**(16): p. 9354-9.

67. Ichiyama, H., et al., *Inhibition of joint inflammation and destruction induced by anti-type II collagen antibody/lipopolysaccharide (LPS)-induced arthritis in mice due to deletion of macrophage migration inhibitory factor (MIF)*. Cytokine, 2004. **26**(5): p. 187-94.
68. Meyer-Siegler, K.L., et al., *Inhibition of macrophage migration inhibitory factor or its receptor (CD74) attenuates growth and invasion of DU-145 prostate cancer cells*. J Immunol, 2006. **177**(12): p. 8730-9.
69. Rendon, B.E., et al., *Regulation of human lung adenocarcinoma cell migration and invasion by macrophage migration inhibitory factor*. J Biol Chem, 2007. **282**(41): p. 29910-8.
70. Repp, A.C., et al., *Human uveal melanoma cells produce macrophage migration-inhibitory factor to prevent lysis by NK cells*. J Immunol, 2000. **165**(2): p. 710-5.
71. Culp, W.D., et al., *Interference of macrophage migration inhibitory factor expression in a mouse melanoma inhibits tumor establishment by up-regulating thrombospondin-1*. Mol Cancer Res, 2007. **5**(12): p. 1225-31.
72. Martin, J., et al., *Macrophage migration inhibitory factor (MIF) plays a critical role in pathogenesis of ultraviolet-B (UVB) -induced nonmelanoma skin cancer (NMSC)*. FASEB J, 2009. **23**(3): p. 720-30.
73. Fingerle-Rowson, G., et al., *A tautomerase-null macrophage migration-inhibitory factor (MIF) gene knock-in mouse model reveals that protein interactions and not enzymatic activity mediate MIF-dependent growth regulation*. Mol Cell Biol, 2009. **29**(7): p. 1922-32.
74. Yang, L., et al., *Targeted disruption of Smad4 in mouse epidermis results in failure of hair follicle cycling and formation of skin tumors*. Cancer Res, 2005. **65**(19): p. 8671-8.
75. Miettinen, P.J., et al., *TGF-beta induced transdifferentiation of mammary epithelial cells to mesenchymal cells: involvement of type I receptors*. J Cell Biol, 1994. **127**(6 Pt 2): p. 2021-36.
76. Honda, A., et al., *Deficient deletion of apoptotic cells by macrophage migration inhibitory factor (MIF) overexpression accelerates photocarcinogenesis*. Carcinogenesis, 2009. **30**(9): p. 1597-605.
77. Loeser, S., et al., *Spontaneous tumor rejection by cbl-b-deficient CD8+ T cells*. J Exp Med, 2007. **204**(4): p. 879-91.
78. Horn, S., H. Pfister, and P.G. Fuchs, *Constitutive transcriptional activator of Epidermodysplasia verruciformis-associated human papillomavirus 8*. Virology, 1993. **196**(2): p. 674-81.
79. Majewski, S., S. Jablonska, and G. Orth, *Epidermodysplasia verruciformis. Immunological and nonimmunological surveillance mechanisms: role in tumor progression*. Clin Dermatol, 1997. **15**(3): p. 321-34.
80. de Villiers, E.M., C. Whitley, and K. Gunst, *Identification of new papillomavirus types*. Methods Mol Med, 2005. **119**: p. 1-13.
81. Pfister, H. and J. Ter Schegget, *Role of HPV in cutaneous premalignant and malignant tumors*. Clin Dermatol, 1997. **15**(3): p. 335-47.
82. Harwood, C.A., et al., *Human papillomavirus infection and non-melanoma skin cancer in immunosuppressed and immunocompetent individuals*. J Med Virol, 2000. **61**(3): p. 289-97.

83. Berkhout, R.J., J.N. Bouwes Bavinck, and J. ter Schegget, *Persistence of human papillomavirus DNA in benign and (pre)malignant skin lesions from renal transplant recipients*. J Clin Microbiol, 2000. **38**(6): p. 2087-96.
84. Pfister, H., *Chapter 8: Human papillomavirus and skin cancer*. J Natl Cancer Inst Monogr, 2003(31): p. 52-6.
85. Feltkamp, M.C., et al., *Seroreactivity to epidermodysplasia verruciformis-related human papillomavirus types is associated with nonmelanoma skin cancer*. Cancer Res, 2003. **63**(10): p. 2695-700.
86. Masini, C., et al., *Evidence for the association of human papillomavirus infection and cutaneous squamous cell carcinoma in immunocompetent individuals*. Arch Dermatol, 2003. **139**(7): p. 890-4.
87. Bouwes Bavinck, J.N., E.I. Plasmeijer, and M.C. Feltkamp, *Beta-papillomavirus infection and skin cancer*. J Invest Dermatol, 2008. **128**(6): p. 1355-8.
88. Steger, G. and H. Pfister, *In vitro expressed HPV 8 E6 protein does not bind p53*. Arch Virol, 1992. **125**(1-4): p. 355-60.
89. Kiyono, T., A. Hiraiwa, and M. Ishibashi, *Differences in transforming activity and coded amino acid sequence among E6 genes of several papillomaviruses associated with epidermodysplasia verruciformis*. Virology, 1992. **186**(2): p. 628-39.
90. Scheffner, M., et al., *The E6 oncoprotein encoded by human papillomavirus types 16 and 18 promotes the degradation of p53*. Cell, 1990. **63**(6): p. 1129-36.
91. Iftner, T., et al., *Involvement of human papillomavirus type 8 genes E6 and E7 in transformation and replication*. J Virol, 1988. **62**(10): p. 3655-61.
92. Jackson, S. and A. Storey, *E6 proteins from diverse cutaneous HPV types inhibit apoptosis in response to UV damage*. Oncogene, 2000. **19**(4): p. 592-8.
93. Yamashita, T., et al., *Biological and biochemical activity of E7 genes of the cutaneous human papillomavirus type 5 and 8*. Oncogene, 1993. **8**(9): p. 2433-41.
94. Fuchs, P.G., et al., *Epidermodysplasia verruciformis-associated human papillomavirus 8: genomic sequence and comparative analysis*. J Virol, 1986. **58**(2): p. 626-34.
95. Muralidhar, S., S.P. Becerra, and J.A. Rose, *Site-directed mutagenesis of adeno-associated virus type 2 structural protein initiation codons: effects on regulation of synthesis and biological activity*. J Virol, 1994. **68**(1): p. 170-6.
96. Warrington, K.H., Jr., et al., *Adeno-associated virus type 2 VP2 capsid protein is nonessential and can tolerate large peptide insertions at its N terminus*. J Virol, 2004. **78**(12): p. 6595-609.
97. Merad, M., F. Ginhoux, and M. Collin, *Origin, homeostasis and function of Langerhans cells and other langerin-expressing dendritic cells*. Nat Rev Immunol, 2008. **8**(12): p. 935-47.
98. Hagemann, T., et al., *Macrophages induce invasiveness of epithelial cancer cells via NF-kappa B and JNK*. J Immunol, 2005. **175**(2): p. 1197-205.

99. Honda, A., et al., *Interleukin-1beta and macrophage migration inhibitory factor (MIF) in dermal fibroblasts mediate UVA-induced matrix metalloproteinase-1 expression*. J Dermatol Sci, 2008. **49**(1): p. 63-72.
100. Shiroeda, H., et al., *Association between functional promoter polymorphisms of macrophage migration inhibitory factor (MIF) gene and ulcerative colitis in Japan*. Cytokine, 2010. **51**(2): p. 173-7.
101. Shimizu, T., et al., *Increased production of macrophage migration inhibitory factor by PBMCs of atopic dermatitis*. J Allergy Clin Immunol, 1999. **104**(3 Pt 1): p. 659-64.
102. Hamasaka, A., et al., *DNA vaccination against macrophage migration inhibitory factor improves atopic dermatitis in murine models*. J Allergy Clin Immunol, 2009. **124**(1): p. 90-9.
103. Serarslan, G., et al., *Macrophage migration inhibitory factor in patients with vitiligo and relationship between duration and clinical type of disease*. Clin Exp Dermatol, 2010. **35**(5): p. 487-90.
104. Jin, Y., et al., *NALP1 in vitiligo-associated multiple autoimmune disease*. N Engl J Med, 2007. **356**(12): p. 1216-25.
105. Ashcroft, G.S., et al., *Estrogen modulates cutaneous wound healing by downregulating macrophage migration inhibitory factor*. J Clin Invest, 2003. **111**(9): p. 1309-18.
106. Ito, T., et al., *Maintenance of hair follicle immune privilege is linked to prevention of NK cell attack*. J Invest Dermatol, 2008. **128**(5): p. 1196-206.
107. Freeman, G.J., et al., *The BB1 monoclonal antibody recognizes both cell surface CD74 (MHC class II-associated invariant chain) as well as B7-1 (CD80), resolving the question regarding a third CD28/CTLA-4 counterreceptor*. J Immunol, 1998. **161**(6): p. 2708-15.
108. Allan, R.S., et al., *Epidermal viral immunity induced by CD8alpha+ dendritic cells but not by Langerhans cells*. Science, 2003. **301**(5641): p. 1925-8.
109. Ritter, U., et al., *CD8 alpha- and Langerin-negative dendritic cells, but not Langerhans cells, act as principal antigen-presenting cells in leishmaniasis*. Eur J Immunol, 2004. **34**(6): p. 1542-50.
110. Valladeau, J., et al., *Langerin, a novel C-type lectin specific to Langerhans cells, is an endocytic receptor that induces the formation of Birbeck granules*. Immunity, 2000. **12**(1): p. 71-81.
111. Kissenpfennig, A., et al., *Dynamics and function of Langerhans cells in vivo: dermal dendritic cells colonize lymph node areas distinct from slower migrating Langerhans cells*. Immunity, 2005. **22**(5): p. 643-54.
112. Bennett, C.L., et al., *Inducible ablation of mouse Langerhans cells diminishes but fails to abrogate contact hypersensitivity*. J Cell Biol, 2005. **169**(4): p. 569-76.
113. Kaplan, D.H., et al., *Epidermal langerhans cell-deficient mice develop enhanced contact hypersensitivity*. Immunity, 2005. **23**(6): p. 611-20.
114. Poulin, L.F., et al., *The dermis contains langerin+ dendritic cells that develop and function independently of epidermal Langerhans cells*. J Exp Med, 2007. **204**(13): p. 3119-31.
115. Ginhoux, F., et al., *Blood-derived dermal langerin+ dendritic cells survey the skin in the steady state*. J Exp Med, 2007. **204**(13): p. 3133-46.

116. Bursch, L.S., et al., *Identification of a novel population of Langerin+ dendritic cells*. J Exp Med, 2007. **204**(13): p. 3147-56.
117. Ginhoux, F. and M. Merad, *Ontogeny and homeostasis of Langerhans cells*. Immunol Cell Biol, 2010. **88**(4): p. 387-92.
118. Ueno, H., et al., *Dendritic cells and humoral immunity in humans*. Immunol Cell Biol, 2010. **88**(4): p. 376-80.
119. Henri, S., et al., *Disentangling the complexity of the skin dendritic cell network*. Immunol Cell Biol, 2010. **88**(4): p. 366-75.
120. Lutz, M.B., A. Dohler, and H. Azukizawa, *Revisiting the tolerogenicity of epidermal Langerhans cells*. Immunol Cell Biol, 2010. **88**(4): p. 381-6.
121. Bedoui, S., et al., *Cross-presentation of viral and self antigens by skin-derived CD103+ dendritic cells*. Nat Immunol, 2009. **10**(5): p. 488-95.
122. Qu, M., H.K. Muller, and G.M. Woods, *Chemical carcinogens and antigens contribute to cutaneous tumor promotion by depleting epidermal Langerhans cells*. Carcinogenesis, 1997. **18**(6): p. 1277-9.
123. Ruby, J.C., G.M. Halliday, and H.K. Muller, *Differential effects of benzo[a]pyrene and dimethylbenz[a]-anthracene on Langerhans cell distribution and contact sensitization in murine epidermis*. J Invest Dermatol, 1989. **92**(2): p. 150-5.
124. Schaper, I.D., et al., *Development of skin tumors in mice transgenic for early genes of human papillomavirus type 8*. Cancer Res, 2005. **65**(4): p. 1394-400.
125. Byrne, C., M. Tainsky, and E. Fuchs, *Programming gene expression in developing epidermis*. Development, 1994. **120**(9): p. 2369-83.
126. Helfrich, I., et al., *Increased incidence of squamous cell carcinomas in Mastomys natalensis papillomavirus E6 transgenic mice during two-stage skin carcinogenesis*. J Virol, 2004. **78**(9): p. 4797-805.
127. Sethi, N. and J. Palefsky, *Transcriptional profiling of dysplastic lesions in K14-HPV16 transgenic mice using laser microdissection*. FASEB J, 2004. **18**(11): p. 1243-5.
128. Miyagi, J., et al., *Extremely high Langerhans cell infiltration contributes to the favourable prognosis of HPV-infected squamous cell carcinoma and adenocarcinoma of the lung*. Histopathology, 2001. **38**(4): p. 355-67.

7 PUBLICATIONS

Fingerle-Rowson G, Kaleswarapu DR, Schlander C, Kabgani N, **Brocks T**, Reinart N, Busch R, Schütz A, Lue H, Du X, Liu A, Xiong H, Chen Y, Nemajerova A, Hallek M, Bernhagen J, Leng L, Bucala R.

A tautomerase-null macrophage migration-inhibitory factor (MIF) gene knock-in mouse model reveals that protein interactions and not enzymatic activity mediate MIF-dependent growth regulation.

Mol Cell Biol. 2009 Apr;29(7):1922-32. Epub 2009 Feb 2.

Congress Participation and Poster Presentation

- **Tania M. Brocks**, Astrid Stein, Hans-Peter Dienes, Michael Hallek, Günter Fingerle-Rowson. Macrophage Migration Inhibitory Factor (MIF) – A Novel Tumor Suppressor in Skin Tumorigenesis.

→ Annual Meeting of the DGHO, ÖGHO, SGMO and SGH, 2008, Vienna.

- **Tania M. Brocks**, Astrid Stein, Hans-Peter Dienes, Michael Hallek, Günter Fingerle-Rowson. Macrophage Migration Inhibitory Factor (MIF) - A Novel Tumor Suppressor in Murine Skin Tumorigenesis.

→ 7th World Congress on Melanoma/5th Congress of the European Association of Dermato-Oncology (EADO), 2009, Vienna.

8 CURRICULUM VITAE

Name	Tania Marina Brocks
Date of birth	26 th September 1976
Place of birth	Dortmund
Nationality	German
Family status	married, no children
Father	Ulrich Brocks, M.D.; married
Mother	Dr. med. Veronika Gressner-Brocks, M.D.; divorced

Academic career

07/10	Research Scholar (RO1 and U19 grant) University of California Los Angeles (UCLA) David Geffen School of Medicine, Radiation Oncology
03/09	Student in Economics and International Management Open University Hagen IWW
02/06-	Ph.D. Candidate, Research Associate
01/10	University Hospital Cologne Clinic I for Internal Medicine, Hematology & Oncology

Ph.D. thesis: "*The Role of Macrophage Migration Inhibitory Factor in Murine Skin Tumorigenesis*"

10/95- Studies in Biology

06/05 University of Cologne

Majors: Biochemistry

Developmental biology

Genetics

Diploma degree: Very good (1,0); date: June 24th 2005

Diploma thesis: "*Characterisation of the Activation Mechanism of CaMKI Through Calmodulin in Presence of Mg²⁺*"

10/95- Student in Philosophy, Japanese Studies and Data Processing

06/05 University of Cologne

09/86- Grammar school

06/95 Stadtgymnasium Dortmund

A-levels ("Abitur") degree: 1,9; date: June 12th 1995

09/82- Primary school

06/86 Graf-Spee-Schule, Essen

Professional experience

06/05- Reserch Associate

01/06 University Hospital Cologne

CMMC, NG IV

Junior Research Group of Dr. rer. nat. C. Niemann

Project: „Role of Indian Hedgehog in proliferation and differentiation of sebocytes and sebaceous adenomas in K14ΔNLef1-transgenic C57BL/6 mice“

03/04- Scientific Assistant

09/04 University of Cologne

Institute for Biochemistry

Research Groups of Professors H.-W. Klein and R. Sterner

10/02- Marketing Department Fellow

12/02 QIAGEN Operon GmbH, Cologne

10/01- Scientific Assistant

03/02 caesar, Bonn

09/00- Content Assistant

06/01 Bioropa GmbH, Cologne

Practical experience

08/03- Scientific practical in genetics

11/03 University of London, Queen Mary & Westfield College

Prof. Conrad P. Lichtenstein's lab

08/01- Laboratory in histology

10/01 caesar, Bonn

A handwritten signature in black ink, consisting of several overlapping loops and a long horizontal stroke at the end.

SIGNATURE

Print- & Copyhaus

Grindelallee 32

20146 Hamburg